Neuron-microglia interactions induce aberrant inflammatory mechanisms in schizophrenia

Dissertation

der Mathematisch-Naturwissenschaftlichen Fakultät

der Eberhard Karls Universität Tübingen

zur Erlangung des Grades eines

Doktors der Naturwissenschaften

(Dr. rer. nat.)

vorgelegt von

Ricarda Breitmeyer geb. Stock

aus Bonn

Tübingen

2020

Gedruckt mit Genehmigung der Mathematisch-Naturwissenschaftlichen Fakultät der Eberhard Karls Universität Tübingen.

Tag der mündlichen Qualifikation:	11.03.2021
Stellvertretender Dekan:	Prof. Dr. József Fortágh
1. Berichterstatter:	Prof. Dr. Ulrich Rothbauer
2. Berichterstatter:	apl. Prof. Dr. Hansjürgen Volkmer

Eidesstaatliche Erklärung

Ich erkläre hiermit, dass ich die zur Promotion eingereichte Arbeit mit dem Titel: „Neuron-microglia interactions induce aberrant inflammatory mechanisms in schizophrenia“ selbständig verfasst, nur die angegebenen Quellen und Hilfsmittel benutzt und wörtlich oder inhaltlich übernommene Stellen als solche gekennzeichnet habe.
Ich erkläre, dass die Richtlinien zur Sicherung guter wissenschaftlicher Praxis der Universität Tübingen (Beschluss des Senats vom 25.5.2000) beachtet wurden. Ich versichere an Eides statt, dass diese Angaben wahr sind und dass ich nichts verschwiegen habe. Mir ist bekannt, dass die falsche Abgabe einer Versicherung an Eides statt mit Freiheitsstrafe bis zu drei Jahren oder mit Geldstrafe bestraft wird.

Tübingen, den

Ricarda Breitmeyer geb. Stock

Table of Contents

List of Figures

List of Tables

List of Abbreviations

°C	degree celsius
αMTG	αMono-thio glycerol
AA2P	ascorbic acid 2 phosphate
AAV	adeno-associated virus
AB	antibody
ASD	autism spectrum disorder
BDNF	brain-derived neurotrophic factor
BMB	blocking reagent
bFGF	basic fibroblast growth factor
BMP4	bone morphogenic protein 4
bp	base pairs
cAMP	N^6,2′-O-Dibutyryladenosine 3′,5′-cyclic monophosphate sodium salt
CHIR99021	highly selective GSK-3 inhibitor
CO_2	carbon dioxide
CNS	central nervous system
dibutyryl cAMP	dibutyryladenosine cyclic monophosphate sodium salt
DMSO	dimethyl sulfoxide
DNA	desoxyribonucleic acid
DPBS	Dulbecco´s Phosphate Buffered Saline
EB	embryoid body
EGFP	enhanced green fluorescent protein
ELISA	enzyme linked immunosorbent assay
FACS	fluorescence activated cell sorting
FBS	fetal bovine serum
FGA	first generation antipsychotic drugs
FWHM	full width half maximum
GCDR	gentle cell dissociation reagent
gDNA	genomic desoxyribonucleic acid
GDNF	glial cell line-derived neurotrophic factor
GFAP	glial fibrillary acidic protein
GM-CSF	granulocyte macrophage colony stimulating factor
H_2O	water
HEK cells	human embryonic kidney cells
HLA	human leukocyte antigen
hNGN2	human Neurogenin 2
HSC	hematopoietic stem cell
Iba1	ionized calcium-binding adapter molecule
IFN	interferon

IL	interleukin
iPSC	induced pluripotent stem cells
ITS-X	Insulin-transferrin selenium ethanolamine
KLF4	Kruppel-like factor 4
Lam	laminin
LPS	lipopolysaccharide
M-CSF	macrophage colony stimulating factor
MAP2	microtubule associated protein 2
MG	microglia
MFI	mean fluorescence intensity
min	minute
MPC	myeloid progenitor cell
MuLV RT	moloney murine leukemia virus reverse transcriptase
NEAA	non-essential amino acids
NFκB	nuclear factor kappa-light-chain-enhancer of activated B-cells
NPC	neuronal progenitor cells
OCT3/4	octamer-binding transcription factor 3/4
PCR	polymerase chain reaction
Pen/Strep	Penicillin / Streptomycin
PFA	paraformaldehyde
PLO	poly-L-ornithine
PVA	poly vinyl alcohol
RNA	ribonucleic acid
ROI	region of interest
ROS	reactive oxygen species
RT	room temperature
RT-PCR	reverse transcriptase polymerase chain reaction
SB 431542	potent, selective inhibitor of TGF-βRI, ALK4 and ALK7
SCF	stem cell factor
s.e.m.	standard error of the mean
SOX2	sex determining region Y-box 2
STR	short tandem repeat
Syn1	synapsin 1
SZ	schizophrenia
TGFβ	tumor growth factor beta
TNFα	tumor necrosis factor alpha
TPO	thrombopoietin
VEGF	vascular endothelial growth factor
VGlut1	presynaptic vesicular glutamate transporter 1
Y-27632 dihydrochloride	ROCK Inhibitor

Abstract

Inflammation in the human brain is suggested to contribute to several diseases of the central nervous system. Human microglia, the resident immune cells of the brain, have essential functions for maintenance of the central nervous system, synaptic organization and immune defense. During brain development and until late adolescence, the elimination of weak and inactive synapses is a mandatory process for sculpting mature, neuronal circuits. Excessive synaptic elimination by reactive microglia is suggested to contribute to the pathology of several neurodegenerative, neurodevelopmental and neuropsychiatric disorders, such as autism spectrum disorder or schizophrenia. Schizophrenia is a complex and highly heterogeneous disease with detrimental impairments for affected patients. Aberrant microglial activation, release of pro-inflammatory cytokines and ungoverned phagocytosis of synaptic structures is considered a central cause for the development and progression of schizophrenia. So far, there is no cure for schizophrenia and antipsychotic drug therapy can only reduce symptom severity. Targeting microglia by anti-inflammatory treatment is hypothesized to be highly beneficial for the integrity of neuronal networks in neuropsychiatric diseases.

To better understand how neuroinflammatory processes and excessive synaptic elimination contribute to pathological phenotypes of schizophrenia, somatic fibroblasts from four patients with schizophrenia and three healthy controls were reprogrammed successfully into induced pluripotent stem cells (iPSCs). iPSCs were completely characterized and reproducible protocols for the differentiation into microglia and glutamatergic neurons were established. Both cell types were separately analyzed for mature phenotypes. Neurite outgrowth, intracellular calcium signaling and synaptic density was reduced in schizophrenia patient-derived neurons. Microglia derived from patients with schizophrenia displayed increased expression of microglial activation marker HLA-DR. Finally, the cells generated were introduced in a co-culture system comprising iPSC-derived neurons and microglia to study neuroinflammatory mechanisms in the early development of schizophrenia. Addition of microglia led to reduced synaptic density with microglia from patients with schizophrenia engulfing and eliminating more synapses compared to control microglia. Likewise, neuronal cultures derived from patients with schizophrenia activated microglia in a more pronounced way than healthy control neurons. Pro-inflammatory pre-treatment amplified microglial activation and synaptic pruning by control and patient-derived microglia. Most interestingly, application of the anti-inflammatory antibiotic minocycline could reverse excessive synaptic elimination by microglia derived from patients with schizophrenia.

The established co-culture model of microglia and neurons offers the possibility to study neuroinflammatory processes in the development of schizophrenia and detect pathological mechanisms in patient-derived microglia and neurons.

Zusammenfassung

Entzündungen des zentralen Nervensystems tragen zu zahlreichen neuropsychiatrischen und neurodegenerativen Erkrankungen bei. Gesteuert werden diese Prozesse normalerweise durch Microglia, den Immunzellen des humanen Gehirns, deren Hauptaufgabe in der Aufrechterhaltung der Homöostase, der synaptischen Organisation und vor allem der Immunantwort liegt. Während der Entwicklung des Gehirns bis hin zur späten Jugend ist die Eliminierung schwacher und inaktiver Synapsen ein notwendiger Prozess, damit ein reifes und funktionell intaktes, neuronales Netzwerk entstehen kann. Es wird vermutet, dass ein fehlregulierter, exzessiver Abbau von Synapsen durch reaktive Microglia zum Verlauf verschiedenster entwicklungsneurobiologischer oder psychiatrischer Erkrankungen beiträgt. Dazu gehört etwa die Autismus-Spektrums-Störung oder die Schizophrenie. Schizophrenie ist eine hoch komplexe und sehr heterogene Erkrankung mit schweren kognitiven Einschränkungen für betroffene Patienten. Deregulierte microgliale Aktivität, die Freisetzung pro-inflammatorischer Zytokine oder die ungesteuerte Phagozytose synaptischer Strukturen sind potentielle Ursachen für die Entstehung und den Fortschritt einer Schizophrenie-Erkrankung. Bis heute ist eine Heilung für Schizophrenie nicht möglich, verfügbare antipsychotische Medikamente können nur die Schwere der Symptome vermindern. Um die Integrität neuronaler Netzwerke zu verbessern und vor überaktivierten Microglia zu beschützen, gilt die anti-inflammatorische Behandlung von Microglia als vielversprechender Ansatz in der Entwicklung neuartiger Therapeutika für neuropsychiatrische Erkrankungen.

Um besser zu verstehen wie neuroinflammatorische Prozesse mit übermäßigem Abbau von Synapsen und dem pathologischen Erscheinungsbild der Schizophrenie zusammenhängen, wurden somatische Fibroblasten von vier Schizophrenie-Patienten und von drei gesunden Kontrollprobanden in induziert pluripotente Stammzellen reprogrammiert. Die generierten Zellen wurden vollständig charakterisiert und anschließend in Microglia und glutamaterge Neurone differenziert und sorgfältig analysiert. Neuritenwachstum, intrazelluläre Calcium-Messungen und die synaptische Dichte waren in neuronalen Kulturen von Schizophrenie-Patienten signifikant reduziert. Zudem zeigten Microglia, die von Schizophrenie-Patienten stammten, eine erhöhte Expression des immunologischen Aktivierungsmarkers HLA-DR.

Das stammzellabgeleitete Co-Kultursystem aus Microglia und Neuronen wurde anschließend genutzt, um entzündliche Prozesse in der frühen Entwicklung von Schizophrenie zu untersuchen. Patienten-basierte Co-Kulturen wiesen eine reduzierte Synapsendichte und einen vermehrtem Synapsenabbau durch aktivierte Microglia auf. Gleichzeitig stimulierten patienten-abgeleitete Neurone die Phagozytose durch Microglia deutlicher als neuronale Kulturen gesunder Kontrollen. Eine pro-inflammatorische Vorbehandlung von Microglia verstärkte die immunologische Aktivierung der Zellen und führte zu einem verstärkten

Synapsenabbau durch Microglia. Eine Behandlung der Immunzellen mit dem anti-inflammatorisch wirkenden Antibiotikum Minocycline führte interessanterweise zu einer Prävention des exzessiven Eliminierens von Synapsen durch Microglia von Schizophrenie-Patienten.

Das in dieser Studie etablierte Co-Kulturmodell bietet eine neue Methodik, um fehlregulierte Interaktionen und die wechselwirkende Kommunikation zwischen neuronalen und immunologischen Zellen in der Entwicklung von Schizophrenie zu untersuchen und potentielle Therapieansätze zu entwickeln.

1. Introduction

1.1. Schizophrenia

Schizophrenia is a complex and devastating mental disorder with a worldwide prevalence of approx. 1 % affecting emotion, perception, cognition and social behavior of women and men equally. First psychotic symptoms can appear in the early adulthood and comprise hallucinations, delusions and social and cognitive impairments [1, 2]. Schizophrenia is considered a neurodevelopmental disorder with symptoms appearing during adolescence. Causes for schizophrenia are as multifactorial and heterogeneous as the disease itself and the precise pathogenesis varies from patient to patient. Genetic predisposition is most likely to contribute to the development of schizophrenia, but also environmental factors like prenatal stress, drug abuse or childhood trauma are equivalent risk factors [3, 4].

Schizophrenia and other neuropsychiatric diseases like autism spectrum disorder (ASD) or bipolar depression share several developmental phenotypes and symptoms, making discrimination among neuropsychiatric diseases difficult for physicians and scientists. For classification of patients with schizophrenia, the Positive and Negative Syndrome Scale for Schizophrenia (PANSS) was developed in 1987 [5]. Symptoms of schizophrenia can thereby be used to measure and segregate symptoms and their severity on a comparable scale [6]. Schizophrenia patients can experience three types of symptoms, namely positive, negative and cognitive deficits. Positive symptoms describe delusions, hallucinations and paranoia, experiences that healthy human beings are not capable of [7]. Negative symptoms are impaired social behavior, emotional withdrawal or poor communicative skills [8]. Cognitive deficits comprise disorganized thought and speech, reduced attention or impaired concentration capability [9]. Generally, also depression, anxiety, disorientation and social withdrawal are common comorbid disorders of schizophrenia [10]. The combination of different symptoms, the diverse course of disease progression and the variable genetic background of each patient make it a challenge to diagnose, treat and give therapy to individual patients.

1.1.1. Induced pluripotent stem cells as a human *in vitro* model for schizophrenia

Studying human neurobiological and neuroimmunological processes and mechanisms *in vitro* was always limited by the lack of human test systems. The only useful basis was the use of post mortem brain tissues, but effects caused by death and age of the respective donor always restricted the significance of achieved results. Therefore, *in vivo* animal models, e.g. rodent or primate studies, were established to study mammalian disease mechanisms but translation of

results to human systems remains difficult. Human pluripotent stem cells represent the complex genomic background of the specific donor and finally offer the possibility to study early human developmental processes *in vitro*.

Pluripotent stem cells have the capability for self-renewal and are able to be differentiated in each germ layer, with the exception of germ cells. Over a decade ago, Yamanaka et al. established a protocol for the reprogramming of somatic cells back into a stem-cell like, naïve status [11]**.** Forced expression of key stem cell and pluripotency genes such as OCT3/4, SOX2, KLF4 and c-MYC, leads to the reprogramming into induced pluripotent stem cells (iPSC). The generated iPSCs comprise the whole, complex genome of the donor, making them especially valuable for personalized medicine and developmental and functional disease modeling. Within the last years, the procedure of reprogramming was more and more simplified, resulting in protocols to gain iPSC within a few weeks [12]. iPSCs offer an unlimited source for disease-relevant cell types and are by now used to model a variety of human *in vitro* patient-derived disease systems, to develop and screen new drugs or for regenerative therapy and personalized medicine.

For neuropsychiatric research, neuronal and glial subtypes can be differentiated reproducibly *in vitro* that reflect *in vivo* morphological and functional characteristics. There are two different types of possible cellular *in vitro* models to study disease mechanisms of schizophrenia: Patient-specific models representing diagnosed patients with schizophrenia in a dish on the one hand and gene-specific isogenic models with introduced mutations into loci of schizophrenia risk genes on the other hand. Patient-derived model systems comprise the complete genetic background of each individual patient, including all postnatal modifications and epigenetics. As schizophrenia is suggested not to arise from one single mutation but from many different aspects together, patient-based models appear to reflect more precisely the diversity, heterogeneity and complex interplay of various factors of the disease. However, the combination and comparison of both models clarifies putative causes and pathogenic phenotypes of schizophrenia paving the way for the identification of new targets for drug development and approaches for personalized therapy.

1.1.2. Putative genetic and environmental causes for schizophrenia

Within the last decades, several putative causes for schizophrenia have been discussed. Heritable, genetic risk genes are major factors driving schizophrenia. The tendency of schizophrenia to impact several members of one family highlights the high rate of heritability and is considered to be the cause in approximately 66 % of all schizophrenia cases [13, 14]. Additionally, aberrant neurobiological or neuroinflammatory mechanisms, epigenetics, environmental factors and prenatal stress have been shown to separately or collectively be able to trigger psychoses [3, 15, 16].

Within the last years, several genome-wide association studies (GWAS) ranging from small cohorts up to large scale studies have been published and identified more than 150 risk genes that are associated to schizophrenia [17, 18]. Affected loci are for example the transcription factor *TCF4* that is needed for initiation of neuronal differentiation [19], the major histocompatibility complex (MHC) [20] or DISC1, the most prominent risk gene that has been extensively modified and studied in animal and human *in vitro* systems [21]. The somatic *DISC1* mutation was first discovered in a scottish family with several family members having a history of psychiatric disorders and mental illnesses [22]. DISC1 is a scaffold protein involved in many cellular processes and signaling pathways that are essential for neuronal migration, network structures and cortical neurodevelopment [23, 24]. *DISC1* deletion in human iPSC has been shown to lead to reduced neuronal outgrowth, impaired neuronal differentiation [25] and disorganized structural morphology [26]. Also glutamatergic synaptic function is impaired in *DISC1* knockout models [27]. The implication of DISC1 in a variety of neurodevelopmental processes make it a valuable target for genome-editing and disease modeling of schizophrenia *in vitro*.

Other bioinformatical techniques like next-generation sequencing and transcriptome analysis offer the possibility to detect further patient- and disease-specifically deregulated genes. Broadly, deregulated genes are predominantly related to neurodevelopmental processes, synapse plasticity, neuronal connectivity and the immune system. More precisely, identified genes comprise several protein-coding genes for glutamatergic and dopaminergic transmission and signaling [28]. Additional genes were identified that are involved in early neuronal migration and proliferation, synaptogenesis and axonal outgrowth implicating that schizophrenia is considered a neurodevelopmental rather than a neurodegenerative disorder [29].

The developing brain depends on genetically determined processes and precisely timed developmental mechanisms that are sensitive to specific environmental signals. Clinical studies and animal models revealed infection-induced maternal immune activation during pregnancy to be clearly associated with an increased potential of developing neuropsychiatric

disorders like schizophrenia but also ASD or bipolar depression [30-33]. Together with genetic predispositions, environmental factors, diet or parental age, viral or bacterial infections can have massive short and long term effects on the fetus' developing brain. Mouse models and human studies of maternal immune activation reported that an imbalance of maternal cytokine levels, especially of the pro-inflammatory cytokines IL-6, TNFα or the C-reactive protein negatively influence the environment *in utero* [34-36]. The subsequent activation of the innate and adaptive immune system and inherent complement pathways, increased reactivity of microglia and other inflammatory stress signals impact the integrity of the blood-brain barrier and negatively affect developing neuronal circuits [37, 38].

1.1.3. The neuropsychiatric side of schizophrenia

Human post mortem tissue analysis and *in vivo* neuroimaging reported reduced brain volumes across all affected brain regions [39, 40], lower levels of dendritic spines [41-43] and reduced expression of postsynaptic marker PSD-95 [44, 45]. First iPSC-based results reported reduced neurite number and decreased PSD-95 levels in reprogrammed iPSC-derived neurons from idiopathic schizophrenia (SZ) patients [46]. Following studies confirmed similar phenotypes in glutamatergic SZ-neurons with decreased neurite numbers and lengths [47, 48] and decreased glutamate receptor expression [48, 49]. Likewise, reduced synaptogenesis and defects in neuronal connectivity were reported for glutamatergic SZ-neurons [46, 50, 51].

Anomalies in neuronal connectivity were also found in iPSC-derived cultures of dopaminergic neurons [49] and deficits in hippocampal neurogenesis were reported for the generation of dentate gyrus granule neurons with reduced levels of neurotransmitter release and neuronal activity [52]. Neuronal activity appears to be one major parameter for detecting disturbances in SZ-derived cells. Several studies reported reduced evoked or spontaneous neuronal activity in different neuronal SZ-cell types [48, 53, 54]. The respective findings on neuronal activity however differ among studies. No significant abnormalities in intracellular calcium signaling were reported in 2011 [46], while newer studies detected differences between control and SZ-derived neuronal cell types [48]. Hippocampal dentate gyrus SZ-neurons showed reduced levels of neurogenesis in association with reduced neuronal activity in 6-week-old neuronal cultures [52]. Additionally, multi-electrode array recordings of 6-week-old dentate gyrus hippocampal SZ-cultures revealed a significantly reduced number of spikes and network bursts and deficits in spontaneous and evoked activity compared to healthy controls [54]. Pattern analysis of intracellular calcium signals of 8-week-old cortical SZ-cultures revealed decreased peak frequency with significantly increased peak areas [48].

Lately, also mitochondrial dysfunction and oxidative damage came into focus of schizophrenia research. Oxidative stress with aberrant release of reactive species leads to intra- and extracellular damage of lipids, enzymes, proteins and DNA, ultimately affecting not only neurons but also immune cells or glial cells of the CNS. Impaired mitochondrial respiration and alterations of mitochondrial networks were reported [49, 55], as well as increased oxidative stress [50]. Deregulated gene expression of genes involved in oxidative phosphorylation was shown for cortical interneurons but not for glutamatergic neurons [51].

All gathered results of iPSC-based neuronal cell culture system derived from patients with schizophrenia indicate that mitochondrial function, synaptic plasticity and neuronal network formation are deregulated, but functional assays like neuronal activity or neurotransmitter release can only give suggestive hints about characteristic phenotypes of schizophrenia. The recruitment of a cohort of carefully diagnosed and selected patients seems to be the most important point to consider when robust assays and disease-specific phenotypes and parameters need to be implemented, as the cellular and functional variability among patients differs significantly.

1.1.4. Therapies and treatment opportunities

Treatment of schizophrenia patients with commonly used antipsychotics mostly aims at the reduction of positive symptoms. Treatment to stop the onset or slow down the progression is until today impossible, as the etiology of schizophrenia is still unclear and the disease cannot be determined before first symptoms and psychoses appear. However, the development of effective early stage antipsychotics is desirable to prevent symptom worsening over time.

Commonly used drugs, so called antipsychotics, act by reducing positive symptoms and prevent relapses. Until today, schizophrenia is not curable but quality of life of affected patients can be increased significantly by antipsychotic application and constant psychotherapy [56]. Antipsychotic drugs can be separated in two groups, the first- and second-generation antipsychotics. First-generation antipsychotics (FGA), such as haloperidol or chlorpromazine, block as an antagonist the postsynaptic dopamine-D2-receptors resulting in reduced positive symptoms, but their efficacy can be very low and varies significantly among patients [57]. Additionally, FGA tend to induce several neurological side effects, like tremors or tardive dyskinesia, i.e. involuntary body movements like grimacing or abnormal tongue and lip movements [5, 58, 59]. With only little improved quality of life and massive side effects, usage of FGA is not beneficial for some patients [60].

Clozapine is the most prominent drug that belongs to the second-generation or so called atypical antipsychotics. Clozapine is usually administered in patients that are non-responsive

to FGA. By blocking as a serotonin-dopamine antagonist not only D2 and D4 receptors but also serotonin $5HT_{2A}$ receptors, clozapine can reduce negative and cognitive symptoms [61, 62]. However, also atypical antipsychotics have the tendency to induce severe side effects affecting not only neurological but also metabolic functions, causing agranulocytosis or myocarditis [4, 63].

The urge to develop improved antipsychotics with lower side effects and subsequent improved quality of life is immense. A combination of knowledge about genetic risk factors and molecular phenotypes of the molecular pathophysiology of schizophrenia is essential for the development of more efficient drugs [64].

1.2. Neuroinflammation

Inflammation is a natural response to infection, pathogens or damaged tissue and is mediated by the precisely timed release of a specific cocktail of pro- or anti-inflammatory cytokines that recruit immune cells to the point of inflammation and induce wound healing. Signaling cascades trigger defense mechanisms of responsible immune cells, such as monocytes or macrophages in the blood or microglia in the central nervous system (CNS), to combat the source of inflammation and reduce inflammation by minimizing tissue damage and systemic consequences. Once the threat has been eliminated and wound healing was initiated, symptoms of inflammation as redness, swelling or itching decline [65]. In healthy conditions, inflammation is a precisely regulated process essential for homeostasis, but inflammation can get off balance, when microglia and other immune cells become reactive. Harmful effects of uncontrolled inflammation are observable in many infectious and autoimmune diseases [66].

Inflammation in the CNS, the so called neuroinflammation, is mostly mediated by microglia and can have neuroprotective or neurotoxic effects on neuronal circuits [67]. An imbalanced inflammatory response is considered a common feature of neurodevelopmental, neuropsychiatric and neurodegenerative disorders [68]. An acute inflammation such as acute encephalitis that can be life-threatening within hours needs to be distinguished from chronic infections as multiple sclerosis that can impair patients for a lifetime. Schizophrenia is considered to be caused or at least influenced by a mild, chronic inflammation of the CNS [69].

But if the characteristic decline of neuronal connectivity, signaling and synaptic density is the cause or consequence of neuroinflammation and if so, how exactly neuroinflammation contributes to the progression of schizophrenia still remains elusive. Cellular *in vitro* models focusing on microglia rather than neuronal cells represent promising approaches to better understand the immunological, immunopsychiatric pathology of schizophrenia and to establish models for biomarker discovery or drug development and may ultimately improve therapy outcomes [70-72].

1.2.1. Microglia as mediators of neuroinflammation

Microglia are tissue-resident macrophages in the brain. While macrophages originate from circulating monocytes in the blood that are constantly renewed in the bone marrow, microglia evolve during embryogenesis in the yolk sac, migrate into the brain and do not depend on blood-monocyte infiltration after blood-brain-barrier formation [73]. Microglia have the ability to self-renew within their specific CNS niche and are long-lived glia cells [74, 75]. Microglia and macrophages are professional phagocytes with important functions during acute immune response, tissue protection and repair or phagocytosis of apoptotic cells and cellular debris.

Microglia comprise approximately 10 % of the total CNS population and are mainly involved in CNS maintenance, homeostasis and control of developmental processes, such as neurogenesis and synaptogenesis [76, 77]. During early brain development, microglia sculpt immature circuits by elimination of synapses, a process called synaptic pruning [78-80]. Additionally, microglia play a crucial role in regulating the CNS innate immune system by initiating and controlling inflammatory reactions [81]. It is believed that in the pathogenesis of several neurodevelopmental, neuropsychiatric and neurodegenerative disorders, immunological processes are compromised and it is hypothesized that microglia contribute to pathological phenotypes of different diseases significantly [82, 83].

Microglia are motile, surveying protective cells of the CNS [84]. Upon stimulation by stress signals within their environment by cytokine secretion of activated astrocytes or damage signaling by necrotic and apoptotic neurons, microglia become activated to induce neuroprotective repair mechanisms [85]. This beneficial activation state depends on a combination of different environmental stimuli, such as pro- and anti-inflammatory cytokines. Microglia and also macrophages are broadly classified into two broad sub phenotypes upon activation and polarization. Pro-inflammatory activated microglia are generally termed M1 microglia, while anti-inflammatory microglia are classified as M2 microglia [86]. However, within the last years, microglia and macrophage M1 and M2 classification is not considered as black and white anymore, but rather a gray scale of activation and phenotype, depending on the individual and specific conditions within the local environment [87, 88].

Neuroinflammation can lead to a deregulation of microglial activation resulting in overreactive microglia and the induction of neurotoxic functions, secretion of pro-inflammatory cytokines and unguided phagocytosis of synaptic structures [81]. Imbalance of microglial activation has been associated with a variety of neurodevelopment and neurodegenerative disorders. For example, mouse models of Alzheimer's Disease have identified aberrant synaptic depletion by inappropriately activated microglia [89], increased microglial phagocytosis [90], and deregulated levels of released cytokines [91] or reactive oxygen species [92].

Similar pathological phenotypes of activated microglia have been observed in other neurodegenerative disease models, like Parkinson's Disease or Frontotemporal Dementia [83] and in neurodevelopment disorders like schizophrenia and autism spectrum disorder (ASD) [93-95].

Post mortem studies revealed increased microglial density within the prefrontal cortex of ASD patients and GWAS identified deregulated expression of inflammatory genes [96, 97]. But if the microglial pro-inflammatory phenotype arises from changes in the neuronal environment or if the aberrant activation is the cause and origin for impaired synaptic and neuronal integrity remains to be determined to fully understand the role of microglia in the individual disease pathology.

1.2.2. The immunopsychiatric side of schizophrenia

For schizophrenia, post mortem tissue analysis and *in vivo* neuroimaging studies of diagnosed SZ patients reported repeatedly the loss of cortical volume and reduced synapse density [40, 98]. Concomitantly, increased microglial density was observed in brain from SZ patients [99]. It is suggested that the loss of synaptic structures and neuronal connectivity in the progression of schizophrenia is a consequence of the excessive elimination of synapses by imbalanced, reactive microglia [100-102].

During childhood and until late adolescence and early adulthood, synaptic connections and dendritic spines decline due to synapse elimination by microglia. This process is called synaptic pruning and is essential for precise synaptic connectivity and brain wiring [103, 104]. Usually during that time, early symptoms of schizophrenia appear and become clinically relevant. Excessive or reduced synaptic pruning by reactive microglia can lead to neurological disorders and has been proposed to be responsible for reduced synapse numbers observed in schizophrenia patients [105, 106].

Animal models of the postnatal retinogeniculate system first observed that microglia are able to actively phagocytose and degrade synaptic structures [107]. This process is mediated and controlled by two proteins of the complement system, C1q and C3, that are bound to the surface of pathogens, necrotic cells or other cellular artifacts to label them for degradation and engulfment by microglia. The complement system is a central and important pathway of the innate immune system for foreign pathogen recognition and subsequent elimination by responding immune cells [108]. Mouse models revealed that C1q and C3 were deposited on synaptic and neuronal structures as so called "Eat-me" signals for synaptic elimination by patrolling microglia [79, 107]. Likewise, inhibition of C1q or C3 reduced microglia-mediated

synapse loss and revealed aberrant synaptic elimination in an Alzheimer's Disease mouse model [89].

Large scale genomic association studies of SZ-patients identified within the MHC region, a single nucleotide polymorphism (SNP) associated with complement component C4 gene expression in SZ-patients that may affect synaptic pruning [109]. Droplet-based PCR identified increased haplotype *C4A* expression as a putative contribution to enhanced schizophrenia susceptibility. Mouse models further proved that the loss of C4 led to reduced synaptic pruning, indicating the important role of C4 for synaptic refinement [109]. C4 is, just as C1q or C3, a central component of the classical complement system [108].

However, microglial function varies greatly between mouse models and the complex human system and the urge for human *in vitro* model systems reflecting the development of the human brain including synaptic and neuronal network formation is immense.

Today, aberrant and increased synaptic pruning is suggested to be the cause for reduced synaptic density in post mortem tissue brain from patients with schizophrenia. First studies in human iPSC-based systems reported increased synaptic pruning by microglia derived from schizophrenia patients [71]. In these experiments, peripheral blood monocytes were differentiated and matured into microglia-like cells and co-cultured with synaptosomes extracted from iPSC-derived excitatory neurons. Increased synapse elimination and PSD-95 uptake was reported for microglia-like cells derived from patients with schizophrenia in comparison to healthy control microglia. Interestingly, this effect could be reversed by application of the anti-inflammatory drug minocycline in a dose-dependent manner. Additionally, neural cell lines with increased copy numbers of risk variant complement protein C4 induced increased synapse elimination by microglia-like cells [71].

RNA sequencing experiments with peripheral blood-monocyte-derived microglia-like cells from twenty SZ patients revealed differential expression of inflammatory genes such as CCR2, CD44, CD95 or HLA-DR compared to control cells [110]. Similarly, patient-derived microglia showed an increased baseline expression of pro-inflammatory cytokines like IL-1β, IL-6 or TNFα and an increased response to LPS. These initial findings in human *in vitro* models of neurodevelopment underline the putative inflammatory phenotype and deregulation of microglial functionality in the pathology of schizophrenia.

1.2.3. Treatment of pro-inflammatory, reactive microglia

Anti-inflammatory agents are of high interest for investigations and clinical trials to treat neuropsychiatric disorders by targeting neuroinflammatory processes by overreactive microglia [111]. The semisynthetic tetracycline minocycline can pass the blood-brain barrier and has been identified as a potential new agent to treat depression or schizophrenia. The precise mode of action of minocycline is not completely understood, but a neuroprotective impact in the adult brain is observable [112]. Adult patients administered with minocycline as adjunctive therapy to standard antipsychotic treatment experienced a decline in pro-inflammatory cytokine levels and an improvement of negative and cognitive symptoms [113].

Minocycline has been shown to decrease the inflammatory response of mice to viral infections, and to reduce maternal immune activation during pregnancy [114]. In iPSC-derived systems, minocycline treatment of microglia reduced synapse uptake in a dose-dependent matter [71]. However, minocycline was found to be detrimental to neuronal survival in rodent models when application occurred in early postnatal stages. Minocycline-mediated inactivation of microglia resulted in increased cell death of cortical neurons [115, 116] and also induced apoptosis in the hippocampus or nucleus accumbens [117]. Additionally, minocycline application impaired neurogenesis and gliogenesis [118]. It appears that minocycline can have detrimental effects on the developing brain, while the adult brain can benefit from inactivated microglia. Further studies will have to analyze how exactly minocycline treatment affects microglial activation, synaptic and neuronal plasticity and if minocycline application can improve neuroinflammatory pathologies in humans. For that, reproducible human test systems are needed to replace rodent models that are not capable of precisely reflecting all the complex human neuronal and immunological circuits.

1.3. Aim of this thesis

Aim of this thesis is to investigate the versatile and bidirectional communication between microglia and neurons and pathological phenotypes of this interplay in the etiology of schizophrenia. Neurodevelopmental aspects and inflammatory mechanisms will be analyzed using a human iPSC-based *in vitro* system that precisely reflects the patient's genetic background and the complex interplay between microglia and neurons in the early development of schizophrenia.

Human fibroblasts from a cohort of patients with schizophrenia and healthy controls will be reprogrammed into naïve iPSC and differentiated into excitatory, glutamatergic neurons and separately into functionally active microglia. Neurodevelopmental aspects of generated cells will be assessed by mean neurite outgrowth and determination of synaptic density as indicators for the capability to form mature neuronal networks with synaptic connections. Additionally, neuronal functionality will be characterized by pattern analysis of intracellular calcium signalling. Separately, inflammatory mechanisms by activated microglia will be evaluated.

Subsequent co-culture models of iPSC-derived microglia and glutamatergic neurons will shed light on synapse densities levels in neuronal cultures derived from SZ-patients after addition of microglia. Microglial activation states and synaptic elimination by untreated and pretreated microglia will be quantified by immunocytochemistry and confocal laser scan microscopy to understand how pathological microglia-neuron crosstalk contributes to the putative immunopsychiatric and neurodevelopmental phenotypes of schizophrenia.

2. Material and Methods

2.1. Material

2.1.1. Patient-derived iPS cell lines

Table 1. Generated iPS cell lines and respective unique cell line identifiers of fully characterized clones registered at the Human Pluripotent Stem Cell Registry, Charité, Berlin (www.hpscreg.eu). Four donors (italicized in grey) were excluded after karyotyping revealed minor and major chromosomal aberrations in several independent clones that were introduced during reprogramming. The study has been approved by the Ethics Committee of the University Hospital and Faculty of Medicine Tübingen, approval and project number: 311/2013BO1.

Donor	**Gender**	**Age at donation**	**Fibroblast label**	**iPSC label**	**Unique cell line identifier**
healthy individual number	female	28	HF1G	CTR1	NMIi001-A
healthy individual number	*female*	*57*	*HF2G*	*CTR2*	*chromosomal aberrations*
healthy individual number	*male*	*34*	*HF3G*	*CTR4*	*chromosomal aberrations*
healthy individual number	*male*	*53*	*HF5G*	*CTR3*	*chromosomal aberrations*
patient with schizophrenia	male	37	HF1P	SZ1	NMIi002-A; NMIi002-B
patient with schizophrenia	female	54	HF2P	SZ2	NMIi003-A
patient with schizophrenia	*male*	*46*	*HF3P*	*SZ3*	*chromosomal aberrations*
patient with schizophrenia	male	50	HF4P	SZ4	NMIi004-A
patient with schizophrenia	female	27	HF5P	SZ5	NMIi005-A; NMI005-B

2.1.2. Cell culture media

Table 2. Commercially available and ready-to-use media used during this study

Medium	**Manufacturer**	**Catalogue Number**
Brain Phys™ Neuronal Medium	STEMCELL Technologies	05790
Dulbecco's modified eagle's medium (DMEM/F12) + Glutamax	Gibco	21331-020
Fibroblast Growth Medium 2	PromoCell	C-23020
mTeSR1 Plus™	STEMCELL Technologies	05825
Neurobasal™ Medium	Thermo Fisher Scientific	21103049
Neurobasal Plus™ Medium	Thermo Fisher Scientific	A3582901
Opti-MEM™	Gibco	51985-026
RPMI-1640	Gibco	21875-034
STEMdiff™ Neural Induction Medium	STEMCELL Technologies	05839
STEMdiff™ Neural Progenitor Freezing Medium	STEMCELL Technologies	05838
STEMdiff™ Neural Progenitor Medium	STEMCELL Technologies	05833
TeSR™-E7™	STEMCELL Technologies	05910

Table 3. iPSC freezing medium

component	final concentration	stock concentration
Knockout serum replacement	90%	100%
DMSO	10%	100%

Table 4. Astrocyte cultivation medium

component	final concentration	stock concentration
DMEM + Glutamax	1x	1x
FBS	10%	100%
Sodium pyruvate	1%	100%
Pen/Strep	1%	100%

Table 5. Astrocyte freezing medium

component	final concentration	stock concentration
FBS	90%	100%
DMSO	10%	100%

Table 6. HEK293FT culture medium

component	final concentration	stock concentration
DMEM + Glutamax	1x	1x
FBS	10%	100%
G418	500 µg/ml	50 mg/ml
NEAA	1%	100%
Pen/Strep	1%	100%

Table 7. HEK293FT freezing medium

component	final concentration	stock concentration
HEK293FT culture medium	90%	100%
DMSO	10%	100%

Table 8. HEK293FT seeding medium used for lentivirus production

component	final concentration	stock concentration
DMEM + Glutamax	1x	1x
FBS	10%	100%
NEAA	1%	100%
Pen/Strep	1%	100%

Table 9. HEK293FT transfection medium used for lentivirus production

component	final concentration	stock concentration
OptiMEM	1x	1x
FBS	5%	100%
Pen/Strep	1%	100%

Table 10. **Basal medium** for monocyte, macrophage and microglia differentiation

component	final concentration	stock concentration
IMDM without phenol red	0.5x	1x
Ham's F12 Nutrient Mix	0.5x	1x
Poly Vinyl Alcohol (PVA)	10 µg/ml	10 mg/ml
Ascorbic acid 2 phosphate (AA2P)	64 µg/ml	64 mg/ml
Chemically defined lipid concentrate	0.1x	100x
ITS-X	2x	100x
αMTG (in IMDM)	0.0039%	1.3%
Glutamax	1x	100x
NEAA	1x	100x
Pen/Strep	1x	100x

Table 11. **Myeloid differentiation medium 1 (days 0+1)**: supplements for mesodermal induction that were added to the basal medium (Table 10)

component	final concentration	stock concentration
BMP4	50 ng/ml	50 µg/ml
Activin A	15 ng/ml	50 µg/ml
CHIR99021	1.5 µM	10 mM

Table 12. **Myeloid differentiation medium 2 (days 2-4)**: supplements for endothelial fate exclusion that were added to the basal medium (Table 10)

component	final concentration	stock concentration
VEGF	50 ng/ml	50 µg/ml
bFGF	50 ng/ml	50 µg/ml
SCF	50 ng/ml	50 µg/ml
SB431542	10 µM	10 mM

Table 13. **Myeloid differentiation medium 3 (days 5-9)**: supplements for hematopoietic induction that were added to the basal medium (Table 10)

component	final concentration	stock concentration
VEGF	50 ng/ml	50 µg/ml
bFGF	50 ng/ml	50 µg/ml
SCF	50 ng/ml	50 µg/ml
IL-6	50 ng/ml	50 µg/ml
TPO	50 ng/ml	50 µg/ml
IL-3	10 ng/ml	50 µg/ml

Table 14. **Myeloid differentiation medium 4 (from day 9) and microglia-neuron co-culture medium**: supplements for microglia maturation that were added to the basal medium (Table 10)

component	final concentration	stock concentration
IL-34	100 ng/ml	50 µg/ml
TGFβ	50 ng/ml	50 µg/ml
GM-CSF	25 ng/ml	50 µg/ml

Table 15. **Myeloid differentiation medium 5 (days 9-14)**: supplements for monocyte differentiation that were added to the basal medium (Table 10)

component	final concentration	stock concentration
IL-6	50 ng/ml	50 µg/ml

Table 16. **Myeloid differentiation medium 6 (days 15-18):** supplements for macrophage differentiation and maturation that were added to the basal medium (Table 10)

component	final concentration	stock concentration
M-CSF	80 ng/ml	100 µg/ml

Table 17. **Myeloid differentiation medium 6a (days 19-21):** supplements for macrophage polarization towards the **M1 phenotype** that were added to the basal medium (Table 10)

component	final concentration	stock concentration
LPS	100 ng/ml	100 µg/ml
IFNγ	100 ng/ml	100 µg/ml

Table 18. **Myeloid differentiation medium 6b (days 19-21):** supplements for macrophage polarization towards the **M2 phenotype** that were added to the basal medium (Table 10)

component	final concentration	stock concentration
IL-4	40 ng/ml	100 µg/ml
IL-10	20 ng/ml	100 µg/ml

Table 19. **Neuronal differentiation and maturation medium** for hNGN2-induction

component	final concentration	stock concentration
Neurobasal Plus™ Medium	1x	1x
B27 Plus	1x	50x
N2	1x	100x
Laminin	1 µg/ml	1 mg/ml
BDNF	20 ng/ml	50 µg/ml
GDNF	20 ng/ml	50 µg/ml
L-Ascorbic Acid	35 µg/ml	50 mg/ml
Pen/Strep	1x	100x

Table 20. **3N-Medium** for long term neuronal differentiation

component	final concentration	stock concentration
DMEM/F12	0.5x	1x
Neurobasal™ Medium	0.5x	1x
N2	1x	50x
B27	1x	100x
L-Glutamine	1 mM	100 mM
NEAA	1x	100x
β-Mercaptoethanol	100 µM	300 mM
Pen/Strep	1x	100x

Table 21. **BrainPhys™ neuronal medium** for calcium imaging

component	final concentration	stock concentration
BrainPhys™ Neuronal medium	1x	1x
Neurocult™ SM1 Supplement	2%	100x
N2	1%	100x
BDNF	20 ng/ml	50 µg/ml
GDNF	20 ng/ml	50 µg/ml
dibutyryl cAMP	500 µg/ml	50 mg/ml
L-Ascorbic Acid	35 µg/ml	50 mg/ml

2.1.3. Cellular seeding densities for differentiations

Table 22. Cell numbers and seeding densities of iPSC

Format	Surface area (cm^2)	Seeding density for cultivation	Seeding density for microglia differentiation	Seeding density for endodermal differentiation	Seeding density for mesodermal differentiation
6-well	9.5	3×10^5	2.5×10^5	-	3×10^5
12-well	3.8	1.2×10^5	1×10^5	-	1.5×10^5
24-well	1.9	6×10^4	-	4×10^5	7×10^4
48 well	0.95	3×10^4	-	2×10^5	3.5×10^4
96 well	0.32	1.1×10^4	-	7×10^4	1.2×10^4

Table 23. Cell numbers and seeding densities of NPCs

Format	Surface area (cm^2)	Seeding density for cultivation	Seeding density for neuronal differentiation (hNGN2)
6-well	9.5	7×10^4	3×10^5
12-well	3.8	2.8×10^4	1.2×10^5
24-well	1.9	-	6×10^4
48 well	0.95	-	3×10^4
96 well	0.32	-	1×10^4

Table 24. Cell numbers and seeding densities of murine astrocytes

Format	Surface area (cm^2)	Seeding density for cultivation	Seeding density for neuronal differentiation (hNGN2)
T75 flask	75	$1x10^6$	-
T25 flask	25	$5x10^5$	-
6-well	9.5	$3x10^5$	$3x10^5$
12-well	3.8	-	$1.2x10^5$
24-well	1.9	-	$6x10^4$
48 well	0.95	-	$3x10^4$
96 well	0.32	-	$1x10^4$

2.1.4. General material and equipment

Table 25. Consumables and general material used during this study

Consumables	**Manufacturer**
AggreWell™800	STEMCELL Technologies
37 µm Reversible Strainers	STEMCELL Technologies
24 well µ-plate	ibidi GmbH
96 well µclear plate	Greiner Bio-One
Cell Culture Flasks (25, 75, 175 cm²)	Corning
Cell Scraper	Costar
Cyro tubes	Greiner Bio-One
Eppendorf Tubes (1.5, 2 ml)	Eppendorf AG
Falcon Tubes (15, 50 ml)	Greiner Bio-One
Parafilm	Pechiney Plastic Packaging
Plastic pipets	Greiner Bio-One
Well plates (96, 48, 24, 12, 6 well)	Corning

Table 26. Instruments used during this study

Instrument	**Manufacturer**
Amaxa 4D Nucleofector® system	Lonza, Germany
C25 Incubator shaker	New Bunswick Scientific, USA
Cell Observer SD	Zeiss, Germany
Centrifuge	Andreas Hettich GmbH & Co KG, Germany
Centrifuges (5415R, 5424, 5810R, MiniSpin)	Eppendorf AG, Germany
CO_2 incubator CB 150	WTC Binder, Germany
DNA agarose gel fluorescence system	IntasScience Imaging Instruments GmbH, Germany
FACS Melody	BD Biosciences, USA
Gel electrophoresis chamber HU13	Thermo Fisher Scientific, USA
ImageXpress micro XL	Molecular Devices, USA
IncuCyte	Sartorius AG, Germany
Mr. Frosty™ Freezing Container	Thermo Fisher Scientific, USA
Nanodrop, Spectrophotometer ND-100	Thermo Fisher Scientific, USA
Neubauer Counting chamber	Marienfeld GmbH & Co. KG, Germany
Nucleocounter NC-200	Chemometech A/S, Denmark
PCR-Gerät Primus 96 plus MWG	Biotech AG, Germany
pH-Meter	Mettler Toledo, Germany
Pipetboy	INTEGRA Biosciences GmbH, Germany
Pipette (0.1-2.5 µl; 0.5-10 µl; 10-200 µl; 100-1000 µl)	Eppendorf AG, Germany
T3000 Thermocycler	Biometra GmbH, Germany
Tecan Plate reader	Tecan Trading AG, Switzerland
Thermomixer (comfort)	Eppendorf AG, Germany
Vortex Genie 2	Scientific Industries Inc., USA
Water bath	GFL®, Germany

2.1.5. Reagents

Table 27. Reagents used during this study

Reagents	Manufacturer	Catalogue Number
1 kb DNA marker	New England Biolabs	N3232
Agarose	Carl Roth GmbH & Co. KG	3810
Ampicillin	Carl Roth GmbH & Co. KG	HP62
B27 Plus™ supplement	Life Technologies	A3582801
B27 supplement	Life Technologies	17504044
Blocking Reagent BMB	Roche	11112589001
Cal520® AM	AAT Bioquest	21130
Cal590® AM	AAT Bioquest	20511
CHIR99021	Tocris	4423
CloneR	STEMCELL Technologies	05888
Clozapine	Sigma-Aldrich	C6305
CS&T RUO Beads	BD Biosciences	661414
Dimethylsulfoxid (DMSO)	Carl Roth GmbH & Co. KG	A994.1
dN-Primer Mix	Roche	11969920
dNTPs	New England Biolabs	N0447
Dorsomorphin dihydrochloride	bio-techne	3093
Doxycycline	Sigma-Aldrich	D9891
Dulbecco's phosphate buffered saline	Gibco	14190-094
Fetal Bovine Serum	Gibco	10270
Fluoresence Mounting Medium	Dako Deutschland	S302380
G418	Carl Roth GmbH & Co. KG	2039
Gentle Cell Dissociation Reagent	STEMCELL Technologies	07174
GlutaMAX	Invitrogen	35050-038
Gurr Buffer Tablets	Life Technologies	10582103
Haloperidol	Sigma-Aldrich	H1512
Hank’s Balanced Salt Solution	Gibco	14170112
Insulin	Sigma-Aldrich	I6634
Insulin-Transferrin-Selenium-Ethanolamine	Gibco	51500056
Knockout Serum Replacement	Thermo Fisher	10828010
Laminin	Sigma-Aldrich	L2020
L-Ascorbic Acid	Sigma-Aldrich	A2078
L-Glutamine	Gibco	25030-024
Matrigel ® hESC-qualified Matrix	Corning	354277
M-MulV Reverse Transcriptase	New England Biolabs	M0253L
N2 Supplement	Life Technologies	17502048
N^6,2′-O-Dibutyryladenosine 3′,5′-cyclic monophosphate sodium salt (cAMP)	Sigma-Aldrich	D0627
NeuroCult SM1 Neuronal Supplement	STEMCELL Technologies	05711
Non-essential amino acids	Gibco	11140-035
Olanzapine	Sigma-Aldrich	O1141
Paraformaldehyd (PFA)	Carl Roth GmbH & Co. KG	335
Penicillin/Strepomycin	Gibco	15140-122
pHrodo™ Red E. coli BioParticles™ Konjugat für Phagozytose	Invitrogen	P35361
Poly-L-Ornithine Solution	Sigma-Aldrich	P4957
Poly Vinyl Alcohol	Sigma-Aldrich	P8136
Puromycin	Gibco	111138-03
Ready-to-Use Packaging Plasmid Mix (pC-Pack2 Lentiviral Packaging Plasmid Mix)	Cellecta	CPCP-K2A

Recombinant Human Noggin FC Chimera	R&D Systems GmbH	719-NG-050
RQ1 RNase-free DNase	Promega	M6101
SB 431542	bio-techne	1614
STEMdiff™ Neural Rosette Selection Reagent	STEMCELL Technologies	05832
StemPro Accutase	Life Technologies	A1110501
Triton-X-100	Carl Roth GmbH & Co. KG	3051
TrypLE	Gibco	12604-054
Trypsin/EDTA 0.025%	Gibco	25300-054
Trypsin 2.5%	Gibco	15090046
UltraPure™ Ethidium Bromide	Thermo Fisher Scientific	15585011
Y-27632	STEMCELL Technologies	72304

2.1.6. Antibodies

Table 28. Unconjugated primary antibodies used for immunocytochemistry during this study

Antibody target	**Species**	**Manufacturer**	**Catalogue Number**	**Dilution**
Arginase 1 (24H4L3)	rabbit	Thermo Fisher Scientific	702730	1:100
β-III-tubulin (AA10)	mouse IgG2a	STEMCELL Technologies	60100	1:250
β-III-tubulin	rabbit	Synaptic Systems	302302	1:1000
Cardiac Troponin T	mouse IgG1	Thermo Fisher Scientific	MA5-12960	1:200
DISC1 (B-2)	mouse IgG	Santa Cruz Biotechnology	sc-365591	1:250
Gephyrin	mouse IgG1	Synaptic Systems	147021	1:100
GFAP	rabbit	Dako	Z0334	1:500
Hoechst 33258	-	Sigma-Aldrich	94403	1:1000
HLA-DR, DP, DQ (Tü39)	mouse IgG2	BioLegend	361702	1:200
iNOS (4E5)	mouse IgG1	Invitrogen	MA5-17139	1:200
Iba1	rabbit	Wako Pure Chemical Industries	019-19741	1:1000
MAP2	rabbit	Synaptic Systems	188 002	1:500
MAP2	chicken	Thermo Fisher Scientific	PA110005	1:5000
Nestin (JP63)	mouse IgG	Synaptic Systems	312011	1:1000
Oct-4A (C30A3)	rabbit	Cell Signaling	2840	1:400
Pax6 (AD2.35)	mouse	BioLegend	862001	1:200
Pax-6	rabbit	BioLegend	PRB-278P	1:300
Phalloidin CruzFluor 488	-	Santa Cruz Biotechnology	SC-363791	1:1000
PSD95	rabbit	Abcam	18258	1:1000
SOX1	rabbit	Abcam	ab22572	1:500
Sox17	rabbit	Cell Signaling	81778S	1:3200
SSEA4 (MC813)	mouse IgG3	Cell Signaling	4755	1:500
Synapsin1	mouse	Synaptic Systems	106011	1:1000
TRA-1-60	mouse IgM	Cell Signaling	4746	1:500
TRA-1-81	mouse IgM	Cell Signaling	4745	1:500
TMEM119	rabbit	Synaptic Systems	400 002	1:500
VGLUT1	mouse IgG1	Synaptic Systems	135511	1:300
ZO-1	mouse IgG1	Thermo Fisher Scientific	339100	1:150

Table 29. Conjugated primary antibodies used for flow cytometry during this study

Antibody target	Species	Manufacturer	Catalogue Number	Dilution
anti-human CD115 (CSF-1R) BV421	rat IgG1	BioLegend	347322	5 µl / test
anti-human CD11b FITC	mouse IgG1	Life Technologies	11-0118-42	2 µl / test
anti-human CD14 PE	mouse IgG2a	BioLegend	301806	5 µl / test
anti-human CD34 PerCP	mouse IgG1	BioLegend	343520	5 µl / test
anti-human CD45 VioBlue	human IgG1	Miltenyi Biotech	130-110-775	1:50
anti-human CD68 FITC	mouse IgG2b	Miltenyi Biotech	130-100-299	1:10
anti-human CD86 BV421	mouse IgG1	BioLegend	374211	5 µl / test
anti-human CD163 PerCP	mouse IgG1	BioLegend	333625	5 µl / test
anti-human CD206 PE-Cy7	mouse IgG1	BioLegend	321123	5 µl / test
anti-human SSEA-4 PE-Vio770	human IgG1	Miltenyi Biotech	130-105-081	1:20
anti-human TRA-1-60 PE	human IgG1	Miltenyi Biotech	130-100-350	1:20

Table 30. Secondary antibodies used during this study

Fluorescence dye	Species	Manufacturer	Catalogue Number	Dilution
AlexaFluor 488	goat anti-mouse IgG (H+L)	Dianova	115-545-003	1:500
AlexaFluor 488	goat anti-chicken (H+L)	Invitrogen	A-11039	1:500
Cy3-AffiniPure	goat anti-mouse IgG (H+L)	Dianova	115-165-146	1:500
Cy3-AffiniPure	goat anti-rabbit (H+L)	Jackson Immuno-Research Labs	111-165-144	1:500
Cy5-AffiniPure	goat anti-mouse IgG (H+L)	Dianova	115-175-146	1:500
Cy5-AffiniPure	goat anti-rabbit IgG (H+L)	Dianova	111-175-144	1:500
AlexaFluor 647	goat anti-rat IgG (H+L)	Life Technologies	A21247	1:500

2.1.7. Cytokines

Table 31. Cytokines used during this study

Cytokine	Manufacturer	Catalogue Number
Human Activin A	Miltenyi Biotech	130-115-008
Human BDNF	PeproTech GmbH	450-02
Human bFGF	biotechne	233-FB-025
Human BMP-4	PeproTech GmbH	120-05ET
Human GDNF	PeproTech GmbH	450-10
Human GM-CSF	Miltenyi Biotech	130-093-864
Human IFN-y	STEMCELL Technologies	78020
Human IL-10	BioLegend	571002
Human IL-3	PeproTech GmbH	200-03
Human IL-34	PeproTech GmbH	200-34
Human IL-4	STEMCELL Technologies	78045
Human IL-6	Miltenyi Biotech	130-095-352
Human M-CSF	Miltenyi Biotech	130-096-485
Human SCF	PeproTech GmbH	300-07
Human TGF-ß1	PeproTech GmbH	100-21
Human TPO	Miltenyi Biotech	130-095-747
Human VEGF	PeproTech GmbH	100-20

2.1.8. Plasmids

Table 32. Plasmids used during this study

Plasmid	Manufacturer	Catalogue Number	Reference
pCE-hOCT3/4	Addgene	41813	[12]
pCE-hSK	Addgene	41814	[12]
pCE-hUL	Addgene	41855	[12]
pCE-mp53DD	Addgene	41856	[12]
pCXB-EBNA1	Addgene	41857	[12]
pLV-TetO-hNGN2-eGFP-Puro	Addgene	79823	[119]
pLV-TetO-hNGN2-Puro	Addgene	79049	[119]
FUdeltaGW-rtTA	Addgene	19780	[120]
psPAX2	Addgene	12260	-
pMD2.G	Addgene	12259	-
pC-Pack2 Lentiviral Packaging Plasmid Mix	Cellecta	CPCP-K2A	-

2.1.9. Oligonucleotides

Table 33. Oligonucleotides used for RT-PCR during this study

Oligo name	Sequence	Amplicon (size in bp)
hOCT3/4-S1165 for	GAC AGG GGG AGG GGA GGA GCT AGG	Endogenous OCT3/4 (144)
hOCT3/4-AS1283 rev	CTT CCC TCC AAC CAG TTG CCC CAA AC	
hSOX2-S1430 for	GGG AAA TGG GAG GGG TGC AAA AGA GG	Endogenous SOX2 (151)
hSOX2-AS1555 rev	TTG CGT GAG TGT GGA TGG GAT TGG TG	
hKLF4-S1128 for	ACG ATC GTG GCC CCG GAA AAG GAC C	Endogenous KLF4 (397)
hKLF4-AS1826 rev	TGA TTG TAG TGC TTT CTG GCT GGG CTC C	
hMYC-S253 for	GCG TCC TGG GAA GGG AGA TCC GGA GC	Endogenous MYC (328)
hMYC-AS555 rev	TTG AGG GGC ATC GTC GCG GGA GGC TG	
ECAT4-macaca-968S for	CAG CCC CGA TTC TTC CAC CAG TCC C	Endogenous NANOG (391)
ECAT4-macaca-1334AS rev	CGG AAG ATT CCC AGT CGG GTT CAC C	
hDNMT3B-S2502 for	TGC TGC TCA CAG GGC CCG ATA CTT C	Endogenous DNMT3B (242)
hDNMT3B-S2716 rev	TCC TTT CGA GCT CAG TGC ACC ACA AAA C	
GAPDH for	TCA CCA TCT TCC AGG AGC G	Endogenous GAPDH (572)
GAPDH rev	CTG CTT CAC CAC CTT CTT GA	
pCE-hOCT3/4 for	GGG CAA CGT GCT GGT TAT TG	Exogenous OCT3/4-Plasmid (167)
pCE-hOCT3/4 rev	TAG CCA GGT CCG AGG ATC AA	
pCE-hSK for	CCC GTT GCA CGA CCA ATA AC	Exogenous Sox2 + Klf4-Plasmid (538)
pCE-hSK rev	GTC ATG GAC AGG AAG CCG AA	

2.1.10. Buffer and solutions

Table 34. Buffer and solutions used during this study

Buffer or solution	Components
4 % (w/v) PFA	40 g PFA dissolved in 1 L pre-warmed PBS, pH 7.4
20 % (v/v) Triton X-100	2 ml Triton X-100 diluted in 8 ml pre-wamed PBS
Staining solution for ICC (for blocking and permeabilization)	1 x BMB, 0.1 % Triton X-100 in PBS
FACS buffer	2 % FBS in PBS
Poly-L-ornithine coating	20 % PLO in PBS
Laminin coating	1 % laminin in DMEM/F12
Matrigel coating	1 % matrigel in cold DMEM/F12
TAE buffer for gel electrophoresis	2 M Tris + 250 mM sodium acetate + 50 mM EDTA, pH 7.8

2.1.11. Commercially available kits

Table 35. Commercially available kits used during this study

Reagent	Manufacturer	Catalogue Number
DNeasy Blood & Tissue Kit	Qiagen	69504
Human TNF-alpha DuoSet ELISA	R&D Systems	DY210
Lenti-X p24 Rapid Titer Kit	Takara Bio Inc.	632200
P2 Primary Cell 4D-Nucleofector X Kit L	Lonza Sales AG	V4XP-2024
P3 Primary Cell 4D-Nucleofector X Kit L	Lonza Sales AG	V4XP-3012
PSC Cardiomyocyte Differentitation Kit	Thermo Fisher Scientific	A2921201
QIAamp DNA Mini Kit	Qiagen	51304
QIAGEN Plasmid Midi Kit	Qiagen	12145
RNeasy Mini Kit	Qiagen	74104
STEMdiff™ Defintive Endoderm Kit	STEMCELL Technologies	05110

2.2. Methods for cell culture

2.2.1. Reprogramming of fibroblasts into iPSC

In cooperation with Prof. Dr. Andreas Fallgatter and Dr. Mark-Christian Eberle at the University Hospital in Tübingen, Department of Psychiatry, skin biopsies from voluntary donors were obtained between 2014 and 2016. Dr. Lena Grunwald prepared and cultivated fibroblasts derived from five patients that were diagnosed with schizophrenia and five healthy voluntary individuals. Reprogramming of fibroblasts into iPSCs was performed by retroviral transduction of five plasmids expressing Oct4, c-Myc, Sox2, KLF4 and CMV-EGFP by Lena-Marie Grunwald beforehand [48]. Within the following years, generated iPSC lost their typical morphology and their capability to form embryoid bodies. High quality iPSC are essential for the success of differentiation, therefore it was decided to reprogram again using a non-invasive, episomal method to reduce the risk of introducing genomic aberrations caused by retroviral reprogramming.

2.2.2. Cultivation and reprogramming of fibroblasts

Patient-derived fibroblasts gained through a skin biopsy at the arm were cultivated in Fibroblast Growth Medium 2 at 37°C and 5 % CO_2 until they reached 80-90 % confluence. For nucleofection, cells were washed with DPBS and dissociated using 0.25% trypsin/EDTA for 5 minutes at 37°C. Cells were spun down at 300 xg for 3 minutes and counted. $7x10^5$ fibroblasts were resuspended in 100 µl nucleofection solution of the P2 Primary Cell Kit and transferred to sterile nucleocuvettes. 2 µg each of the following five plasmids were added to the suspension: pCE-hOCT3/4, pCE-hSK, pCE-hUL, pCE-mp53DD and pCXB-EBNA1. Cuvettes were immediately transferred to the Nucleofector 4D system and electroporated using the program EN-150. Cells within the cuvettes were incubated for 10 minutes at 37°C and subsequently, $5x10^4$ fibroblasts per well were seeded on matrigel-coated 6-well plates in 2 ml Fibroblast Growth Medium 2 per well for 48 hours without medium change. Two days after electroporation, medium was replaced by TeSR-E7 reprogramming medium with daily medium changes for the next weeks.

2.2.3. Expansion of single iPSC colonies

First iPSC-like colonies appeared three weeks after electroporation and were manually picked once they reached at least 500 µm diameter. One iPSC colony was transferred to one well of a matrigel-coated 12-well plate and cultured in mTeSR Plus medium and 10 µM Y-27632 dihydrochloride (ROCK inhibitor) for the first 24 hours with subsequent daily medium changes. Per donor several clones were picked and expanded for characterization.

2.2.4. Passaging of whole colonies or single cell seeding

Once iPSC colonies grew too big, too close to other colonies or started to differentiate, iPSCs were propagated using either enzymatic or enzyme-free passaging methods. Gentle Cell Dissociation Reagent (GCDR) was used during low iPSC passage numbers. Here, whole colonies are lifted up from the matrigel-coated well bottom by gentle scraping using pipette tips and can be transferred as a small colony to a new well. Cells were washed with DPBS, and GCDR was added to the wells. After a few minutes of incubation at room temperature (RT), the edges of the colonies started to lift up from the well. GCDR was carefully removed and medium was added to the cells. Cells were scraped gently from the plate using cell scraper or glass pipettes and whole colonies were transferred to a new matrigel-coated well plate.

For seeding cells in advance for differentiations or passaging of colonies that were higher in passage number, the enzyme accutase was used for seeding single cells that are evenly distributed within the well. Therefore, iPSCs were washed with DPBS and incubated with accutase for a few minutes at 37°C. DMEM/F12 was added to stop the enzymatic reaction and the single cell suspension was centrifuged for 3 minutes at 300 xg. Cells were counted and seeded in proper densities in freshly matrigel-coated well plates.

2.2.5. Matrigel coating

Maintenance of iPSC requires a proper substrate to ensure consistent growth and preservation of an undifferentiated, pluripotent state. For that, culture well plates were coated with matrigel before expanding, seeding or thawing. Matrigel was diluted according to the manufacturer's certificate of analysis, here 1:100 in DMEM/F12. Thawing of matrigel and dilution in DMEM/F12 was always prepared on ice to prevent gelling. 1 ml of the diluted matrigel was added to one well of a 6-well plate and incubated for at least 30 minutes at 37°C. For storage, matrigel-coated well plates could be stored at 4°C for one week and were incubated for 30 minutes at 37°C before usage.

2.2.6. Thawing and freezing of iPSC

For freezing iPSC, cells were detached using enzyme-free or enzymatic agents, washed with DPBS and finally resuspended in iPSC freezing medium, consisting of 90 % knockout serum replacement and 10 % DMSO. Cells were stored for 48 hours at -20°C and were then transferred to liquid nitrogen or -150°C tanks.

For thawing iPSC, well plates were always freshly coated with matrigel to increase viability of thawed cells. iPSC cryo stabilates were thawed quickly in a 37°C water bath and the cell suspension was transferred to pre-warmed 10 ml DMEM/F12. Cells were centrifuged at 300 xg for 3 minutes and resuspended in mTeSR Plus medium supplemented with 10 µM ROCK inhibitor. 24 hours later, medium was completely changed to remove residual DMSO from the culture.

2.2.7. STR analysis

Short tandem repeat (STR) analyses are a commonly used molecular biological method for paternity tests and the detection of STRs. Genomic DNA was extracted from donor-derived fibroblast and generates iPSC cultures using the QIAamp DNA Mini Kit to compare allele repeats at different loci within the genome. By proving 100 % match between fibroblast and iPSC alleles, a mix up of samples could be excluded and the identities of generated iPSC clones were proven. STR analysis targeting 20 loci within the genome was performed under the lead of Prof. Dr. Ulrike A. Mau-Holzmann at the Institute of Medical Genetics and Applied Genomics, University Hospital of Tübingen.

2.2.8. Genomic integrity

Reprogramming of somatic cells, cultivation and expansion of iPSC increases the risk of developing chromosomal aberrations and the loss of genomic integrity. Techniques to verify chromosomal validity are G-Banding, digital karyotyping of highly sensitive methods like the CGH array. Genomic integrity was proven by Thermo Fisher Scientific, USA, by applying cells to a digital visualization of chromosome aberrations within the KaryoStat assay. Chromosomal gains of > 2 Mb and chromosomal losses of > 1 Mb can be detected within the genome covering all 36.000 RefSeq genes (Source: Thermo Fisher Scientific).

For analysis, cell pellets of at least $2x10^6$ iPSC per clone were washed with DPBS and frozen at -80°C and shipped to the United States for further processing. Thermo Fisher Scientific in Carlsbad, California, USA continued to prepare genomic DNA and prepared 250 ng gDNA for insertion into the GeneChip® for KaryoStat™ analysis to detect copy number variants and single nucleotide polymorphisms across the whole genome.

2.2.9. Endodermal differentiation

For endodermal differentiation, iPSCs were dissociated using accutase and $7x10^4$ cells were seeded into matrigel-coated 96-well plates in mTeSR Plus medium supplemented with 10 µM ROCK inhibitor. Endodermal differentiation was induced by scheduled addition of three media with different composition driving endodermal fate using the STEMdiff™ Definitive Endoderm Kit according to the manufacturer's instructions. After fi2.ve days *in vitro*, cells were fixed and stained against Sox17, a transcription factor expressed in cells of the definitive endoderm.

2.2.10. Mesodermal differentiation

For mesodermal differentiation, iPSCs were dissociated using accutase and $7x10^4$ cells were seeded into black matrigel-coated 24-well ibidi plates in mTeSR Plus medium supplemented with 10 µM ROCK inhibitor. The PSC Cardiomyocyte Differentiation Kit was used according to the manufacturer's instructions upon confluence of 80-90 %. After 10 to 14 days *in vitro*, contracting cardiomyocytes were observed and cells were fixed and stained against cardiac troponin T (cTNT) for further validation.

2.2.11. Ectodermal differentiation

Generation of iPSC-derived neurons required a two-step protocol with a first pre-differentiation of high-quality iPSC to neuronal progenitor cells (NPCs) and subsequent maturation of NPC to neurons by lentiviral overexpression of human Neurogenin 2 (hNGN2) [119].

2.2.11.1. PLO/Lam Coating

NPC and maturing neurons require a two-step poly-L-ornithine (PLO) and laminin coating for successful cultivation and efficient differentiation. NPCs and neurons were seeded at all times on pre-coated well plates. Plates were first coated with 20 % PLO diluted in PBS and incubated for at least two hours at RT. After once washing with DPBS and twice with DMEM/F12, wells were coated with 1 % laminin in DMEM/F12 at 37°C and 5 % CO_2 overnight. Coated plates were sealed with parafilm and could be stored at 4°C for a maximum of two weeks. Before seeding, the laminin coating was removed and medium was added, no washing steps were required.

2.2.11.2. Neuronal progenitor cell (NPC) generation

High-quality iPSC with a low percentage of differentiation (< 3 %) were dissociated to a single cell suspension by using accutase for 5 minutes at 37°C, centrifuged at 300 xg for 3 minutes at RT and counted. $2\text{-}3x10^6$ iPSC were required for NPC generation and were seeded into one

well of a AggreWell™ 800 plate that was pre-treated with 1 ml Anti-Adherence Rinsing Solution for at least five minutes at RT and subsequently washed with PBS twice. iPSCs were seeded in a total volume of 2 ml Neural Induction Medium. For proper embryoid body (EB) generation, the plate was centrifuged for one minute at 100 xg and RT and incubated at 37°C and 5 % CO_2 for one week with daily medium changes.

EBs were harvested seven days by separating them from single cells by filtration through a 37 µm reversible strainer. Single cells that were not incorporated into one of the EBs, passed the mesh and could be discarded. All EBs from one well were seeded into one PLO/Lam-coated well of 6-well plate and were cultivated in Neural Induction Medium with daily medium changes. After one week neural rosettes could be selected by removing all medium from the well, washing once with DMEM/F12 and adding 2 ml Neural Rosette Selection per well of a 6-well plate for a duration of 90 minutes at 37°C. Afterwards, dissociated neural rosettes could gently be washed from the plate by adding DMEM/F12 and centrifuged at 300 xg for 3 minutes. Neural progenitor cells (NPCs) were plated on PLO/Lam-coated plates and cultivated in Neural Progenitor Medium (NPC medium) with medium changes every other day for up to ten passages.

All generated NPC were routinely tested for expression of classical neuronal precursor markers like Pax6, Nestin, Sox1 or ZO-1 by immunocytochemistry.

Early passages of NPCs could be frozen and thawed as required. For freezing, confluent cells were dissociated using accutase, centrifuged and resuspended in Neural Progenitor Freezing Medium with at least $2x10^6$ cells per cryoconservation tube. For thawing, cryo tubes were quickly warmed in a 37°C waterbath, transferred to 5 ml DMEM/F12 and centrifuged at 300 xg for 3 minutes. Cells were resuspended in NPC medium and seeded into PLO/Lam-coated well plates.

2.2.11.3. Neuronal differentiation through lentiviral doxycycline-dependent overexpression of human Neurogenin 2

NPCs were dissociated using accutase and seeded at a density of $3x10^4$ cells per cm^2 (Table 23) in NPC medium. 24 hours after seeding, cells were transduced with two viral constructs that induce the overexpression of human Neurogenin 2 (hNGN2) and accelerate neuronal differentiation, network formation and maturation (Figure 1). 24 hours after infection, medium was changed to NPC medium + 10 µg/ml doxycycline to induce tetracycline-dependent expression of reverse tetracycline transactivator (rtTA) and hNGN2 [119, 121, 122]. 24 hours later, medium was changed to NPC medium supplemented with 10 µg/ml doxycycline and 2 µg/ml puromycine to select for only transduced cells. Cells were selected for 48 hours. Minimal toxic concentration of puromycine was tested by different doses in a kill curve experiment

beforehand. After selection, medium was completely changed to neuronal differentiation medium (NeuM) supplemented with 10 µg/ml doxycycline. At this point, murine astrocytes were co-seeded for improved neuronal viability and network formation. Astrocytes were detached using 0.25 % Trypsin/EDTA, centrifuged at 300 xg for 3 minutes and counted. $3x10^4$ Astrocytes were added per cm^2 (Table 24) and 50 % medium was changed every other day until cells were assayed or fixed after at least 14 days *in vitro*.

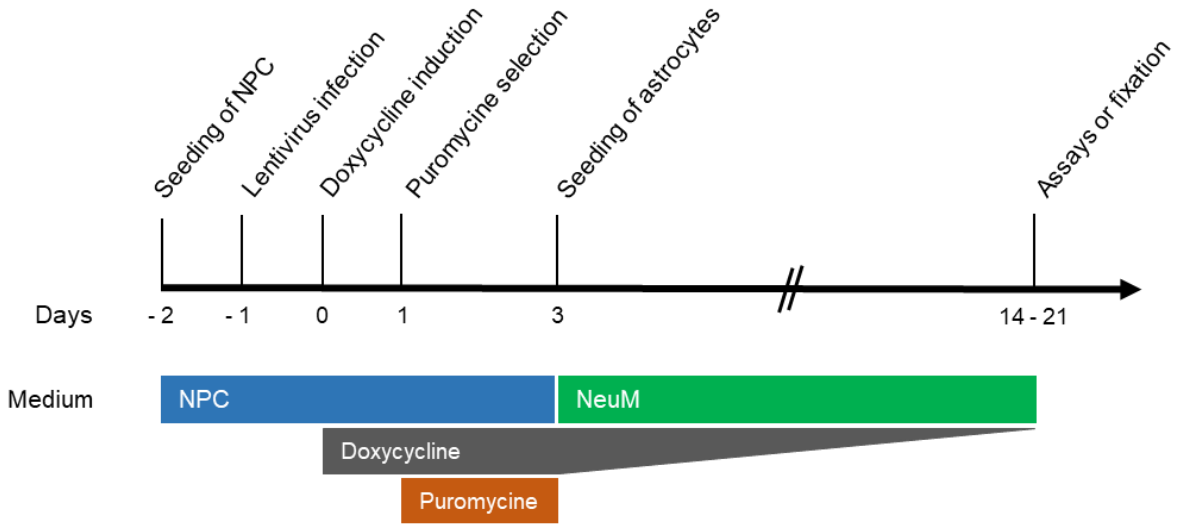

Figure 1. Differentiation and time scheme of hNGN2 induction for neuronal patterning. Seeding, infection, induction of expression by doxycycline administration and puromycine selection was performed in NPC medium. Upon addition of murine astrocytes, medium was switched to neuronal maturation medium (NeuM) with 10 µg/ml doxycycline, followed by 50 % medium changes every other day. First assays were performed after 14 days in culture and cultures could be cultivated up to four weeks before loss of viability.

2.2.12. Calcium imaging

For imaging of intracellular calcium flow, NPCs originating from iPSC that were reprogrammed using the invasive, retroviral method by Dr. Lena-Marie Grunwald. Low passage NPCs were dissociated using accutase, centrifuged at 300 xg for 3 minutes and counted. $3x10^4$ NPC per cm^2 were seeded into PLO/Lam-coated wells of black 24-well plates suitable for immunocytochemical analysis. Differentiation was initiated by changing medium to 3N-Medium (Table 20) the following day. Neuronal differentiation and maturation was continued for six weeks with 75 % medium changes every other day. After 6 weeks in culture, medium was replaced by BrainPhys™ medium (Table 21) to enhance functionality, viability and activity of mature neuronal networks for two more weeks with 75 % medium changes every other day until calcium imaging was performed.

After 8 weeks in culture, neuronal cultures were stained for 30 minutes at 37°C with 1 µM Cal520 staining solution dissolved in BrainPhys™ culture medium to visualize intracellular calcium fluxes. Afterwards, the Cal520 staining solution was replaced by pre-warmed BrainPhys™ culture medium and cells were let sit at 37°C for additional 20 minutes. The incubation chamber of the confocal laser scan microscopy Cell Observer SD was prepared to standard incubator conditions of 37°C and 5% CO_2. Calcium waves were imaged at 20x resolution for 10 minutes with a frame rate of 20 frames per second and with low 488 nm laser settings to minimize laser-induced bleaching of the calcium sensor.

Movies of calcium imaging were analyzed using open source software Fiji. Soma of spontaneous active neurons were defined as regions of interests (ROIs) to determine changes of fluorescence intensity within ROIs representing calcium level changes within single cells. Visualization and further processing of fluorescence intensities was performed manually using Origin software and the calcium signaling script written by Thoralf Herrmann (NMI). Analyzed parameters were the peak frequency over 10 minutes, ΔF/F0 describing the ratio of maximum intensity to baseline intensity, area under the curve and full width half maximum. Three independent experiments and differentiations were performed for each donor. Kruskal-Wallis test and Dunn's post-hoc test were used for quantification.

2.2.13. Neurite outgrowth

For neurite outgrowth assays, NPCs originating from iPSC that were reprogrammed using the invasive, retroviral method by Dr. Lena-Marie Grunwald were seeded into PLO/Lam-coated black 96-well plates and differentiated for four days in 3N medium. Therefore, NPCs were dissociated, centrifuged for 3 minutes at 300 xg and seeded at a density of $3x10^3$ NPC in one well of a 96-well plate in 3N medium (Table 20). 24 hours after seeding, medium was changed completely and NPCs were treated with 1 µM clozapine, 1 µM haloperidol or 1 µM olanzapine. DMSO served as solvent control. 72 hours later, plate was fixed using 4 % PFA and cells were stained with primary antibodies against β-III-tubulin and Hoechst for detection of nuclei.

Images were acquired using the high content microscope ImageXpress micro XL and analyzed using the automated MetaXpress high-content image acquisition and analysis software with at least 9 images taken per well and condition. Nuclei were identified by Hoechst staining and outgrowing neurites were processed and quantified using the Neurite Outgrowth tool (Molecular Devices). Viable nuclei were identified with a size ranging from 8 to 16 µm in width and a minimum gray level intensity above local background of 2500 gray levels. Cell soma were defined as a minimum intensity of 2000 gray levels above local background and a minimum size of 150 µm². Neurite outgrowths of identified cell bodies were detected with a minimum fluorescence of 2500 gray levels above local background and a maximal width of

8 µm and a minimal cell outgrowth of 10 µm. Neurites shorter than 10 µm were excluded from the analysis. Neurite length was determined automatically, for analysis of neurons with neurites, the number of neurons with neurites was divided by the number of all neurons. Neurite outgrowth of treated NPCs were normalized to each individual untreated control and the fold change between different treatments was calculated.

At least three independent experiments and differentiations were performed per clone and treatment with each three technical replicates. Drug response was performed with seven clones from three healthy controls (CTR1-3) and five clones from three patients with schizophrenia (SZ1-3). Kruskal-Wallis test and Dunn's post-hoc test were used for statistics. Imaging and quantification parameters were constant across all independent experiments.

2.2.14. Microglia and macrophage differentiation

The protocol for differentiation of iPSC towards monocytes, macrophages and microglia shared the first steps of myeloid induction, but differed upon maturation [123]. Different cytokine and growth factor combinations induce first the mesodermal germ layer, followed by the generation of hematopoietic cells and subsequent maturation into monocytes, macrophages or microglia.

Confluent and high quality iPSC were dissociated using accutase, centrifuged at 300 xg for 3 minutes and counted. For myeloid differentiation, iPSCs were seeded at a density of $5x10^4$ cells per cm^2 (day -2). iPSCs should have adhered in tiny colonies (10-20 cells per colony) and spread across the whole plate. Wells with colonies that already had grown too big or too close were not suitable for differentiation and were discarded. Two days after seeding (day 0), medium was replaced by the basal medium that was used for all further differentiation steps (Table 10) supplemented with BMP4, Activin A and CHIR99021 for mesoderm induction (Table 11). At day 2, medium supplements were changed to SCF, VEGF, bFGF and SB 431542 (Table 12) to suppress self-renewal in favor of stem cell differentiation (Smad inhibition). At day 5, supplements were replaced by basal medium and the addition of IL-3, IL-6, TPO, bFGF, SCF and VEGF (Table 13), a variety of cytokines inducing hematopoietic patterning. At day 7, medium was refreshed. At day 9, differentiated wells should have grown to full confluence with a few hematopoietic stem cells emerging into the supernatant. The supernatant with all including cells was extracted and saved separately in a 15 ml tube. Remaining adherent cells were dissociated by adding accutase and incubation at 37°C for a few minutes. Dissociated cells were fused with the respective supernatant and centrifuged at 300 xg for 3 minutes. Ultra-low attachment plates were prepared that were coated with Anti-Adherence Rinsing Solution for at least 5 minutes and afterwards rinsed twice with PBS. Cells were resuspended in microglia medium containing IL-34, TGFβ-1 and GM-CSF (Table 14) or monocyte medium

containing IL-6 (Table 15). Microglia differentiation proceeded for another seven days with medium changes every other day. At day 16, microglia could be seeded for microglia-neuron co-culture experiments or were stimulated by adding 100 ng/ml LPS and 100 ng/ml IFN-γ or 10 µM minocycline to assess microglial functionality.

For monocyte and macrophage differentiation, cells were kept as suspension cultures and fresh medium was supplemented at day 12. At day 15, pre-mature macrophages were seeded onto plates that were coated with 1 % matrigel for at least 30 minutes at 37°C and were seeded at a density of $1x10^5$ cells per cm². Medium was switched to macrophage differentiation medium containing high-dose M-CSF (Table 16). Differentiated macrophages adhered within 72 hours and could be polarized towards the pro-inflammatory M1 phenotype by medium change and addition of LPS and IFNγ (Table 17) or towards the anti-inflammatory M2 phenotype by adding IL-4 and IL-10 for 24 hours (Table 18). Finally, macrophages were fixed for immunocytochemistry or prepared for flow cytometry.

2.2.15. Co-culture setup

Neuronal and microglial differentiation started separately from each other. iPSC or NPC were dissociated with accutase and seeded the same day for microglia differentiation as described in 2.2.14. or for neuronal differentiation as described in 2.2.11.3., respectively. At day 16 of neuronal and microglial differentiation, neuronal medium was completely changed to microglia medium, which proved to be the medium with the highest viability outcome for the co-culture system. Microglia were lifted from the ultra-low attachment plates, washed with DPBS, centrifuged at 300 xg for 3 minutes and finally resuspended in microglia medium (Table 14). $5x10^4$ microglia per cm² were co-seeded to $3x10^4$ initially seeded NPCs per cm² in microglia medium (example for one well of a 96 well plate: $1x10^4$ NPC were initially seeded and $1.5x10^4$ microglia were co-seeded at day 16 in a total volume of 200 µl microglia medium). The co-culture plate was transferred to the incubator and left for 72 hours at 37°C and 5 % CO_2.

For some assays, it was useful and necessary to seed microglia only into wells serving as controls without neurons. Therefore, well plates were coated with matrigel for at least 30 minutes beforehand and microglia were seeded at a density of $1x10^5$ cells per cm² in microglia medium. Microglia adhered within 72 hours. Finally, the supernatant of all well plates was saved for cytokine analysis and cells were fixed for immunocytochemistry.

2.2.16. Synaptic pruning and microglial activation

Co-Culture plates and microglia-only plates were fixed using 4 % PFA in PBS after 72 hours of incubation at day 19 of differentiation (as described in 2.2.15). Fixed cells were stained with primary antibodies targeting Synapsin1 (Syn1) for detection of pre-synaptic structures, the allograft inflammatory factor 1 also known as ionized calcium-binding adapter molecule 1 (Iba1) as a general marker for microglia, and the human leukocyte antigen DR (HLA-DR) as a marker for microglial activation. To stain whole neuronal networks, primary antibodies against microtubule-associated protein 2 (MAP2) or class III β-tubulin (β-III-tub) were used.

To determine microglial pruning of synaptic structures, first three-dimensional Z-stacks of neuronal networks were acquired at the confocal laser scan microscopy Cell Observer SD with a 63 x plan-apochromatic oil immersion objective. Per each co-culture condition at least ten Z-stacks with comparable cellular density were taken. Within each experiment the setting for acquisition (such as exposure time, laser intensity and gain) were unchanged for all conditions.

Z-stacks of neuronal mono-cultures or neuron-microglia co-cultures were further processed and quantified using Imaris Bitplane Software. Therefore, a surface was generated covering all MAP2 signal present in the whole stack. Afterwards, the surface was masked using the Syn1 signal creating a new channel for Syn1. Spot detection was applied for the new Syn1 channel and all Syn1 spots over a set threshold were counted as synaptic structures and divided by the MAP2 area. The threshold for Syn1 spot detection was never changed during analysis of one replicate. At least five independent co-culture experiments were performed. Kruskal-Wallis test and Dunn's post-hoc test with multiple comparisons or ordinary two-way ANOVAs with Dunnett's post-hoc test were used for group comparisons. Two-tailed Mann-Whitney U tests were used for pairwise comparisons.

Microglial synaptic pruning was further quantified by determination of the mean fluorescence intensity (MFI) of Syn1 within Iba1 positive microglia. Therefore, Z-stacks of microglia were acquired as described above and further processed using Imaris Bitplane. A first surface was generated using the Iba1 signal to cover whole microglial cells and was subsequently masked with the signal for Syn1. Spots within microglia were assessed and the MFI of Syn1 was determined. At least three independent experiments were performed for every donor combination. Kruskal-Wallis test and Dunn's post-hoc test with multiple comparisons were used for group comparisons. Two-tailed Mann-Whitney U tests were applied for pairwise comparisons.

Microglial activation was assessed by quantification of the MFI of the pro-inflammatory activation marker HLA-DR and Iba1 as readout. For analysis, the same method as described above was used to quantify the MFI of HLA-DR and Iba1 within microglia after mono- and co-

culture. For HLA-DR expression, three independent co-culture experiments and three independent mono-culture experiments with LPS and minocycline treatment were performed. For Iba1 expression, at least five independent co-culture experiments for each donor combination and three mono-culture experiments with LPS and minocycline treatment were performed. Kruskal-Wallis test and Dunn's post-hoc test with multiple comparisons were used for statistics.

2.2.17. Lentivirus Production

The specialized HEK293FT cell line is a fast growing, genetically modified and immortalized cell line ideally suited for the production of high lentiviral titers [124]. HEK293FT are easy to handle and to transfect and were used to produce lentiviral suspension of the hNGN2-expressing plasmid and the reverse transactivator rtTA plasmid for neuronal differentiation.

2.2.17.1. Cultivation of HEK293FT

HEK293FT stably express the neomycin resistance gene and were cultured under presence of 500 µg/ml G418 for selection. HEK293FT were cultured at 37°C and 8 % CO_2 in HEK culture medium (Table 6) and passaged using 0.25 % Trypsin/EDTA once or twice a week.

2.2.17.2. Transfection of HEK293FT

For lentivirus production, HEK293FT medium was changed to HEK293FT seeding medium (Table 8) without G418. When cells reached 90 % confluence, cells were dissociated, centrifuged and counted. Per T175 flask for virus production, $5x10^5$ HEK293FT cells were seeded on Thursday in 30 ml seeding medium with no medium change on Friday. The following Monday, HEK293FT cells should have reached a confluence of 80-90 % or otherwise, the culture medium was refreshed and cells were let grown for additional 24 hours. For transfection, 27 µg pC-Pack2 Lentiviral Packaging Mix for third-generation lentiviruses (hNGN2) or 18 µg each of the two packaging plasmids pxPAX2 and pMD2.G for second-generation lentiviruses (rtTA) were diluted in 4.5 ml Opti-MEM. In a separate tube, 108 µl of the transfection reagent Lipofectamine 2000 Reagent were diluted in 4.5 ml Opti-MEM. Both tubes, the plasmid mix and the Lipofectamine mix, were incubated separately for 5 minutes at RT. Afterwards, the plasmid mix was carefully transferred to the Lipofectamine mix without any mixing and let sit for 20 minutes at RT. In the meantime, the medium was replaced by 21 ml transfection medium (Table 9). After 20 minutes, the whole Lipofectamine-plasmid mix was transferred to one T175 flask, the flask was carefully shaken and incubated at 37°C and 5 % CO_2.

24 hours later, a complete medium change with 30 ml fresh transfection medium was performed under biosafety level 2 conditions. 48 hours and 72 hours after transfection,

supernatants containing released lentiviruses were carefully taken and stored at -80°C until ultracentrifugation. Medium was refreshed on day 2. On day 3, after taking the 72-hours supernatant, HEK293FT cells were discarded.

2.2.17.3. Virus Preparation

Frozen supernatants containing lentiviral suspension were thawed in a 37°C water bath. Lentiviral suspensions were sterile filtered and transferred into buckets suitable for ultracentrifugation. Lentiviral suspensions were centrifuged at 19,600 rpm and 4°C for 80 minutes. The supernatant was poured off slowly and carefully. Pellets were air dried for a few minutes and remaining liquid was removed with sterilized soft tissue papers. Finally, 100 µl PBS + 1 % BSA were added per tube with no pipetting or resuspending. Tubes were sealed with parafilm and let rest overnight at 4°C. The next day, pellets were resuspended by pipetting several times and the lentiviral suspensions were aliquoted for storage at -80°C.

2.2.17.4. Lentivirus titer determination

Titer determination was performed using the Lenti-X p24 Rapid Titer Kit according to the manufacturer's instructions. Lentiviral suspensions were diluted 10-fold and 100-fold and quantified against a p24 standard curve. Yields ranged from $5x10^{10}$ to $5x10^{11}$ particles/ml. For infection, approximately 10 ng/ml or $2x10^{8}$ particles/ml per lentivirus were used in NPC or iPSC medium for 24 hours.

2.2.18. Astrocyte preparation from newborn mice

Astrocytes participate in a variety of developmental and biological mechanisms that contribute to functional neuronal network formation, maturation and CNS repair [125, 126]. To improve neuronal differentiation efficacy *in vitro*, pregnant mice originating from the wildtype mouse strain RjOrl:SWISS were used for astrocyte preparation (Janvier Labs) [127]. One day old newborn pups were decapitated in a sterile hood using sterile scissors. The scalp was carefully cut to reveal the skull along the visible midline from the neck to the nose and additionally cut anterior of the olfactory bulbs and inferior of the cerebellum to allow full access to the brain. The brain was removed carefully with a small spoon and transferred to Hank's Balanced Salt Solution (HBSS) and immediately stored on ice. The olfactory bulbs and the cerebellum were removed under a stereomicroscope and the hemispheres were separated using a one-way scalpel. The meninges were removed from the cortex by gentle pulling with fine forceps and the cortex was cut into small pieces and stored in a tube filled with cold astrocyte cultivation medium (Table 4) until further processing.

Once all prepared cortices sunk to the bottom of the tube, the medium was carefully removed and replaced by 5 ml of trypsin/EDTA and incubated for 20 minutes in a 37°C water bath with occasional inverting every 5 minutes. Finally, cortices were let to sink to the bottom of the tube and the trypsin solution was carefully discarded and replaced by 5 ml of astrocyte culture medium. Using a 5 ml pipette, the cell suspension was rigorously pipetted up and down 35 to 40 times to loosen up dense cell clumps. The suspension was then transferred to a T75 cell culture flask. Cortices from five pups were seeded into one T75. Confluence was reached within one week of cultivation in astrocyte cultivation medium at 37°C and 8% CO_2 with full medium changes every other day.

Remaining neuronal cells, microglia and oligodendrocytes were observed to detach within the first week of cultivation or were lost during the first passaging of astrocytes. Astrocytes were seeded into neuronal cultures at passage number two to four. Astrocytes older than passage five were discarded due to loss of viability and functionality. $3x10^6$ astrocytes in early passage numbers could be frozen in astrocyte freezing medium (Table 5) and thawed into T75 flasks with high viability.

2.3. Methods for molecular biology

2.3.1. RNA Isolation, cDNA Synthesis and RT-PCR

Expression of pluripotency markers was proven by reverse transcriptase polymerase chain reaction (RT-PCR). About $1x10^5$ reprogrammed and expanded iPSCs were washed and lysed for RNA extraction using the RNeasy Mini Kit according to the manufacturer's instructions. Afterwards, remaining DNA was digested using the RQ1 Kit according to the manufacturer's instructions. The RNA amount was measured and prepared RNA could be stored at -20°C. For cDNA synthesis, 500 ng RNA were mixed with 45 ng dN_6-Primer (0,3 µl of 150 µg/ml stock) and 0,5 µl of 25 mM dNTPs and diluted to a total volume of 10 µl in ddH_2O. The mixture was incubated at 70°C for 10 minutes. Afterwards, 2 µl reverse transcriptase buffer and 1 µl M-MuLV reverse transcriptase was added and incubated at 42°C for 70 minutes. To inactivate the enzyme, the solution was heated up to 80°C for 5 minutes and the cDNA amount was measured. cDNA could be stored at -20°C until further use.

For PCR targeting the mRNA-based expression of several pluripotent stem cell markers (e.g. SOX2, NANOG or OCT3/4), the polymerase Platinum II Taq was used according to the following scheme (Table 36) and amplification of cDNA was performed using a thermo cycler (Table 37).

Table 36. Components used for RT-PCR calculated for one reaction.

Component	Amount for one 25 µl reaction
Platinum II Taq Polymerase	0.19 µl
Platinum GC Enhancer	4.8 µl
5x Platinum II PCR Buffer	4.8 µl
dNTP mix (10 mM)	0.48 µl
Forward primer (10 µM)	1 µl
Reverse primer (10 µM)	1 µl
Nuclease-free water	10,73 µl
Template cDNA	800 ng

Table 37. Temperature profile used for RT-PCR in a thermocycler.

Step	Temperature	Duration	
1 - Initial denaturation	94°C	2 min	
2 - Denaturation	94°C	30 sec	35 cycles: steps 2 to 4
3 - Annealing	60°C	30 sec	
4 - Extension	68°C	30 sec / kb	
5 - Final Extension	68°C	2 min	
6 - Hold	4°C	∞	

2.3.2. Gel Electrophoresis

Gel electrophoresis was used to separate DNA fragments or PCR amplicons by size. 1-2 % agarose gels were prepared and for visualization of DNA under UV light, 10 mg/ml ethidium bromide were added. Agarose gels polymerized for 30 minutes at RT and subsequently, DNA samples were combined with 6x DNA loading dye and loaded on the gel. For fragment size determination suitable DNA ladders were added in separate lanes. The voltage was set at 120 Volt and gel electrophoresis ran for 60 minutes at RT.

2.3.3. Immunocytochemistry

Cells were fixed in 4 % PFA for 15 minutes at RT and washed three times with DPBS. For blocking and permeabilization, the staining solution consisting of 1x BMB solution in PBS supplemented with 0.1 % Triton X-100 (Table 34) was prepared and cells were incubated for 30 minutes at RT. Primary antibodies were diluted in BMB-Triton solution accordingly and incubated over night at 4°C (Table 28). Afterwards, cells were washed three times with DPBS before the addition of secondary antibodies for two hours at RT in the dark. Again, cells were washed three times with DPBS and in some cases nuclei were stained for 30 minutes at RT in the dark using Hoechst dye.

2.3.4. Flow cytometry

Cells were detached and dissociated using accutase for 5 minutes at 37°C, followed by a centrifugation at 300 xg for 3 minutes. Cells were resuspended in 100 µl FACS buffer, consisting of PBS + 2 % FCS. First, extracellular antigens were stained with proper conjugated antibodies for 30 minutes at 4°C (Table 29). Cells were washed three times with FACS buffer. For intracellular stainings, cells were first fixed with 4 % PFA for 15 minutes at RT, followed by three washing steps with PBS. For subsequent permeabilization, cells were incubated for 30 minutes in a BMB + 0.1 % Triton solution at 4°C. Antibodies for intracellular antigens were incubated again for 30 minutes at 4°C and cells were washed three times with FACS buffer before analysis using the BD FACSMelody.

2.3.5. ELISA

Secretion of the pro-inflammatory cytokine TNFα in the supernatant of co-culture wells was quantified using a standard sandwich-ELISA, namely the Human TNF-alpha DuoSet ELISA kit according to the manufacturer's instructions. Briefly, 96-well plates were coated with the capture antibody and incubated over night at RT. Wells were washed three times and blocked for at least one hour at RT. Wells were again washed and samples of standards were added and incubated for two hours at RT. After washing, detection antibody was added and incubated at RT for two hours. Wells were washed and the streptavidin / horse radish peroxidase (HRP) mix was added for 30 minutes at RT. Wells were washed again and substrate solution was added for 20 minutes at RT in the dark, stop solution was added and the plate was tapped for mixing and the optical density using a microplate reader set to 450 nm with wavelength corrections set to 540 nm was immediately determined. TNFα concentrations were calculated using an according standard curve.

2.3.6. Transcriptome analysis

Neuronal cultures were differentiated and cultivated for 21 days as described in 2.2.11. Cells were harvested by addition of accutase for 10-15 minutes at 37°C. Afterwards, cells were washed once in PBS and centrifuged at 300 xg for 3 minutes. The supernatant was discarded completely and the cell suspension was stained against CD11b for fluorescence activated cell sorting of microglia as described in 2.3.4. Purified microglia were spun down at 300 xg for 3 minutes and pellets were frozen immediately at -20°C with long term storage at -80°C. Pellets were finally processed for RNA sequencing by CeGaT GmbH, Tübingen.

2.4. Programs / Statistics

Confocal laser scan microscopy images were acquired using Zen Black and quantified using Imaris Bitplane (Version 8.2.0). Flow cytometry measurements were performed using BD FACS Chorus software and analyzed using FlowJo 10.6.1 (FlowJo Engine, Becton Dickinson & Company). Imaging of calcium signaling were processed using and exported using Zen Blue 2.5 lite (Carl Zeiss Microscopy GmbH). Mean fluorescence intensity over time within single regions of interests were quantified using ImageJ 1.52d (Wayne Rasband, National Institutes of Health, USA). Further quantification of frequency of peaks, area under the curve and $\Delta F/F0$ were assessed using Microsoft Excel 2016 (Microsoft Office 2016) and Origin 2015G (OriginLab Corporation).

Statistical analysis was performed using GraphPad Prism 8.0.1 (GraphPad Software Inc.). Data within experiments was tested for gaussian distribution at all times using the D'Agostino and Pearson test. Mostly, generated data were distributed non-normally. For non-gaussian distribution in pairwise comparisons, the unpaired Mann-Whitney U test was performed and for group comparisons, Kruskal-Wallis test with Dunn's post-hoc multiple comparisons test was used. In the case of normal distributions of values, classical one-way ANOVA was employed. P-values were assigned as follows: * = $p < 0.05$, ** = $p < 0.01$, *** = $p < 0.001$.

3. Results

The overall aim of this thesis was to establish a reproducible human iPSC-based microglia-neuron *in vitro* co-culture system and to identify suitable assays to study neuroinflammatory processes in the pathology of schizophrenia. For that purpose, impaired neuronal functionality in neurons from patients with schizophrenia and autism spectrum disorder was first validated by quantification of intracellular calcium signaling and by neurite outgrowth under the influence of antipsychotics with existing induced pluripotent stem cells (iPSCs) and neuronal progenitor cells (NPCs) from three healthy controls and three patients with schizophrenia.

3.1. Extended analysis of neuronal disease phenotypes

Dr. Lena-Marie Grunwald reprogrammed fibroblasts into iPSC from four healthy controls (CTR), five patients with schizophrenia (SZ) and from five patients diagnosed with autism spectrum disorder (ASD) as part of the work for her PhD thesis submitted in 2018 using an integrative approach based on retroviral transduction of key stem cell genes. Significant decrease in synaptic density by quantification of postsynaptic density protein 95 (PSD-95) and reduced neurite outgrowth were observed in both neurodevelopmental diseases but a discrimination between SZ and ASD was not possible using these parameters [48]. Disease-specific impaired functionality of neuronal networks needed to be further validated in neurite outgrowth test under the influence of drug administration and extended calcium imaging experiments.

The following results described in 3.1.1., 3.1.2 and 3.1.3. are part of the research publication by Grunwald & Stock et al. published in 2019 in the scientific journal Translational Psychiatry [48].

3.1.1. Antipsychotic drug application does not affect neurite outgrowth

Previous experiments by Dr. Lena-Marie Grunwald found mean neurite lengths to be reduced in NPCs from SZ and ASD patients in earlier experiments and the percentage of neurons with neurites was decreased in SZ and ASD cultures compared to healthy control cultures [48]. In this study, the set of experiments was repeated for CTR- and SZ-derived cells to test effects of three different antipsychotics commonly used to treat SZ and to assess how drug administration can affect and potentially rescue the reduced number of neurons with neurites and mean length of neuronal outgrowths in neuronal cultures from SZ-patients. ASD-derived neuronal cells were not included in this particular experiments of schizophrenia specific drug response. Seven healthy control clones derived from three different donors (CTR1-3) and five clones from three donors diagnosed with schizophrenia (SZ1-3) were seeded into PLO/Lam-

coated well plates and treated with the three antipsychotic drugs clozapine, haloperidol and olanzapine.

High-content image acquisition and automated analysis reproduced initial findings that untreated neurite lengths in SZ-neurons were significantly reduced compared to CTR lengths (Figure 2A). Likewise, the percentage of untreated neurons with neurites was reduced in SZ clones, whereas only three clones of donor SZ2 showed significantly reduced percentage of neurons with neurites when compared to healthy controls (Figure 2B).

In order to analyze whether antipsychotics that are commonly used to treat symptoms of schizophrenia can rescue reduced neurite length and the percentage of neurons with neurites, outgrowing NPCs were treated with 1 µM clozapine, 1 µM haloperidol or 1 µM olanzapine for 72 hours. No significant differences were found for neurite lengths when compared to DMSO-treated cells (Figure 2C). Likewise, the analysis of the amount of neurons with neurites did not reveal any distinct alterations compared to DMSO-treated cells (Figure 2D) [48]. All antipsychotics showed a slight tendency to increase the number of neurons with neurites in CTR-NPCs but only application of haloperidol showed a significant increase in the percentage of neurons with neurites for donor CTR1, however no effects were observable when treating SZ-NPCs with antipsychotics.

To conclude, drug application had no to only minor effects on neurite outgrowth and could not rescue SZ-derived phenotypes of reduced neurite lengths and reduced percentage of neurons with neurites. Determination of drug responses by changes in the mean neurite outgrowth appears to be no suitable assay for high-throughput drug discovery and screening.

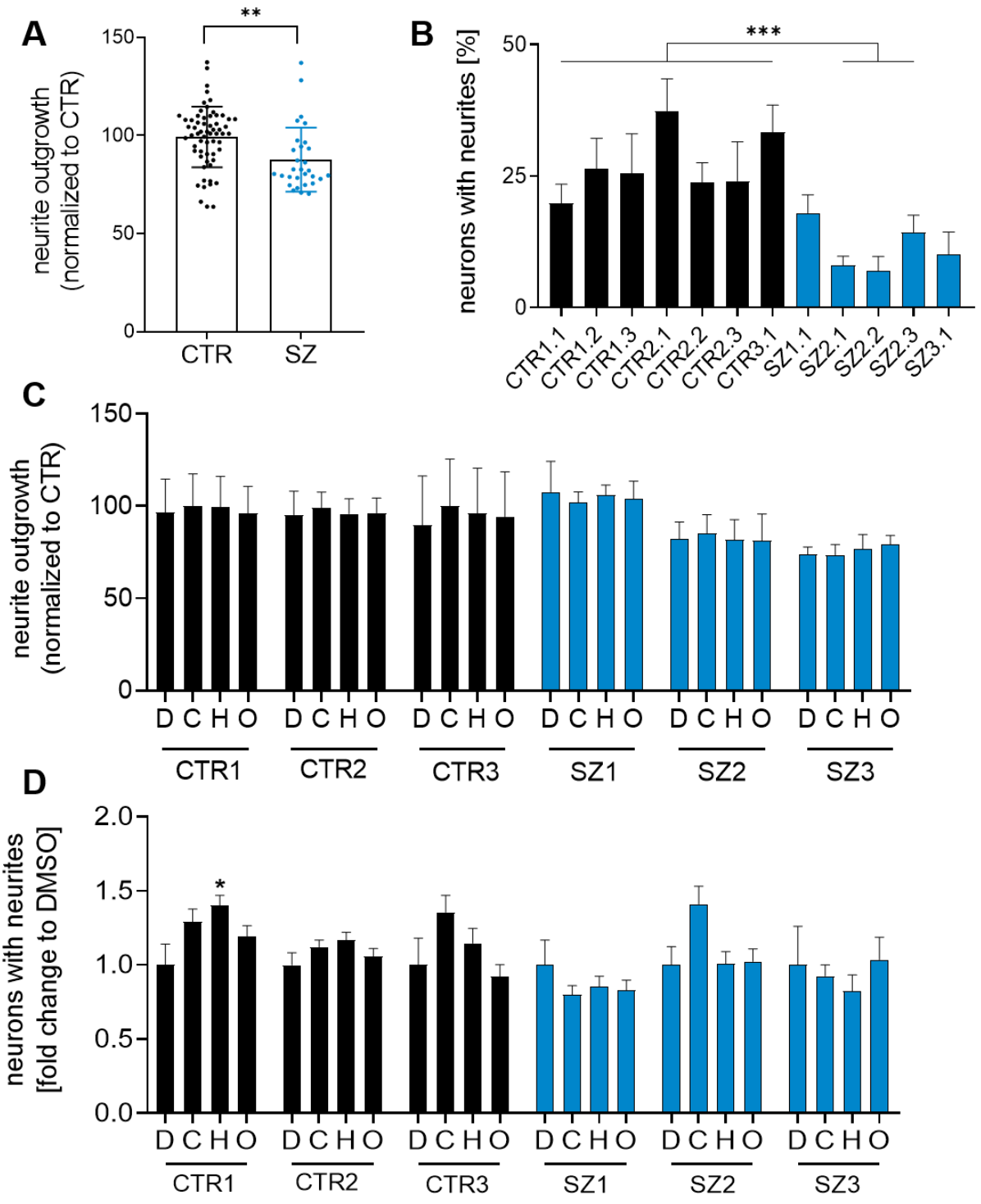

Figure 2. High content analysis of neurite outgrowth in iPSC-derived neurons. (A) Percentage of neuronal outgrowth normalized to control neurons including seven CTR clones and five SZ clones. Unpaired two-tailed Mann Whitney U test, $p = 0.003$, $n > 50$. **(B)** Percentage of neurons with neurites for all individual clones that were included. Unpaired two-tailed Mann Whitney U test for group comparison of all CTR clones versus all SZ2 clones, $p < 0.0001$, $n>25$. **(C)** Normalized mean neurite outgrowth of neurons that were treated with 1 µM clozapine ("C"), 1 µM haloperidol ("H"), 1 µM olanzapine ("O") or DMSO as control ("D"), $n>30$. **(D)** Drug response of neurons treated with 1 µM clozapine ("C"), 1 µM haloperidol ("H"), 1 µM olanzapine ("O") or DMSO as control ("D") is expressed as fold change to DMSO control ("D") for each clone. Kruskal–Wallis Test and Dunn's post hoc test. CTR1 $H(3) = 8.31$, CTR2 $H(3) = 3.66$, CTR3 $H(3)= 7.83$, SZ1 $H(3) =0.76$, SZ2 $H(3)= 7.96$, and SZ3 $H(3) = 35.6$. $p<0.05$ *, $p<0.01$ **, $p<0.001$ ***; $n>80$. Error bars are s.e.m. [48]

3.1.2. Functional discrimination of neuropsychiatric diseases by distinct calcium signaling patterns

For further examination of functional impairment in more mature neuronal networks of neuropsychiatric patients, single cell calcium imaging was performed with neurons derived from three healthy controls, from three SZ-patients and from three ASD-patients (in total nine clones, one clone per donor). After eight weeks of differentiation, iPSC-derived neurons were loaded with 1 µM of the fluorescent calcium sensitive dye Cal520-AM and imaged to quantify intracellular calcium signaling on a single cell level (Figure 3A-C).

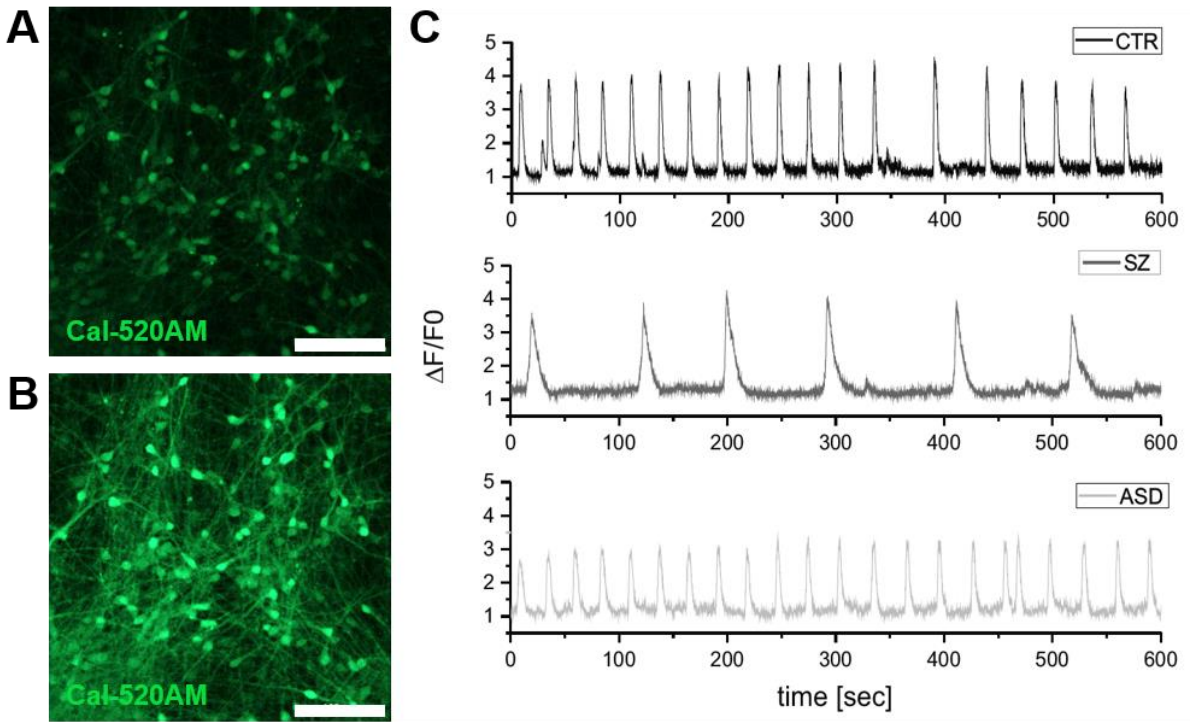

Figure 3. Representative calcium traces of sponteaneously active neurons were imaged over 10 minutes. Cal-520AM™ stained neurons of healthy CTR, SZ, and ASD groups showed a baseline fluorescence of the calcium sensitive dye **(A)** with increased fluorescence upon calcium influx during depolarization of neuronal networks **(B)**. Scale bars indicate 100 µm. **(C)** Exemplary calcium traces of retrieved fluorescence changes, shown as the ratio ΔF/F0, over the time of acquisition.

Calcium imaging of spontaneously active neurons revealed reduced peak frequency in SZ-derived cells compared to the CTR group, which was not observable among ASD clones (Figure 4A+B). The peak amplitude ΔF/F0 describes the ratio of the peak's highest fluorescence intensity divided by the baseline intensity and was not altered when comparing SZ- to CTR-neurons, only ASD-neurons showed a minor but significant decrease describing lower rise of fluorescence during depolarization (Figure 4C).

The two parameters area under the curve and full width half maximum (FWHM) describe the width of individual peaks including the speed of the fluorescence intensity's rise and fall that represent how fast calcium fluxes into and out of the cells occur. In SZ-neurons, peak area and FWHM were increased, whereas ASD-neurons showed no significant difference compared to CTR-neurons (Figure 4D+E).

Analysis of neuronal signaling patterns through visualization of intracellular calcium levels demonstrate a differentially impaired and distinguishable phenotype of SZ- and ASD-neurons upon comparison to control neurons.

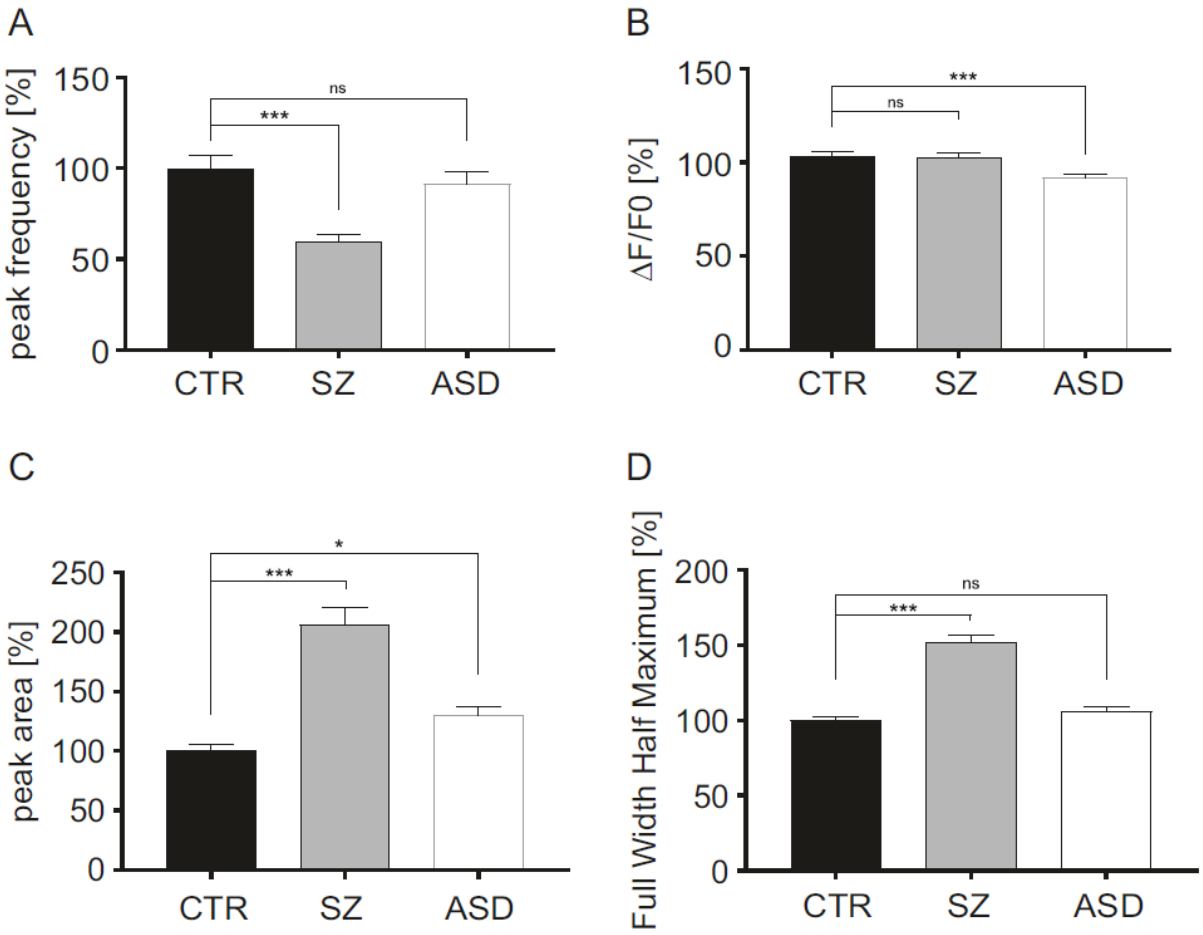

Figure 4. Measurement of intracellular calcium level changes [48]. (A) and signals obtained were used to calculate **(B)** peak frequency, **(C)** peak amplitude determined by fluorescence intensity ΔF/F, **(D)** peak area and **(E)** full width half maximum. Kruskal–Wallis Test and Dunn's post hoc test, peak frequency H(2) =22.56, ΔF/F0 H(2) = 19.44, peak area H(2) = 93.17, and FWHM H(2) = 45.2; $p<0.05$ *, $p<0.01$ **, $p<0.001$ ***; error bars are s.e.m.

3.1.3. MHC class II expression is deregulated in one patient with schizophrenia

Comparative transcriptome sequencing and analysis helps to discriminate disease groups from each other and from healthy control cells. RNA sequencing of 4-week old neuronal cultures revealed distinct disease-specific transcriptomic profiles with several specifically deregulated genes for SZ and ASD neurons compared to CTR neurons. Hierarchical clustering discriminated both neuropsychiatric diseases based on their expression data [48]. The expression data generated here is further reviewed in the review by Stock et al., published in Stem Cells Translational Medicine in 2020 [128].

Most interestingly, comparison of individual SZ with CTR neurons revealed a deregulation of several genes involved in the MHC class II processing and presentation signaling pathway for donor SZ2 (Table 38). In total, 48 genes were deregulated compared to all CTR donors and within those 15 immune-associated genes were found to be highly upregulated. Such an upregulation was not found for donors SZ1 and SZ3 highlighting the genomic heterogeneity and diversity of individual severities and pathologies of schizophrenia cases. Patient SZ2 was the only patient to receive clozapine as only antipsychotic treatment. Interestingly, clozapine treatment of one healthy control CTR1 resulted in equally increased expression rates of the same MHC class II-associated genes [48].

Table 38. Expression analysis of donor SZ2-neuronal culture identified 15 immune-associated genes to be highly upregulated in comparison to CTR groups [48].

Gene ID	Gene	Base mean	Log2 fold change
ENSG00000125730	C3	82,4096708	4,2619802
ENSG00000019582	CD74	12301,8847	5,96186369
ENSG00000179583	CIITA	1020,07467	5,73406923
ENSG00000204257	HLA-DMA	996,195529	4,21815148
ENSG00000242574	HLA-DMB	344,812711	4,53053327
ENSG00000204252	HLA-DOA	1295,47277	6,30186606
ENSG00000231389	HLA-DPA1	5359,91757	5,60631318
ENSG00000196735	HLA-DQA1	1511,60291	5,53599906
ENSG00000237541	HLA-DQA2	711,906614	5,21036505
ENSG00000232629	HLA-DQB2	111,351614	6,02979814
ENSG00000204287	HLA-DRA	9921,96611	5,5392645
ENSG00000196126	HLA-DRB1	3829,96493	4,03211621
ENSG00000198502	HLA-DRB5	930,565252	4,34349265
ENSG00000229391	HLA-DRB6	433,344135	5,6119804
ENSG00000204642	HLA-F	272,374174	3,83280859

Undirected cultivation and differentiation of NPC to neurons over several weeks may lead to the development of microglia or other glial cells. To rule out the possibility that unintended co-differentiated microglia may be the reason for increased expression of immune-associated genes, the protein level of MHC class II in neuronal cultures was examined *in vitro* by immunocytochemistry and fluorescence microscopy.

Three independent experiments of three clones of three CTR donors (one clone per donor) and three independent clones of donor SZ2 were fixed for immunocytochemical analysis as naive NPCs and in the state of 6-week old neurons (Figure 5A). For donor SZ2, MHC class II expression in Pax6-positive NPCs and MAP2-positive neurons was significantly and equally increased in both neuronal maturation states when compared to CTR cells (Figure 5B+C).

Transcriptome analysis and quantification of protein levels *in vitro* identified a significant upregulation of MHC class II expression in three clones from patient SZ2.

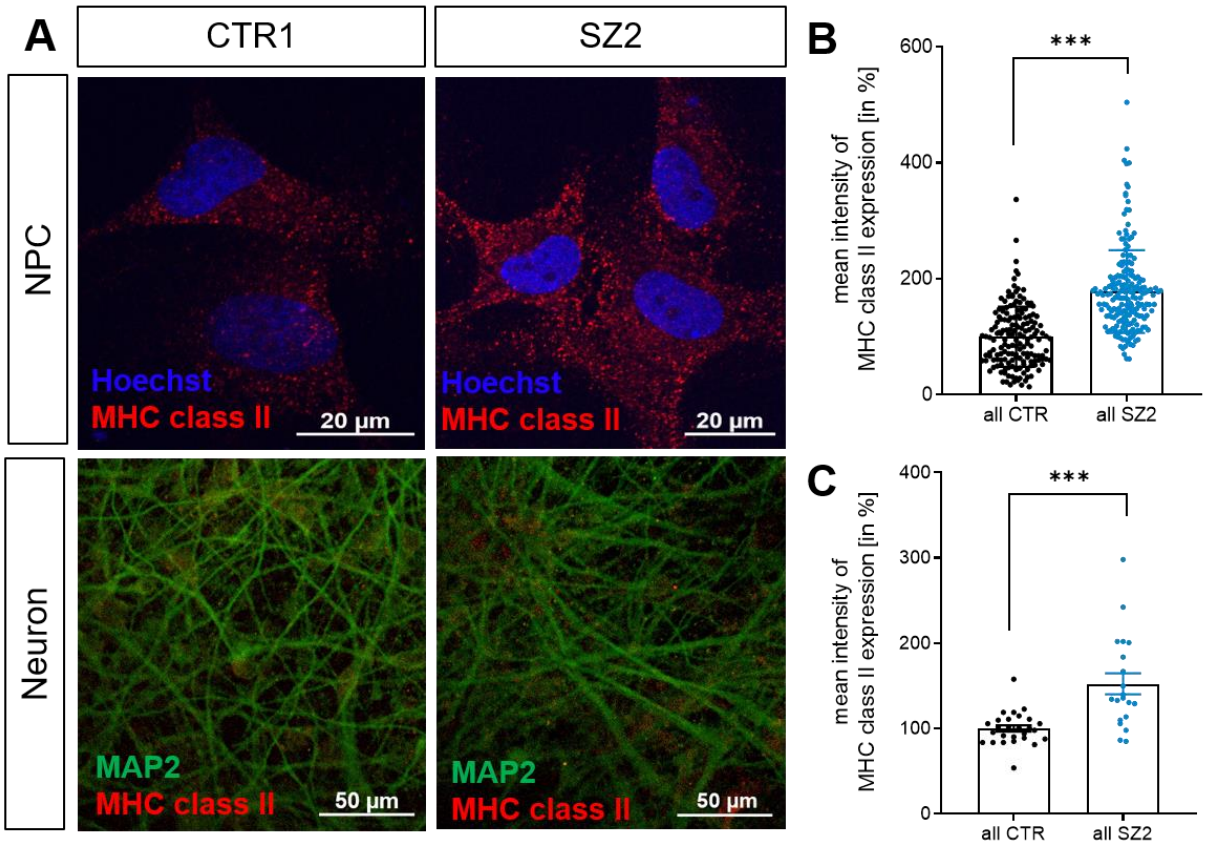

Figure 5. Quantification of MHC class II expression by immunocytochemical staining against human HLA-DR, DP, DQ for three CTR clones and three SZ2 clones **(A)**. **(B)** Expression of MHC class II was increased in SZ2-NPC, unpaired two-tailed Mann Whitney U test, $p < 0.0001$, $n>160$ and **(C)** in 6-week old neurons, unpaired two-tailed Mann Whitney U test, $p < 0.0001$, $n>20$, error bars are s.e.m.

3.2. Non-integrative iPSC generation and characterization

iPSCs were initially derived from patient-derived human skin fibroblasts generated by retroviral transduction [48]. iPSCs typically grow in tightly packed, dense colonies that start to differentiate and lose integrity once the colonies grow too big or too close to neighboring colonies. The morphology of iPSC colonies is probably one of the best quality control features in the lab. Other typical characteristics of iPSC are the expression of standard stem cell surface markers, such as SSEA-4 or TRA-1-60, or the ability to form embryoid bodies, a required step that is crucial in several differentiation protocols.

When iPSCs started to grow rather as single cells than as colonies, the expression of SSEA-4 across the whole colony declined and iPSCs lost the ability to form compact embryoid bodies (Figure 6), the decision was made to reprogram the patient-derived fibroblasts again. To exclude possible effects of integrating retroviruses, a non-invasive episomal approach was chosen this time.

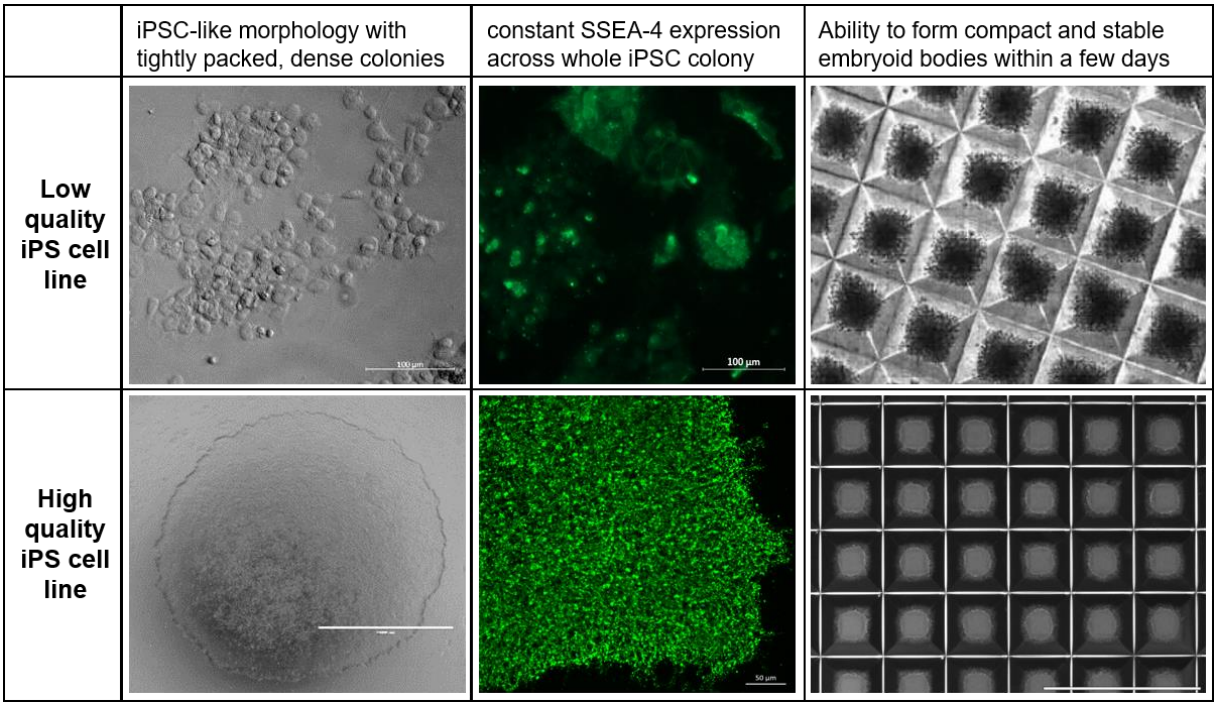

Figure 6. Quality control features of high quality iPSC colonies that are tightly packed colonies, consistent high expression of stem cell surface markers like SSEA-4 or the ability to form embryoid bodies. When iPSC quality declines, the iPSC integrity and potential to be differentiated towards all three germ layers diminishes.

Fibroblasts were transfected with five plasmids encoding OCT3/4, SOX2, L-MYC, KLF4 and LIN28 by nucleofection and seeded onto matrigel-coated plates. Three weeks after electroporation, first iPSC-like colonies appeared and could be transferred manually once a size of 200-300 µm in diameter was reached (Figure 7A+B). Per donor at least 10 colonies were picked and expanded for analysis. Three clones per donor were finally integrated in a

complete characterization, including stem cell marker expression on RNA and protein level (Figure 7C+D), chromosomal integrity (Figure 7E+F) and the potential to differentiate into all three germ layers by directed differentiation into excitatory neurons, cardiomyocytes and cells of the definitive endoderm (Figure 7G-M).

Chromosomal integrity was analyzed by Thermo Fisher, Carlsbad, CA by applying the KaryoStat™ Technology (coordinated by Kirstin K. Melton and Chris C. Gibson). Several minor and major chromosomal aberrations were detected during the screen. Ultimately, only seven clones out of 27 showed chromosomal integrity and were included in the following analyses (Table 39). As only one healthy control, clone CTR1.3, exhibited no chromosomal aberrations, two further control clones with minor aberrations were included in the analysis. The two clones CTR3.3 and CTR4.3 revealed a partial chromosomal gain and mosaic gain on chromosome 11 and were nonetheless included into further experiments to ensure a proper number of control clones for this study. All other clones were excluded from further experiments.

The complete characterization of the seven intact clones was published in 2020 in the publication Stock, Vogel et al. in Stem Cell Research Lab Resources [129]. The two clones CTR3.3 and CTR4.3 revealed robust expression of endogenous stem cell gene expression, showed standard iPSC surface markers and were capable to be differentiated into all three germ layers (Supplementary Figure 2). Conceptualization, planning and establishment of reprogramming and differentiation protocols and initial rounds of reprogramming were performed as part of this thesis. Sabrina Vogel expanded the number of clones up to 27 clones in total (three clones for each of the nine donors) and the characterization of all clones regarding stem cell marker expression on RNA and protein level and differentiation towards all three germ layers was completed. The full description and validation for all 27 clones was part of Sabrina Vogel's master thesis, submitted in 2019.

Table 39. Overview of the remaining seven clones that passed chromosomal integrity evaluation and were included in all following studies and two additional clones from healthy controls CTR3 and CTR4 with minor chromosomal anomalies (shown in italics).

Donor	**Gender**	**Age at donation**	**Label throughout this thesis**
healthy individual number 1	female	28	**CTR1**
healthy individual number 3	*male*	*53*	***CTR3***
healthy individual number 4	*female*	*34*	***CTR4***
patient with schizophrenia 1	male	37	**SZ1a**
patient with schizophrenia 1	male	37	**SZ1b**
patient with schizophrenia 2	female	54	**SZ2**
patient with schizophrenia 4	male	50	**SZ4**
patient with schizophrenia 5	female	27	**SZ5a**
patient with schizophrenia 5	female	27	**SZ5b**

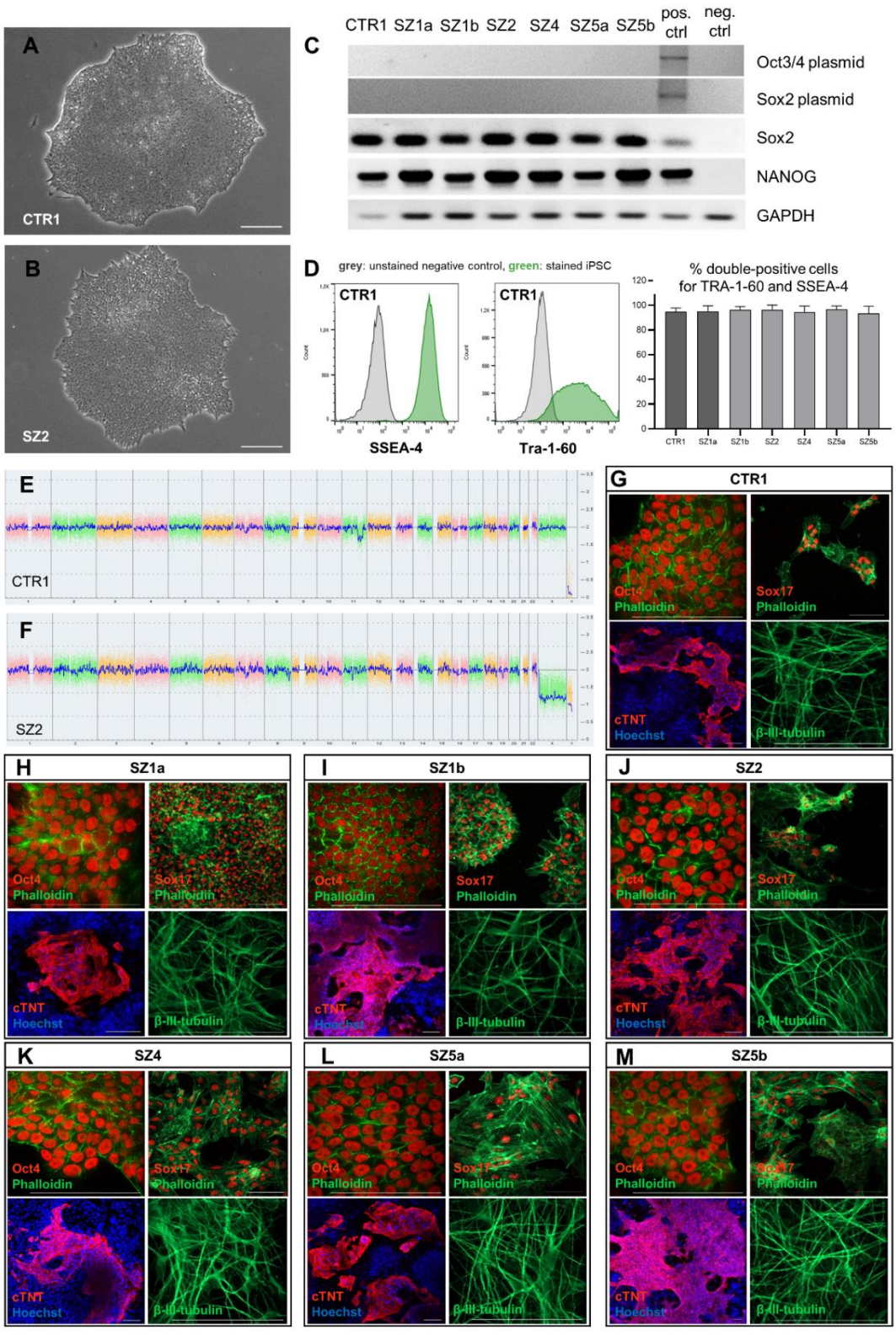

Figure 7. Complete characterization of chromosomally intact iPSC clones [129]. **(A+B)** Typical iPSC morphology with dense and tightly packed colonies. **(C)** Endogenous expression of stem cell genes and loss of exogenously introduced plasmids needed for reprogramming shown by RT-PCR. **(D)** Flow cytometry proved homogenous surface marker expression of SSEA-4 and Tra-1-60 across all iPSC clones. **(E+F)** KaryoStat™ array identified seven clones without chromosomal anomalies, performed by Thermo Fisher Scientific. **(G-M)** All iPSC clones were positive for Oct4 expression in the nucleus and capable to be differentiated towards all three germ layers: Sox17 as marker for definitive endoderm, cTNT for cardiomyocytes of the mesoderm and β-III-tubulin expression for ectodermal neurons.

3.3. Neuronal differentiation reveals developmental phenotype

Undirected neuronal differentiation of iPSCs can be a time-consuming procedure and leads to an undefined mixture of cell types within one well ultimately resulting in high variability among replicates of differentiations and poor reproducibility. Lentiviral overexpression of human Neurogenin 2 (hNGN2) directly induced differentiation of excitatory, cortical neurons with improved reproducibility and the time of differentiation was shortened to three weeks [119]. Additionally, co-cultivation of iPSC-derived neurons with murine astrocytes increased neuronal viability, connectivity and functionality vastly. Analysis of synaptic density in neuronal cultures derived from patients with schizophrenia confirmed reduced synaptic density.

3.3.1. Murine astrocytes increase neuronal maturation and circuity

Mouse astrocytes were extracted from the cortices of newborn mice and expanded and passaged for up to four passages. Afterwards, murine astrocytes showed reduced proliferation and decreased viability. Immunocytochemical staining of the cytoplasmic astrocyte marker glial fibrillary acidic protein (GFAP) proved pure astrocyte cultures to be without remaining murine neuronal or other glial cells (Figure 8). The absence from microglia and other glial cells was especially important for the subsequent co-culture assays with iPSC-derived microglia and neurons.

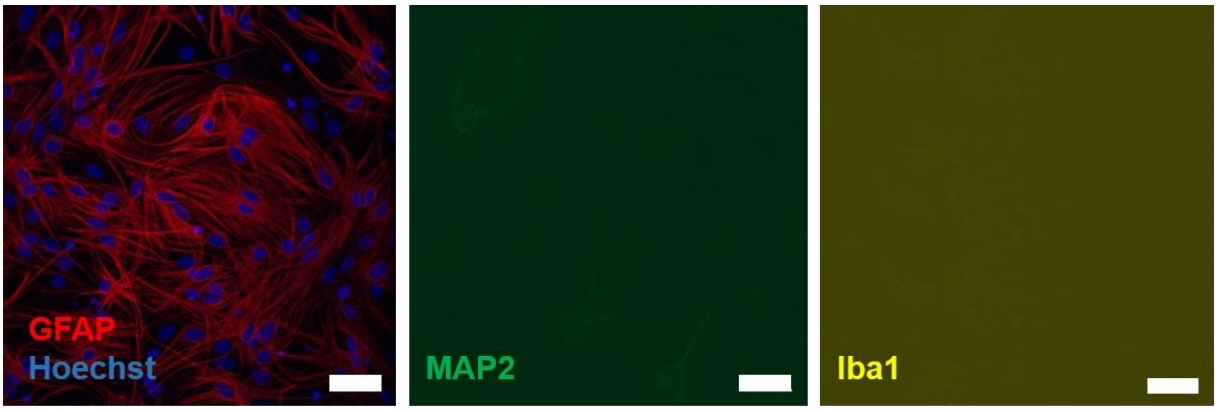

Figure 8. Isolated cultures of murine astrocytes do not contain MAP2-positive neurons or other glial cell types, such as e.g. Iba1-positive microglia, as shown by immunocytochemistry with increased laser intensity and maximum exposure time. Scale bar indicates 50 µm.

MAP2-staining of 3-week old hNGN2-induced neuronal cultures confirmed improved morphology of neuronal networks after co-culture with astrocytes derived from mouse astrocytes compared to neurons cultured alone (Figure 9). Astrocytes were seeded in a ratio of 1:5 to NPCs. This ratio contradicts the actual situation in the human brain where astrocytes are the most abundant cell type. Astrocyte density was reduced to a minimum that still had a

huge beneficial influence by medium conditioning on the neuronal network but did not consume too much medium in favor of neuronal viability and survival. Co-cultivation of neurons and astrocytes in neuronal differentiation medium and in absence of FCS inhibited further astrocyte proliferation but enabled astrocyte survival and neurons-astrocyte interactions *in vitro*.

Likewise, the expression of synaptic markers such as the vesicular glutamate transporter 1 (VGlut1) and Synapsin 1 (Syn1) were significantly increased after astrocyte addition (Figure 9) representing more mature neuronal networks with improved synaptic connectivity.

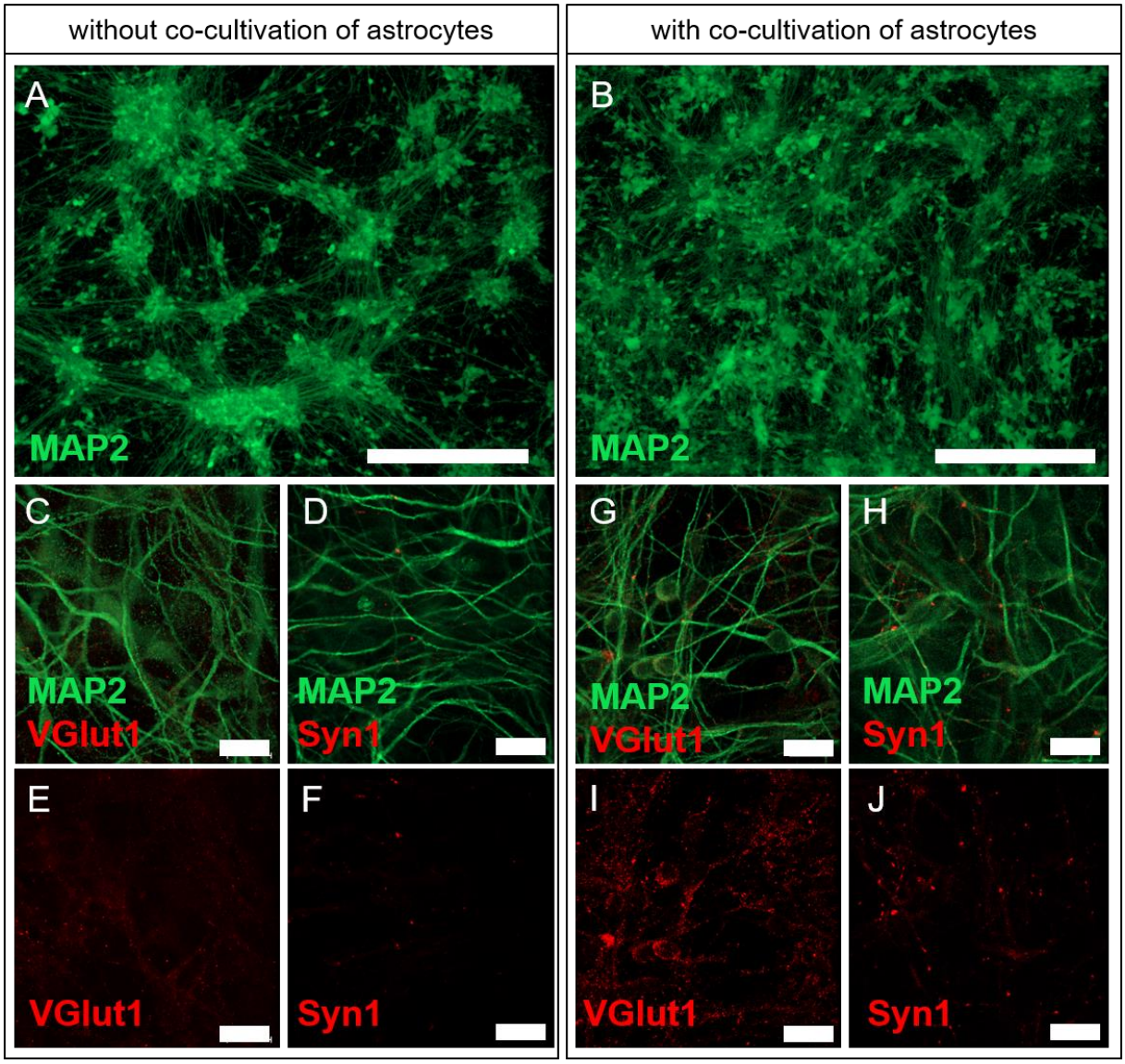

Figure 9. Improved differentiation of iPSC-derived neurons cultured in presence of murine astrocytes. (A+B) Overview images taken at 5x magnification highlight how the absence of astrocytes triggers neurons to cluster tightly, resulting in low cell viability and immature neuronal network formation. Addition of astrocytes enables neurons so spread evenly and build dense neuronal networks. Scale bar indicates 500 µm. **Increased expression of synaptic markers** as VGlut1 and Syn1 after neuronal differentiation in presence of astrocytes. Scale bars indicate 20 µm.

3.3.2. Synaptic density is reduced in SZ-neuronal cultures

Synaptic density was reported to be decreased in patients with schizophrenia in a variety of human post mortem or iPSC-based studies [44-46, 48]. Neuronal networks cultured on murine astrocytes were differentiated for three weeks and fixed for immunocytochemistry. Z-stacks of presynaptic Synapsin1 (Syn1) stainings (Figure 10A) were acquired using high resolution confocal laser scan microscopy and synaptic density was determined by quantification of Syn1-positive spots on MAP2-positive dendrites (Figure 10B).

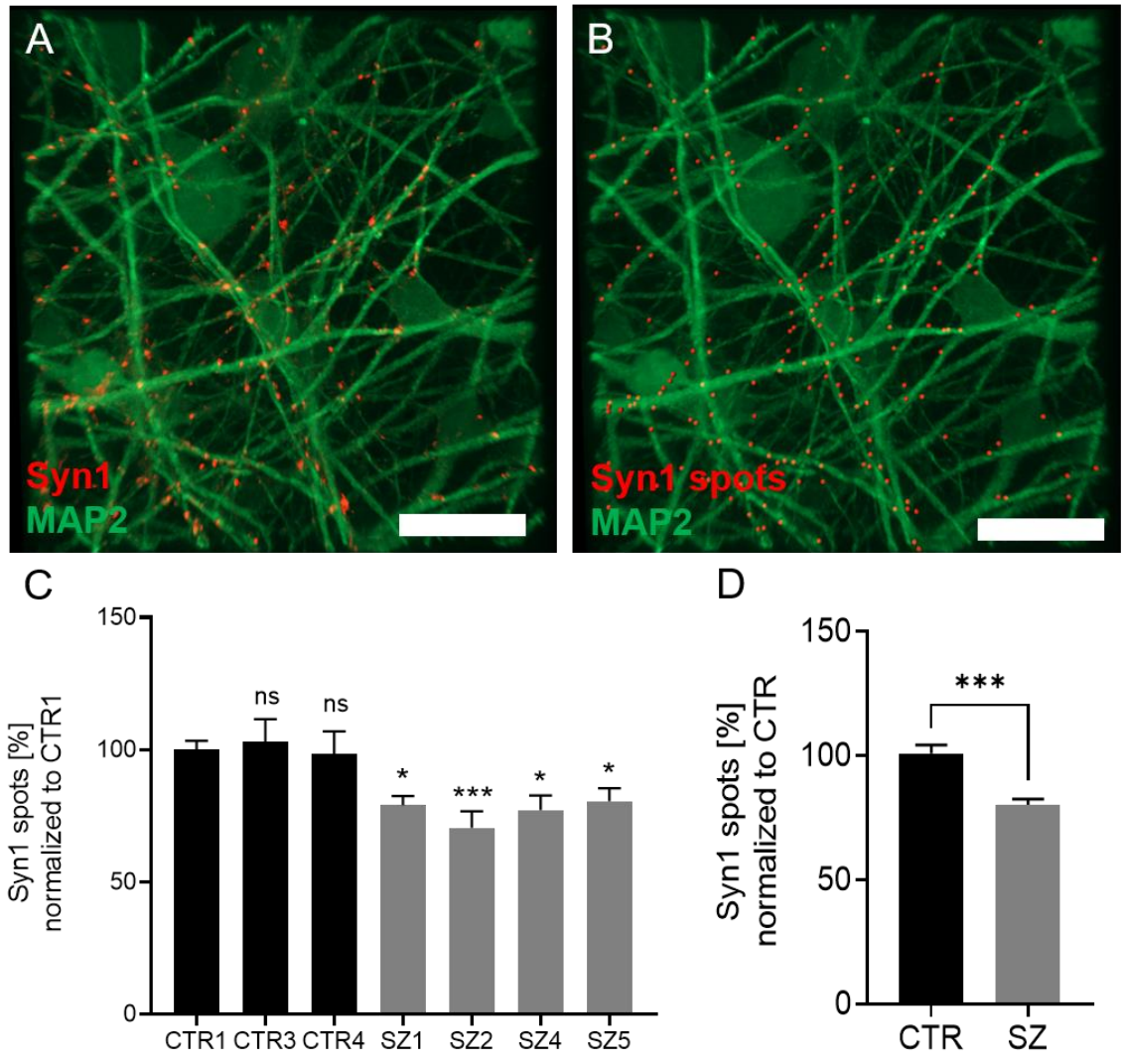

Figure 10. Synaptic density is reduced in iPSC-derived neuronal cultures of SZ patients. **(A)** Immunocytochemical stainings of 3-week old MAP2-positive neuronal cultures with astrocytes but without microglia and Syn1 positive presynaptic structures. Scale bar indicates 20 µm. **(B)** Representative z-stack processing using Imaris Bitplane software with processed Syn1 spots on MAP2 surface mask. Scale bar indicates 20 µm. **(C)** Quantification of donor-specific synapse number reduction in neuronal cultures. Data is normalized and statistically compared to all CTR. Kruskal-Wallis Test with Dunn's post-hoc multiple comparisons test, $H(6)=39.89$, $n>50$. $p<0.05$ *, $p<0.01$ **, $p<0.001$ ***, ns = not significant. **(D)** Donor data was pooled for donor-independent but disease-specific quantification of Syn1 spot reduction. Data is normalized to CTR. Unpaired, two-tailed Mann Whitney U test, *** $p<0.0001$, $n>150$. Error bars are s.e.m.

Donor-specific Syn1 spots in neuronal cultures of each of the seven individual clones were determined and normalized to healthy control clone CTR1. For all subsequent studies, three clones were derived from three control donors (CTR1, CTR3, CTR4) and four clones from four patients (SZ1, SZ2, SZ4 and SZ5). Experiments were always performed with one clone per donor. Syn1 spots were significantly reduced in all four analyzed SZ clones separately, with clone SZ2 having the lowest amount of Syn1 spots consistently throughout all replicates. The two control clones CTR3 and CTR4 showed no significant differences in Syn1 spot density compared to CTR1. Group comparison of pooled control or patient-specific clones confirmed the overall significant tendency that synaptic density was reduced in SZ-derived pure mono-cultures of hNGN2-induced glutamatergic neurons.

3.4. Myeloid immune cell differentiation of iPSC

Microglia are tissue-resident macrophages and phagocytes in the human central nervous system and have important functions during early brain development and constant neuronal circuit shaping and are essential for appropriate long term brain function. During injury or disease, microglia and macrophages can polarize into two different immunological activation states, the pro-inflammatory M1 and the anti-inflammatory M2 phenotype, both of which can have beneficial or detrimental consequences for the peripheral tissue and the CNS.

3.4.1. Myeloid differentiation protocol generates distinct inflammatory macrophage phenotypes

To understand the inflammatory role of microglia in the pathology of schizophrenia using a human *in vitro* model system, iPSCs were differentiated using an adapted version of a fast and straight-forward protocol for macrophage and microglia generation [123]. The quality of generated myeloid progenitor cells and microglia was frequently controlled to ensure protocol efficacy and reproducibility. After one week of differentiation, adherent iPSC differentiated from pluripotent into free floating hematopoietic stem cells (Figure 11A) that uniformly expressed stem cell marker CD45 (Figure 11B). After two weeks of differentiation and myeloid induction, myeloid progenitor cells (MCPs) were positive for myeloid cell markers CD14 and CD11b (Figure 11B).

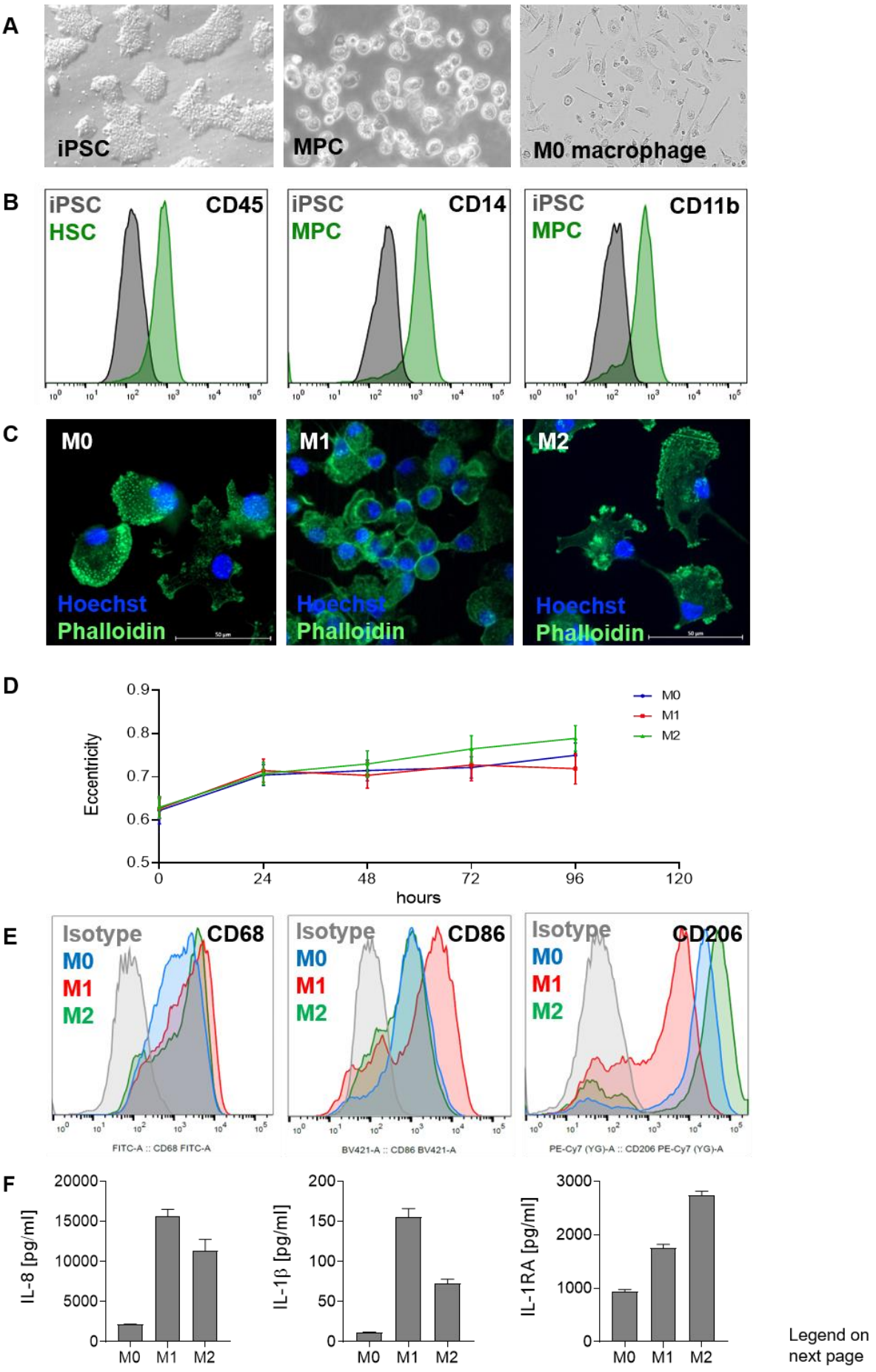

Legend on next page

Figure 11. Myeloid differentiation protocol resulted in functional macrophages. (A) Differentiation was observable by morphological transformation, as myeloid progenitors arose into the supernatant and floated in suspension and mature macrophages re-adhere. **(B)** Flow cytometry identified 7 days old hematopoietic stem cells (HSC) as CD45 positive and 14 days old myeloid progenitor cells (MPC) were positive for classical markers CD14 and CD11b. **(C)** Functional response to polarization stimuli as LPS or IL-10 induced morphological changes in the actin cytoskeleton as shown by immunocytochemistry against phalloidin and could be quantified by determination of the eccentricity, a parameter for the roundness or extension of individual cell bodies **(D)**. **(E)** Expression of the classical macrophage marker CD68 and the pro- and anti-inflammatory cell surface markers CD86 and CD206, respectively, was analyzed in polarized M0, M1 and M2 phenotypes. **(F)** Cytokine secretion of the pro-inflammatory cytokines IL-8 and IL-1β and the anti-inflammatory and pro-wound healing cytokine IL-1RA into the supernatant after M1 or M2 polarization was kindly measured using the Luminex technology by Meike Jakobi, NMI Reutlingen.

At this point, MCPs could be differentiated into peripheral macrophages or CNS-specific microglia. To prove that both differentiation protocols were applicable, MCPs were further differentiated by application of high-dose M-CSF for maturation into macrophages. Polarization using LPS and IFNγ or IL-4 and IL-10 induced the pro-inflammatory M1 or anti-inflamamtory M2 phenotype, respectively. Both subtypes were confirmed by morphology and cell shape analysis (Figure 11C). M1-polarized macrophages displayed a smaller, almost round cell body, while M2-polarized macrophages exhibited a rather spread, large cellular morphology. Quantification of eccentricity, a parameter to determine the cell shape morphology, discriminated macrophages between small, round M1 and large, spread M2 phenotypes (Figure 11D). Additionally, expression of M1 or M2-specific surface markers were assessed using flow cytometry. The expression of pro-inflammatory marker CD86 was increased in M1 macrophages compared to M2 or unstimulated M0 microglia, while the anti-inflammatory marker CD206 was increased in M2 macrophages (Figure 11E). As expected, expression of the standard microglia and macrophage marker CD68 was similar among polarization states. Luminex analysis of secreted cytokines was performed by Meike Jakobi, NMI Reutlingen, and revealed a trend towards M1- and M2- specific secretion patterns of pro- (IL-8 and IL-1β) or anti-inflammatory (IL-1RA) cytokines (Figure 11F).

3.4.2. Differentiation protocol yields fully functional microglia

For full characterization of microglial phenotypes, MCPs were further cultivated and differentiated by high-dose application of IL-34, TGFβ1 and GM-CSF into a mature microglial phenotype (Figure 12A). Generated microglia displayed their typical ramified morphology *in vitro* with several branched extensions (Figure 12B). Additionally, microglia were capable to engulf and phagocytose *Escherichia coli* bacterial particles that were labelled with a pH-sensitive dye leading to increased fluorescence upon phagocytosis within the microglial lysosome (Figure 12C). Additionally, expression of microglial marker Iba1 and HLA-DR was increased in differentiated microglia (Figure 13A).

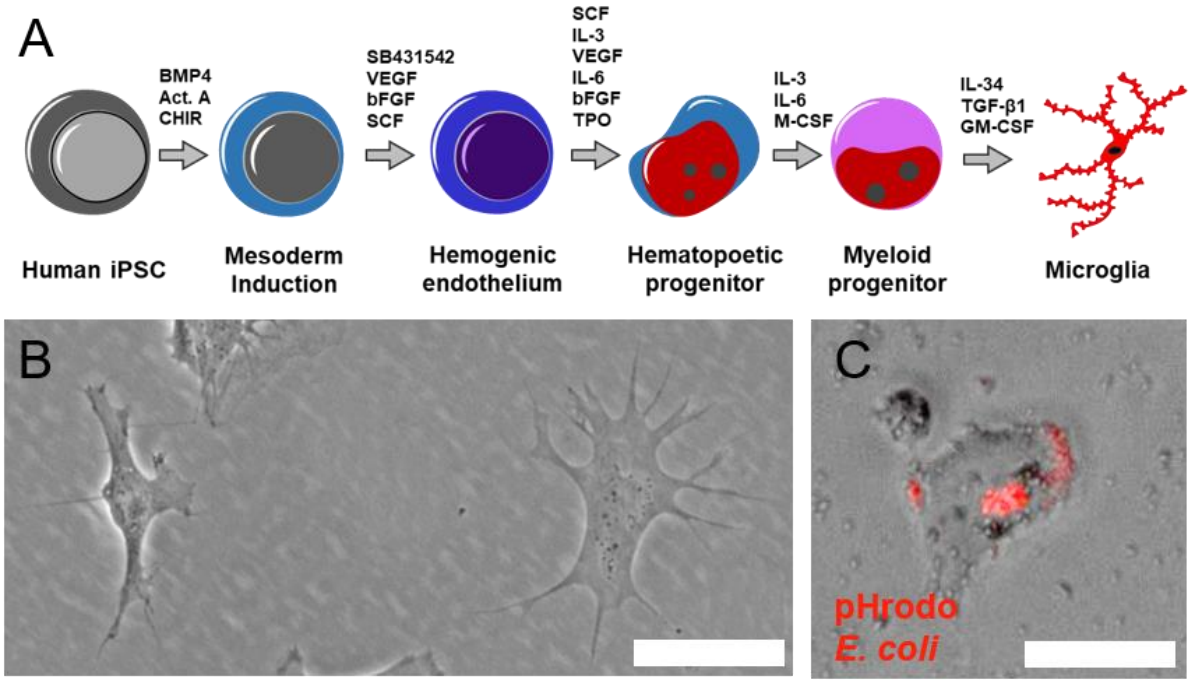

Figure 12. Microglial differentiation protocol. (A) Schematic overview of the cytokines and growth factors used to induce hematopoietic and myeloid fate (protocol modified from [123]). **(B)** Ramified morphology of mature microglia. **(C)** Microglia engulf bacterial particles labelled with a pH-sensitive dye. Scale bars indicate 50 µm.

Next, the response of HLA-DR and Iba1 positive microglia to pro- and anti-inflammatory stimuli was examined (Figure 13A). Pro-inflammatory LPS treatment increased microglial marker expression HLA-DR in CTR-microglia, whereas anti-inflammatory drug treatment using minocycline induced no changes in HLA-DR or Iba1 expression (Figure 13B). In SZ-microglia, LPS treatment had only a small and not significant effect on HLA-DR expression. Interestingly, HLA-DR was increased in untreated SZ-microglia compared to CTR-microglia. In contrast, Iba1 expression was not significantly increased in untreated SZ-microglia (Figure 13C). LPS treatment increased Iba1 expression equally in CTR- and SZ-microglia, whereas minocycline treatment slightly decreased Iba1 expression compared to untreated microglia.

Likewise, LPS treatment increased the secretion of the pro-inflammatory cytokine TNFα significantly for both mgCTR and mgSZ (Figure 13D). The anti-inflammatory drug minocycline slightly suppressed the release of TNFα compared to untreated microglia.

The applied protocol generated active and responsive microglia with distinct immunological and inflammatory response to specific stimuli. Assessment of microglial functionality and the response to pro- and anti-inflammatory triggers revealed full activation capacity of microglia by LPS-induced increased expression of microglial activation marker HLA-DR, Iba1 and increased secretion of TNFα.

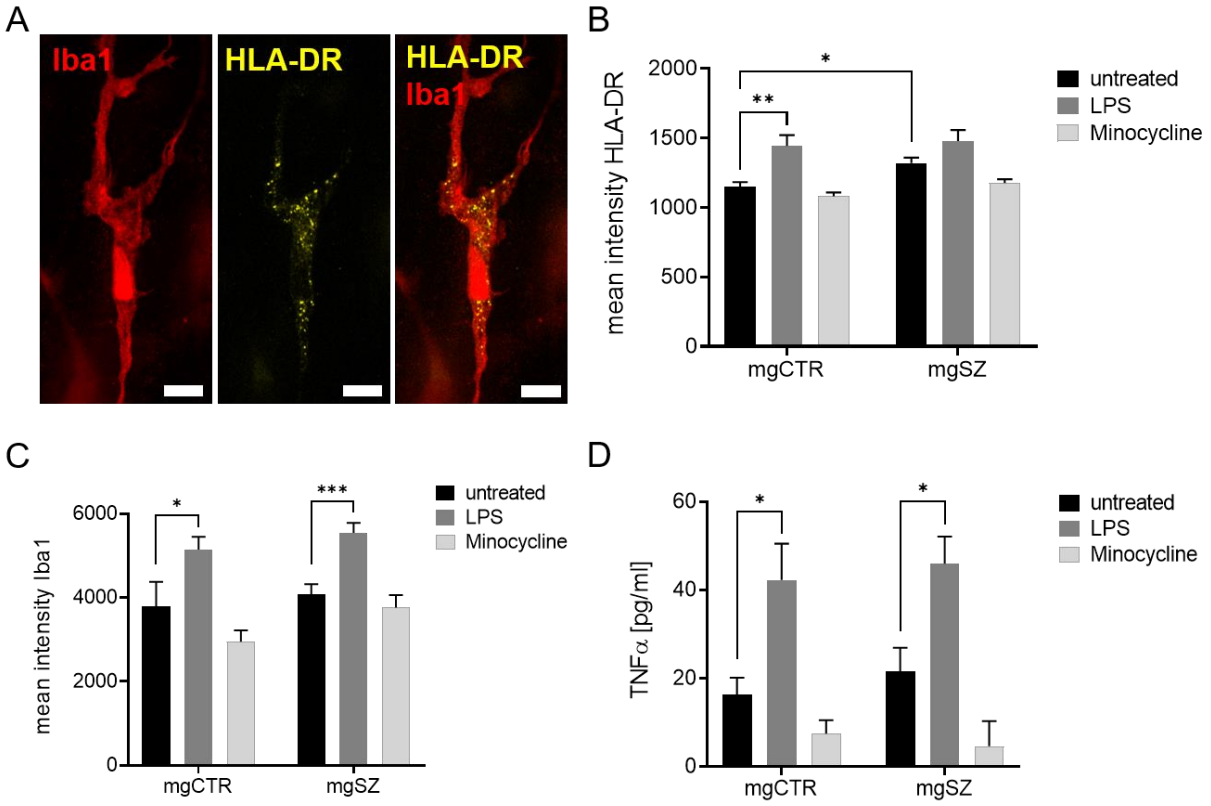

Figure 13. Microglia respond to LPS and Minocycline treatment as assessed by HLA-DR and Iba1 expression and secretion of the pro-inflammatory cytokine TNFα. **(A)** Ramified morphology and increased HLA-DR expression in Iba1-positive microglia. Scale bars indicate 20 µm. **(B)** HLA-DR expression is increased in untreated mgSZ and in LPS-treated mgCTR in comparison to untreated mgCTR. Ordinary two-way ANOVA followed by Tukey's post-hoc multiple comparisons test, n>25. **(C)** LPS treatment induces enhanced Iba1 expression. Ordinary two-way ANOVA followed by Sidak's post hoc multiple comparisons test, n>25. **(D)** TNFα secretion is increased after LPS treatment. Ordinary two-way ANOVA followed by Tukey's post hoc multiple comparisons test, n>15. Error bars are s.e.m., $p<0.05$ *, $p<0.01$ **, $p<0.001$ ***.

3.4.3. RNA expression profiling confirms microglial phenotype

RNA sequencing of differentiated microglia cells was performed to confirm microglial phenotypes at the RNA expression level. Therefore, at least $1x10^6$ microglia or iPSC as control were pelleted and shipped to CeGaT GmbH, Tübingen, for further processing. Total RNA sequencing, normalization of read counts and determination of log2 fold changes (log2FC) comparing deregulated genes in microglia compared to iPSC revealed strong upregulation of several microglia-specific genes proving microglial identity of differentiated cells (Figure 14). The raw count of reads was added up by the factor 1 to be able to determine the log2FC for visualization of specific changes, when zero reads were measured in the undifferentiated iPSC control (FPKM+1: fragments per kilo base million reads + 1). For raw read data and log2FC(FPKM+1) please refer to Supplementary Table 1.

Previously published results identified a panel of highly specific microglia signature genes expressed in iPSC-derived microglia, blood-derived microglia-like cells, primary isolated adult microglia or primary fetal microglia like *Tmem119*, *P2ry12*, *Gpr34*, *Trem2, Mertk* and *Pros1* [110, 130-136]. RNA expression level analysis of all differentiated microglia compared to undifferentiated iPSC revealed a decrease in expression level of pluripotent stem cell markers like *Klf4*, *Lin28a*, *Pou5f1* or *Sox2* and a basal expression of microglia markers like *P2ry12*, *P2ry13, Trem2* or *Tmem119* (Figure 14).

Hierarchical clustering of differentiated microglia for donors CTR1, SZ1, SZ2, SZ4 and SZ5 identified two subsets of microglia (Figure 14, Supplementary Figure 3). Clustering based on expression of microglia-related genes revealed that microglia derived from patients SZ1 and SZ4 (mgSZ1 and mgSZ4) clustered separately in comparison to mgCTR1, mgSZ2 and mgSZ5). Microglia from donors SZ1 and SZ4 showed a higher expression level of microglia signature genes, especially for genes involved in maintaining homeostasis within the CNS (*Siglec7/12/14*) [138], complement system associated and related regulatory genes (*C1qa-c*, *C2*, *C3* or *Vsig4*) or genes correlating with an increased immune response (*Ccl2-4*, *CD14*) [132]. As expected, the expression levels of genes like *P2ry12*, *Olfml3*, *Hexb* or *Tgfbr1* that are usually upregulated not until adolescence, were low in all iPSC-derived microglia [136].

Myeloid differentiation resulted in microglia expressing unique signature markers that resemble expression patterns of fetal or newborn microglia. These findings underline and represent how iPSC-based differentiation protocols give rise to young, premature microglia and that iPSC-based model systems mimic the early cellular development and physiology.

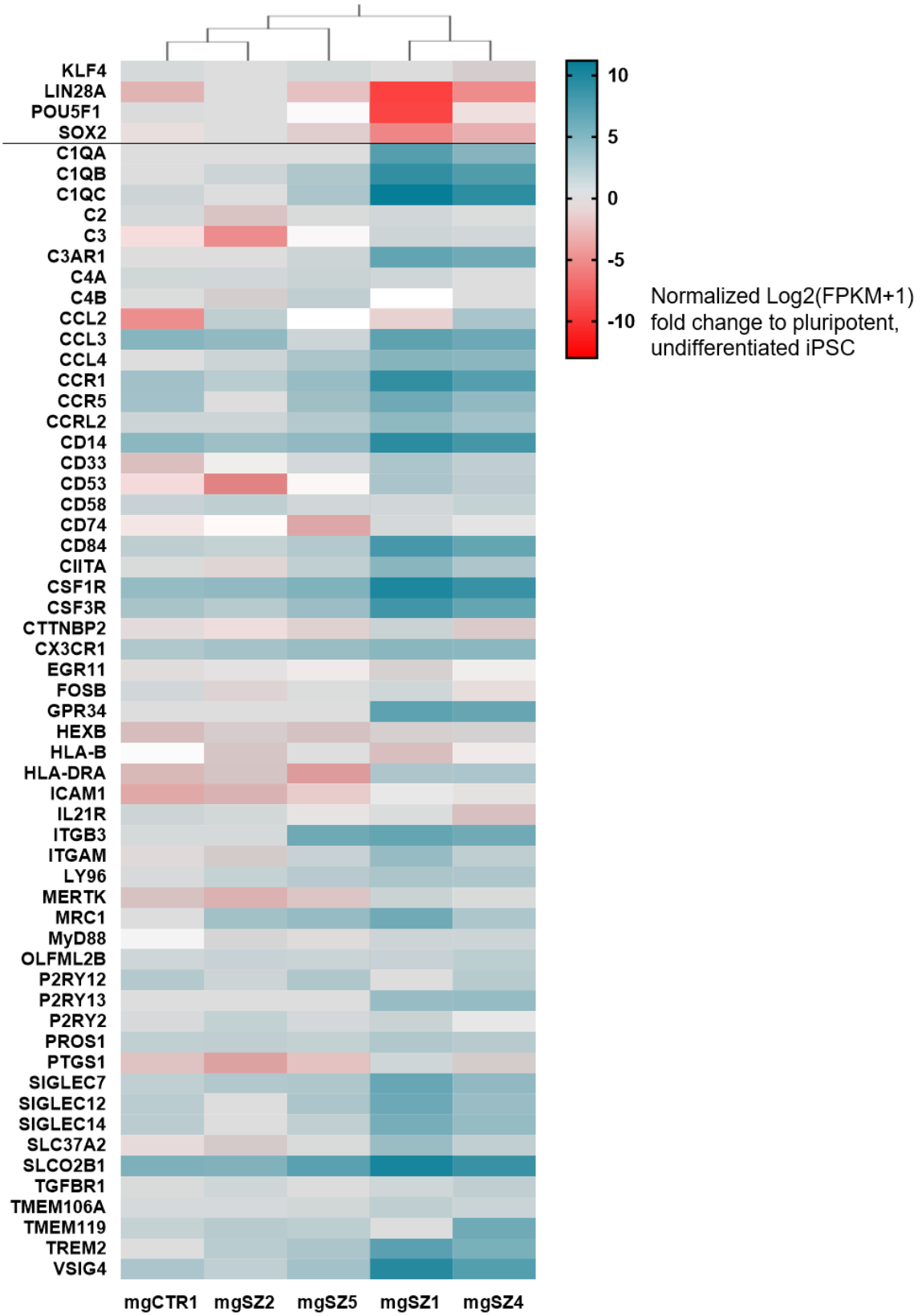

Figure 14. Gene expression analysis revealed upregulation of microglia-specific genes in differentiated microglial cells. Heat map representation of log2 fold change (log2FC) was calculated comparing microglial RNA to RNA derived from undifferentiated iPSC only cultures (FPKM+1). RNA sequencing and bioinformatical analysis was performed by CeGaT GmbH, Tübingen.

3.5. Pathological phenotypes of microglia-neuron interactions

Co-cultures of microglia, neurons and murine astrocytes were established and optimized regarding composition, individual cell densities, culture medium and co-culture duration. Upon co-seeding of microglia at day 16, medium was changed to microglial differentiation medium that proved to be optimal for viability and functionality of all cell types. Microglia-neuron-astrocyte co-cultures were incubated for 72 hours. The pan-microglial marker Iba1, GFAP for astrocytes and MAP2 staining for neurons were used throughout this study for distinct labelling of the three different cell types (Figure 15).

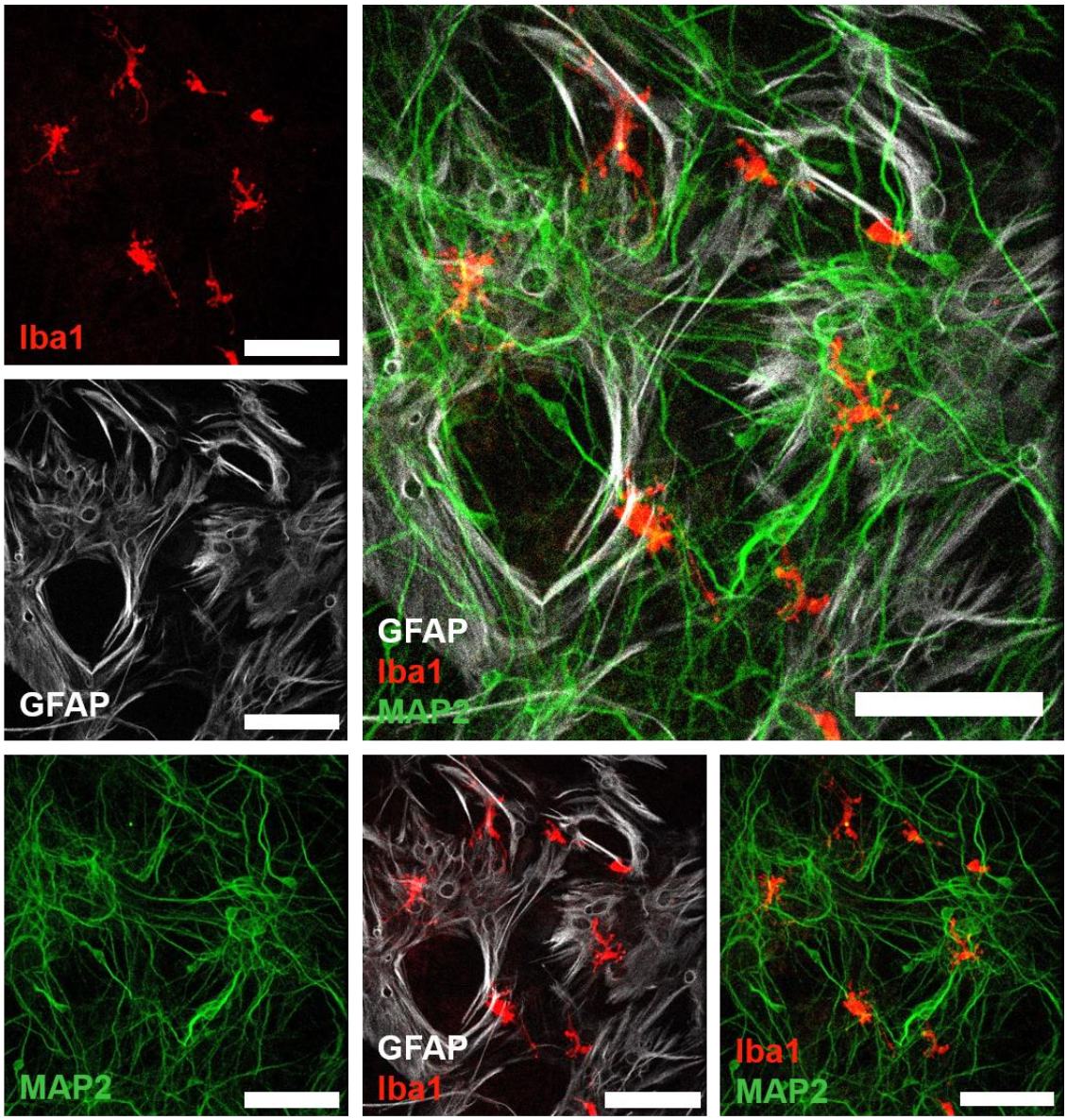

Figure 15. Different cell types can be visualized in a reliable and reproducible way using specific antibodies in co-culture of iPSC-derived microglia and neurons and murine astrocytes. Microglia were stained using Iba1, astrocytes were stained using GFAP and MAP2 was used to stain neurons. Scale bars indicate 100 µm.

Donor-specific Syn1 spots were determined and normalized to healthy control clone CTR1. Syn1 spots were significantly reduced in all four analyzed SZ clones separately, with clone SZ2 having the lowest amount of Syn1 spots consistently throughout all replicates. The two control clones CTR3 and CTR4 showed no significant differences in Syn1 spot density compared to CTR1. Group comparison of pooled control or patient-specific clones confirmed the overall significant tendency that synaptic density was reduced in SZ-derived pure mono-cultures of hNGN2-induced glutamatergic neurons.

In all subsequent experiments, always one clone per donor were included in differentiations into microglia and neurons derived from control donors (CTR1, CTR3, CTR4) or patients with schizophrenia (SZ1, SZ2, SZ4, SZ5). Analyzed data from three control clones or from five patient clones were pooled together to determine disease-specific phenotypes. Donor-specific phenotypes were not further evaluated as initial experiments, as synaptic density or microglia-dependent decrease of synaptic density, did not reveal any significant differences among donors (Figure 10, Figure 16).

3.5.1. Co-Culture of neurons and microglia leads to significant decrease in synaptic density

Aberrant synaptic pruning and an increased inflammatory response has been reported for microglia derived from schizophrenia patients in iPSC-based models [71, 110]. While those model systems relied on co-cultures of peripheral blood monocyte-derived microglia-like cells and iPSC-derived neurons, the co-culture model used during this study is the first one to study microglia-neuron interactions in a full iPSC-based model.

iPSC-derived microglia and neurons were co-seeded on day 16 of each individual differentiation and co-incubated for 72 hours. Microglial impact on synaptic density was determined by Syn1 spot detection on MAP2-positive networks (Figure 16A) and data was normalized to neuronal cultures of healthy control neurons without microglia (nCTR only). Syn1 spot density was significantly reduced by the presence of microglia (Figure 16B). Interestingly, synaptic reduction was significantly more profound by addition of SZ-derived microglia (mgSZ) compared to CTR-microglia (mgCTR), independent of the neuronal origin (nCTR or nSZ). However, the comparison of control and SZ-microglia was only significant when cultured on CTR-neurons, not on SZ-neurons.

To compare donor-dependent effects of microglial influence on synaptic density, microglia derived from three healthy and five patient-derived clones were analyzed individually and compared (Figure 16C). All CTR-microglia showed the tendency to reduce the amount of Syn1

spots independent of the neuronal culture by roughly 10-12 %, while neuronal co-culture with SZ-microglia revealed by 20 % decreased numbers of Syn1 spots.

iPSC-based co-culture of microglia and neurons revealed that addition of microglia directly or indirectly influences synaptic stability and induces a decrease of presynaptic Syn1 positive structures. Microglia derived from patients with schizophrenia induced a more extensive decline in synaptic density compared to control microglia in healthy control or patient-derived neuronal networks.

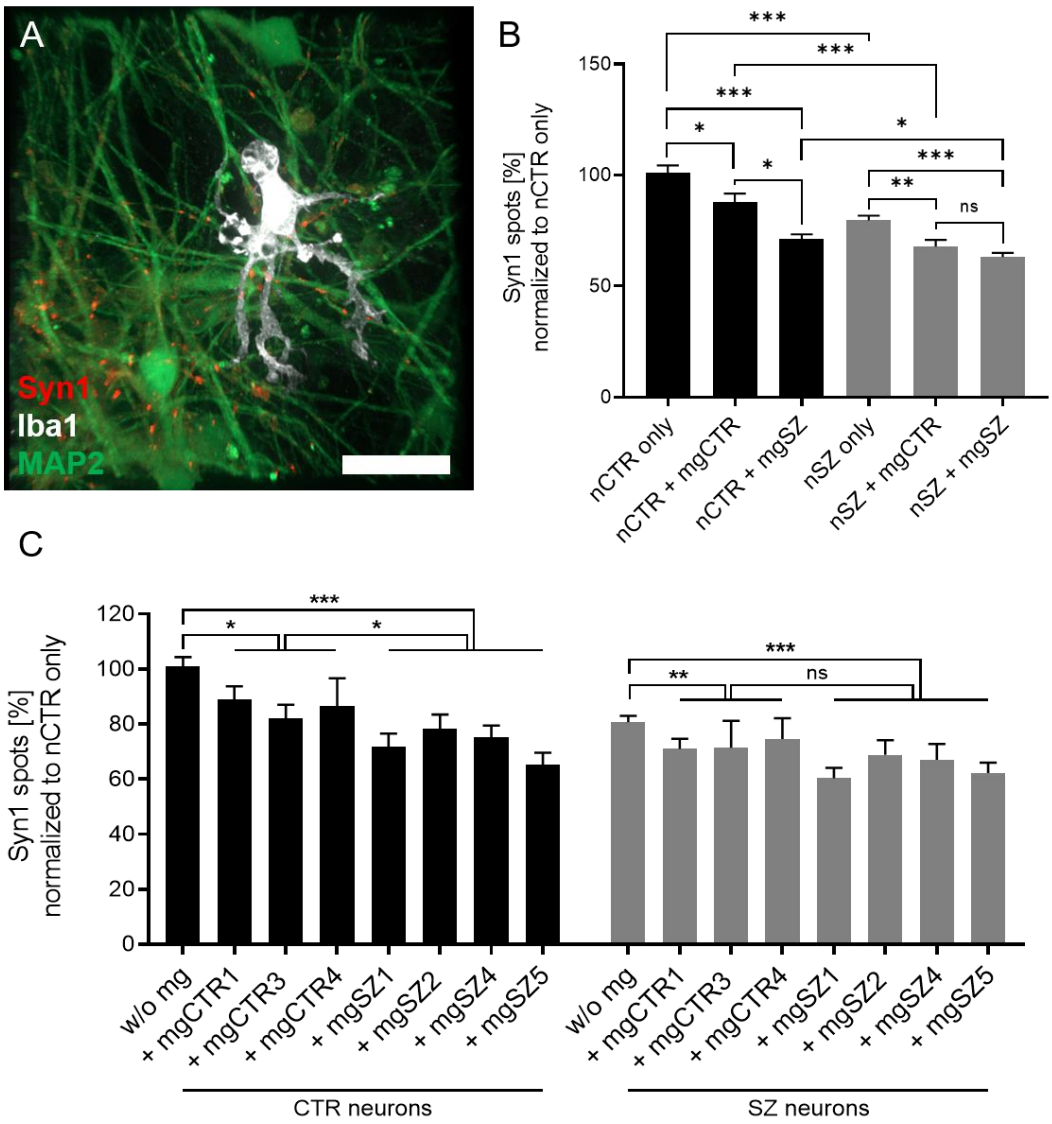

Figure 16. Microglia-neuron interactions resulted in decreased spot density. (A) Representative image acquired using confocal laser scan microscopy depicting Iba1-positive microglia on a MAP2- and Syn1- positive neuronal network. Scale bar indicates 20 µm. **(B)** Co-culture of healthy control microglia (mgCTR) or SZ-microglia (mgSZ) on healthy control neuronal networks (nCTR) or SZ-derived neuronal networks (nSZ) induced reduction of Syn1 spot density. Data is normalized to nCTR only. Kruskal-Wallis Test with Dunn's post hoc multiple comparisons test, H(5)=120.5, n>135. **(C)** Visualization of donor-dependent microglial effects of three healthy CTR-microglia (mgCTR1-3) and four SZ-microglia (mgSZ1,2,4,5) clones on CTR- or SZ-neurons. Data is normalized to nCTR only. Group-comparison using ordinary two-way ANOVA followed by Dunnett's post-hoc multiple comparisons test, n>50. $p<0.05$ *, $p<0.01$ **, $p<0.001$ ***, ns = not significant. Error bars are s.e.m.

3.5.2. Conditioned medium has no effect on synaptic density

The decline of synaptic density may be an effect of direct cell-cell interactions between microglia and neurons or can be the reaction to the presence of pro-inflamamtory cytokines, hormones or other soluble factors that have been secreted into the shared culture medium by activated microglia. To test this hypothesis, neuronal cultures were exposed to conditioned medium from previous co-cultures of intra- and inter-disease specific combinations of neurons and microglia at day 19. No further microglia were added to the neuronal culture. However, for better and easier comparison, direct co-cultures of differentiated microglia and neurons were analyzed in parallel to be able to evaluate possible changes in Syn1 spot density.

Cultivation of neuronal cultures with supernatants from previous co-cultures induced no significant changes in neuronal Syn1 spot density (Figure 17). Direct co-cultures over the same time period confirmed again the preliminary results of microglia reducing presynaptic structures.

Therefore, the decline in synapse density was suggested to be directly mediated by the active presence of microglia and their close interactions with neuronal structures. Plasticity and stability of presynaptic structures was not affected by soluble factors or cytokines that had been secreted by microglia into the supernatant beforehand.

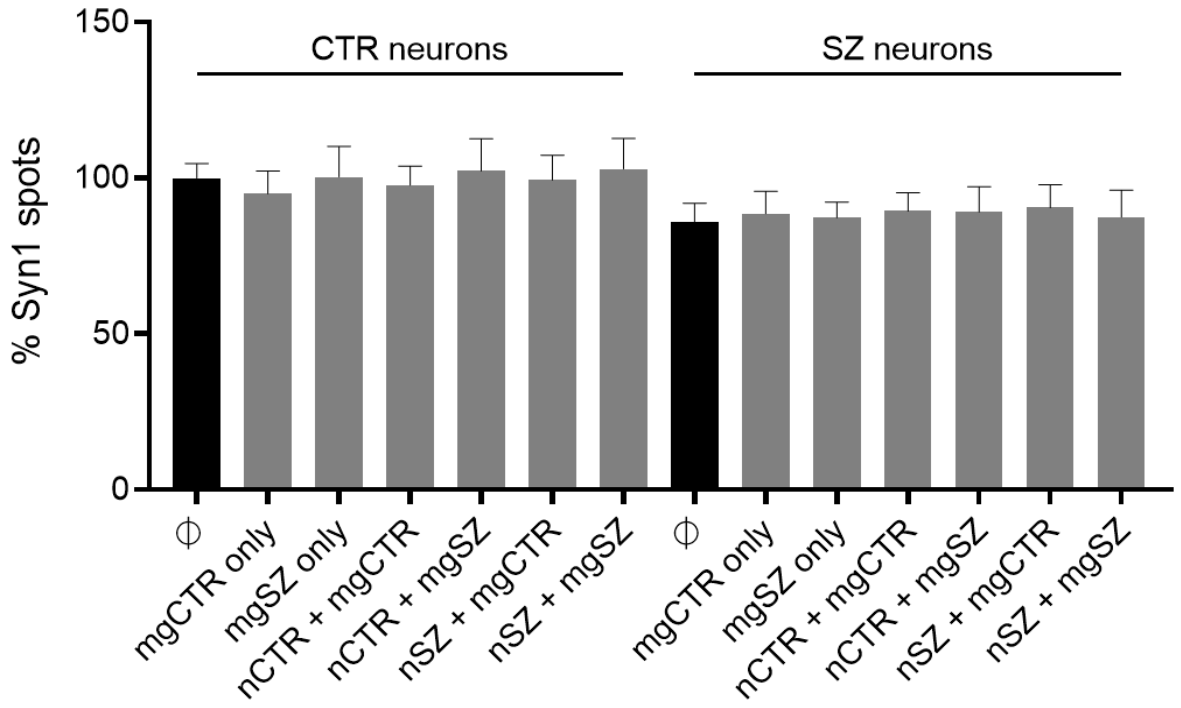

Figure 17. Syn1 spot density is not affected after incubation of neuronal networks with conditioned medium from previous co-culture experiments. CTR or SZ neurons were treated without any supernatant, here shown as black bars, or with conditioned medium from previous co-culture combinations of CTR and SZ neurons and microglia, here shown as grey bars, n>25.

3.5.3. Synaptic pruning is increased in patient-derived microglia

Direct cell-cell contact was found to be responsible for decreased numbers of Syn1 spots after co-culture of neurons with microglia. Alzheimer's Disease studies in mouse models visualized active engulfment of synaptic structures and elimination by activated microglia [79] and iPSC-based models identified increased synaptic elimination by microglia-like cells derived from patients with schizophrenia [71]. To understand if iPSC-derived microglia actively engulfed and eliminated presynaptic structures in our co-culture model, fixed microglia-neuron co-cultures were additionally stained against the pan-microglial marker Iba1 (Figure 18A). Surfaces for Iba1 positive microglia were generated and a mask for the specific Syn1 signal within individual microglia was generated. Individual Syn1 spots within microglia were binarized after thresholding (Figure 18B). Syn1 spots inside microglia were clearly perceptible as phagocytosed structures and distinguishable from Syn1 spots that still co-localized to MAP2 positive dendrites and had not been phagocytosed (Figure 18C). As control, microglia that had been cultured alone without neuronal networks were stained negatively against Syn1.

Three different parameters were applied for assessment of synaptic elimination of iPSC-derived microglia. Changes in Syn1 mean fluorescence intensity (MFI) of whole Iba1 positive microglia determined synaptic specificity of phagocytosis. Here, the Syn1 MFI fold change of co-cultured microglia to Syn1 spot negative mono-cultures of microglia was determined (Figure 18D). Microglia derived from patients with schizophrenia displayed a slight, but not significant, increase in Syn1 MFI compared to CTR-microglia, when cultivated together with CTR-neurons. Cultivation of CTR- or SZ-microglia on SZ-neurons induced for both combinations a significantly increased Syn1 MFI compared to each microglia cultured on CTR-neurons.

Additionally, microglia positive for at least one Syn1 spot were counted as phagocytosing cells resulting in a percentage of Syn1 positive cells compared to not actively phagocytosing Syn1-negative microglia that gave hints about the overall phagocytosis rate. A higher percentage of Syn1 positive cells was detected for SZ-microglia compared to CTR-microglia (Figure 18E). Equally to the mean fluorescence changes in Syn1 expression, culture of microglia on SZ-neurons slightly increased the percentage of Syn1 positive cells compared to microglia cultured on CTR-neurons.

The total amount of phagocytosed spots was a third approach to assess Syn1 positive synaptic structures in association with activation of microglia. Quantification of the total amount of phagocytosed Syn1 spots within Syn1 positive microglia showed slight but not significant tendencies that SZ-neurons promote synaptic pruning rather than CTR-neurons (Figure 18F).

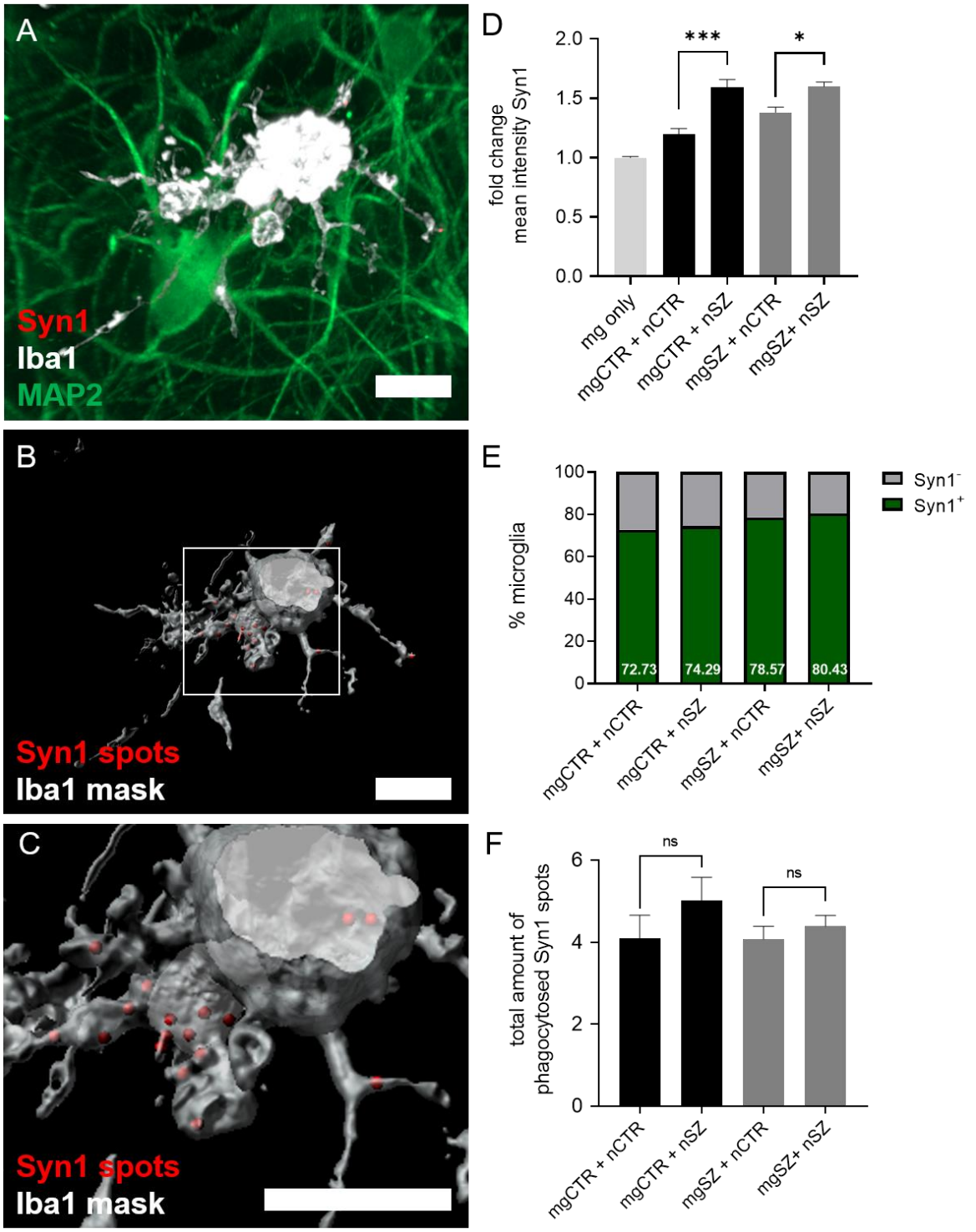

Figure 18. Quantification of synaptic elimination by microglia. (A) Representative confocal laser scan z-stack of ramified Iba1-positive microglia surveying the MAP2-positive neuronal environment. Scale bar indicates 20 µm. **(B)** Processed Imaris surface mask of Iba1-positive microglia with intracellular Syn1 spots. Scale bar indicates 20 µm. **(C)** Magnification of (B) to visualize intracellular Syn1-positive spots representing engulfed and phagocytosed synaptic structures. Scale bar indicates 20 µm. **(D)** Quantification of mean fluorescence intensity (MFI) of Syn1 signal across whole microglial cells. MFI is calculated as fold change referring to microglia not cultured on neurons (mg only). Kruskal-Wallis Test with Dunn's post hoc multiple comparisons test, $H(4)=40.25$, $n>35$. **(E)** Microglia positive for at least one Syn1 spot were considered as Syn1-positive phagocytosing cells. Determination of percentage of Syn1-positive or negative microglia. **(F)** Quantification of the total amount of phagocytosed spots within microglia. Kruskal-Wallis Test with Dunn's post hoc multiple comparisons test, $n>35$. Error bars are s.e.m., $p<0.05$ *, $p<0.01$ **, $p<0.001$ ***, ns = not significant.

To evaluate synaptic elimination by microglia, all three parameters need to be evaluated together. In this study, our co-culture model indicated that synaptic pruning is increased by SZ-derived neuronal cultures compared to CTR-neurons for both microglial cultures. Additionally, we found that activated SZ-microglia take up more synaptic structures than CTR-microglia. To conclude, both cell types, microglia and neurons, influence each other through complex intracellular mechanisms, while SZ-cultures reveal increased synaptic decline compared to CTR-cultures.

3.5.4. Co-culture activates microglia significantly but independent of neuronal pathological phenotype

Inflammatory processes involving the complement system are thought to contribute to aberrant synaptic pruning in schizophrenia [71]. Microglial mono-cultures identified HLA-DR but not Iba1 expression in SZ-microglia being increased compared to CTR-microglia (Figure 13b). To assess the effect of co-culture on the microglial activation status, the mean HLA-DR fluorescence intensity in Iba1 positive microglia was determined (Figure 19A). Co-culture with healthy control or disease-neurons increased microglial activation and HLA-DR expression for CTR- and SZ- microglia significantly compared to microglia mono-cultures (Figure 19B). Likewise, the mean Iba1 expression was significantly increased after co-culture with neurons (Figure 19C). A possible differential effect of CTR- or SZ-neurons on microglial activation was only slightly observable. Control and SZ-microglia showed a slightly, but not significantly lower activation grade when cultured with control neurons than upon co-culture with SZ-neurons. That effect was only detected for Iba1 expression, HLA-DR expression identified no effects of the neuronal culture on microglial activation.

To assess if increased microglial activation came along with increased secretion of pro-inflammatory cytokines, levels of TNFα within the supernatant were determined by ELISA (Figure 19D). Microglia-neuron co-cultures overall increased the release of the pro-inflammatory cytokine TNFα. Cultivation of CTR-microglia on SZ-neurons significantly increased secretion of TNFα in comparison to CTR-microglia cultures with CTR-neurons indicating an increased stimulation of microglia by SZ-neurons. However, this tendency was only slightly detectable for SZ-microglia.

These results suggested that increased synaptic pruning by SZ-microglia is significantly affected by neurons derived from healthy controls or patients with schizophrenia, while the activation state of microglia was increased but not differentially impacted by control or SZ-derived neuronal cultures. Additionally, no significant differences in activation were found for CTR- and SZ-microglia.

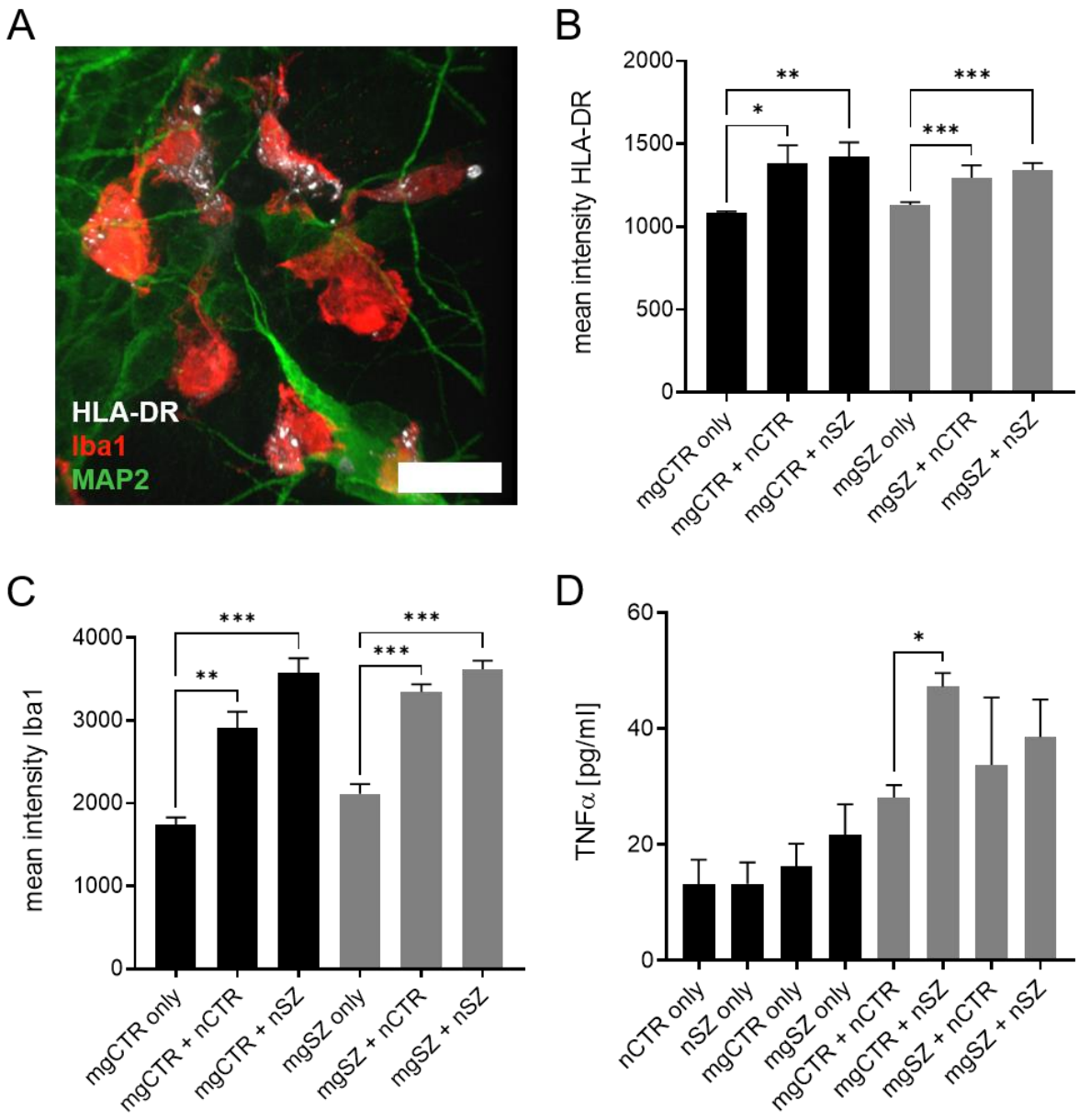

Figure 19. Co-culture significantly increases three aspects of microglial activation. (A) Representative image of HLA-DR staining in Iba1-positive microglia on MAP2-positive neuronal networks. Scale bar indicates 20 µm. **(B)** HLA-DR mean fluorescence intensity (MFI) after co-culture with neurons. Kruskal-Wallis test with Dunn's post hoc multiple comparisons test, $H(5)=54.49$, $n>40$. **(C)** Iba1 MFI after co-culture with neurons. Kruskal-Wallis Test with Dunn's post hoc multiple comparisons test, $H(5)=105.3$, $n>50$. **(D)** Classical sandwich-ELISA for detection of TNFα levels in the supernatant of microglia-neuron co-cultures. Kruskal-Wallis Test with Dunn's post hoc multiple comparisons test, $H(7)=44.50$, $n>25$. Error bars are s.e.m., $p<0.05$ *, $p<0.01$ **, $p<0.001$ ***.

3.5.5. LPS stimulation enhances synaptic elimination, while minocycline treatment partially prevents aberrant pruning

Minocycline is a highly brain-penetrant tetracycline antibiotic that has been proposed as an anti-inflammatory agent with beneficial effects in neuropsychiatric and neurodegenerative disorders [139]. In contrast, LPS is commonly used to activate NFκB mediated signaling pathways and to finally induce pro-inflammatory mechanisms in immune cells [140]. In the context of schizophrenia, LPS is usually used to mimic maternal immune activation in rodent studies [30, 141].

iPSC-derived microglia were pro- and anti-inflammatorily pretreated with 100 ng/ml LPS or 10 µM minocycline, respectively, for 60 minutes, before being washed and co-seeded to neuronal cultures. Co-culture of neurons with LPS-treated microglia resulted in significantly decreased synaptic density as measured by Syn1 spots within MAP2-positive structures in all inter- or intra-disease specific combinations of neurons and microglia (Figure 20).

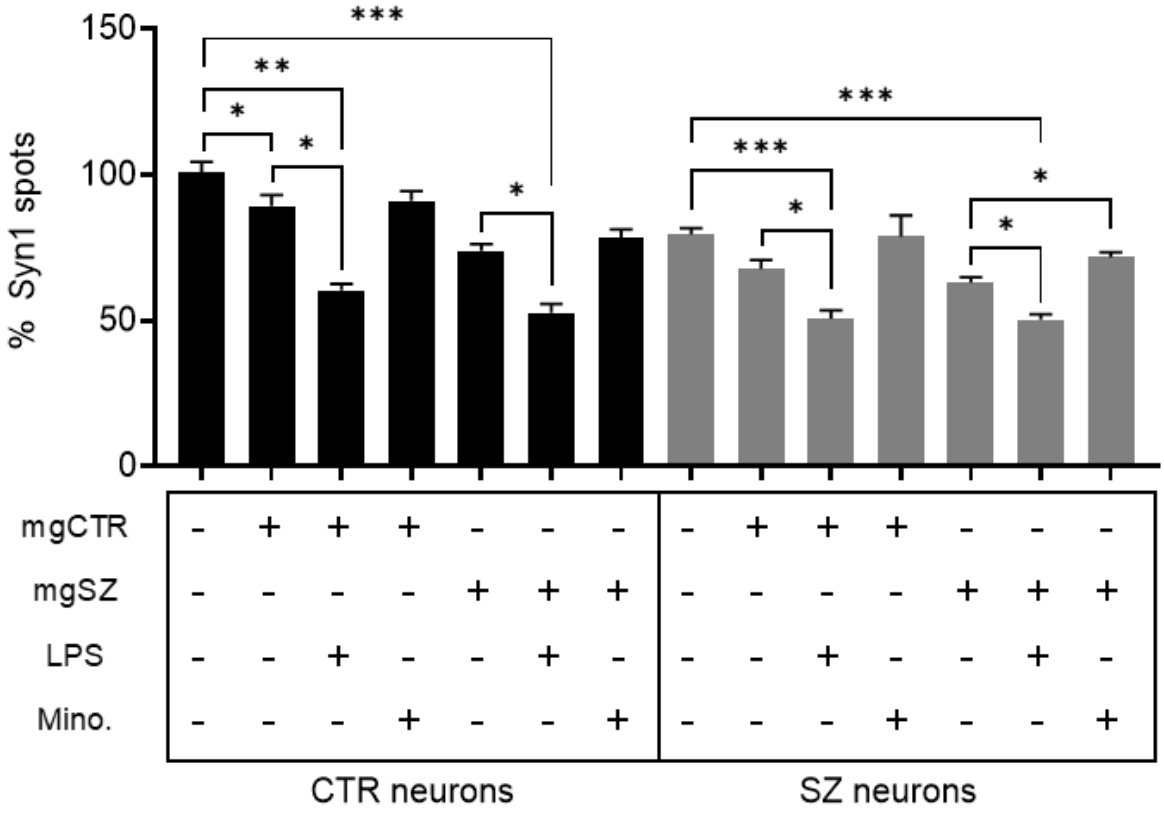

Figure 20. Pro-inflammatory stimulation of microglia increases decline of Syn1-positive synaptic density. Microglia were stimulated for 60 minutes with 100 ng/ml LPS or 10 µM minocycline before being seeded into co-culture with neurons. Syn1 positive spots within MAP2-positive neuronal networks were detected and all values were normalized to healthy control neurons only (nCTR1 only). Kruskal-Wallis test with Dunn's post hoc multiple comparisons test, $H(14)=267.90$, $n>50$, error bars are s.e.m., $p<0.05$ *, $p<0.01$ **, $p<0.001$ ***.

Most interestingly, minocycline treatment of SZ-microglia co-cultured on SZ-neurons (71.68 % Syn1 spots) could significantly rescue the decrease of Syn1 spots mediated by untreated SZ-microglia (63.07 % Syn1 spots, $p = 0.0129$). By contrast, LPS-treatment exacerbated the decline in synapse density significantly. For all other intra- or inter-disease combinations, anti-inflammatory minocycline priming slightly, but not significantly, enhanced Syn1 spot density compared to untreated microglia.

To understand if the decline in synaptic spot density was associated with over-activated microglia, several parameters to determine synapse elimination and microglial activation were analyzed. The effect of pro- or anti-inflammatory priming on synaptic phagocytosis by microglia was assessed by measurement of fold changes in mean fluorescence intensity of Syn1 signal, the total amount of Syn1 positive spots within microglia and the percentage of actively phagocytosing cells.

LPS stimulation increased the mean Syn1 fluorescence intensity for CTR-microglia cultured on CTR- and SZ-neurons compared to untreated microglia (Figure 21A). The *per se* increased Syn1 MFI in untreated SZ-microglia compared to untreated CTR-microglia was slightly increased after LPS stimulation when cultured on CTR-neurons but cultivation on SZ-neurons did not further intensity this effect. This may be caused by a maximal SZ-microglia activation state induced by present SZ-neurons and LPS stimulation could not further increase microglial activation. Interestingly, minocycline application reduced the Syn1 MFI of CTR- and SZ-microglia cultured on SZ-neurons compared to untreated microglia. This tendency was also observed but not significant for microglia cultured in combination with CTR-neurons indicating that priming of microglia with minocycline inactivates microglia and leads to decreased phagocytosis.

Results were confirmed when analyzing the total amount of microglia with at least one intracellular Syn1-positive spot. Those cells were considered as actively phagocytosing cells. LPS pre-treatment of microglia led to significantly increased uptake of Syn1 structures for all microglia-neuron combination (Figure 21B). Minocycline had no to only small effects on the total amount of phagocytosed Syn1 spots. Microglia pre-treated with minocycline showed a minor decrease of phagocytosed spots compared to untreated microglia. Disease-specific phenotypes or combination-dependent differences were not observable in the total amount of phagocytosed spots. LPS treatment increased the rate of phagocytosis, but variability among cells and replicates was high and must be considered when interpreting these results.

Likewise, LPS treatment led to 100 % Syn1-positive and actively phagocytosing CTR microglia, while only 83 % of all untreated CTR microglia took up Syn1-positive structures from CTR-neurons (Figure 22A). Here, minocycline treatment of CTR-microglia had the strongest effect by decreasing the percentage of actively phagocytosing cells down to 50 % cultured on

CTR-neurons. The percentage of untreated CTR-microglia phagocytosing structures from SZ-neurons was low (59 %), while LPS treatment likewise increased the percentage up to 100 %. Minocycline treatment had no effect (62 %) on CTR-microglia in this case. For SZ-microglia, LPS treatment led to minor increased rates of phagocytosis on CTR-neurons (89 %) or SZ-neurons (79 %) compared to untreated microglia, but the difference was by far not as pronounced as for CTR-microglia. Likewise, minocycline application only slightly reduced the percentage of actively phagocytosing SZ-microglia on CTR- or SZ-neurons.

Microglial activation was assessed by measurement of the mean Iba1 intensity. As expected, LPS treatment led to significantly increased levels of Iba1 for all microglia-neuron combinations, while minocycline treatment did not significantly affect Iba1 intensity (Figure 22B). Differences in Iba1 intensity were not observable between CTR- and SZ-microglia.

Microglial activation and synaptic pruning is largely increased after co-culture of microglia and neurons when microglia are pre-treated with LPS. Mean Syn1 intensity, the total amount of Syn1 spots and the percentage of Syn1-positive microglia is increased in all control- or patient-derived microglia-neuron combinations after LPS treatment. Most interestingly, minocycline treatment of SZ-microglia cultured in combination with SZ-neurons reversed effects of excessive pruning of untreated microglia (Figure 20). Additionally, minocycline application led to significantly decreased mean Syn1 intensity in microglia cultured on SZ-neurons compared to untreated microglia.

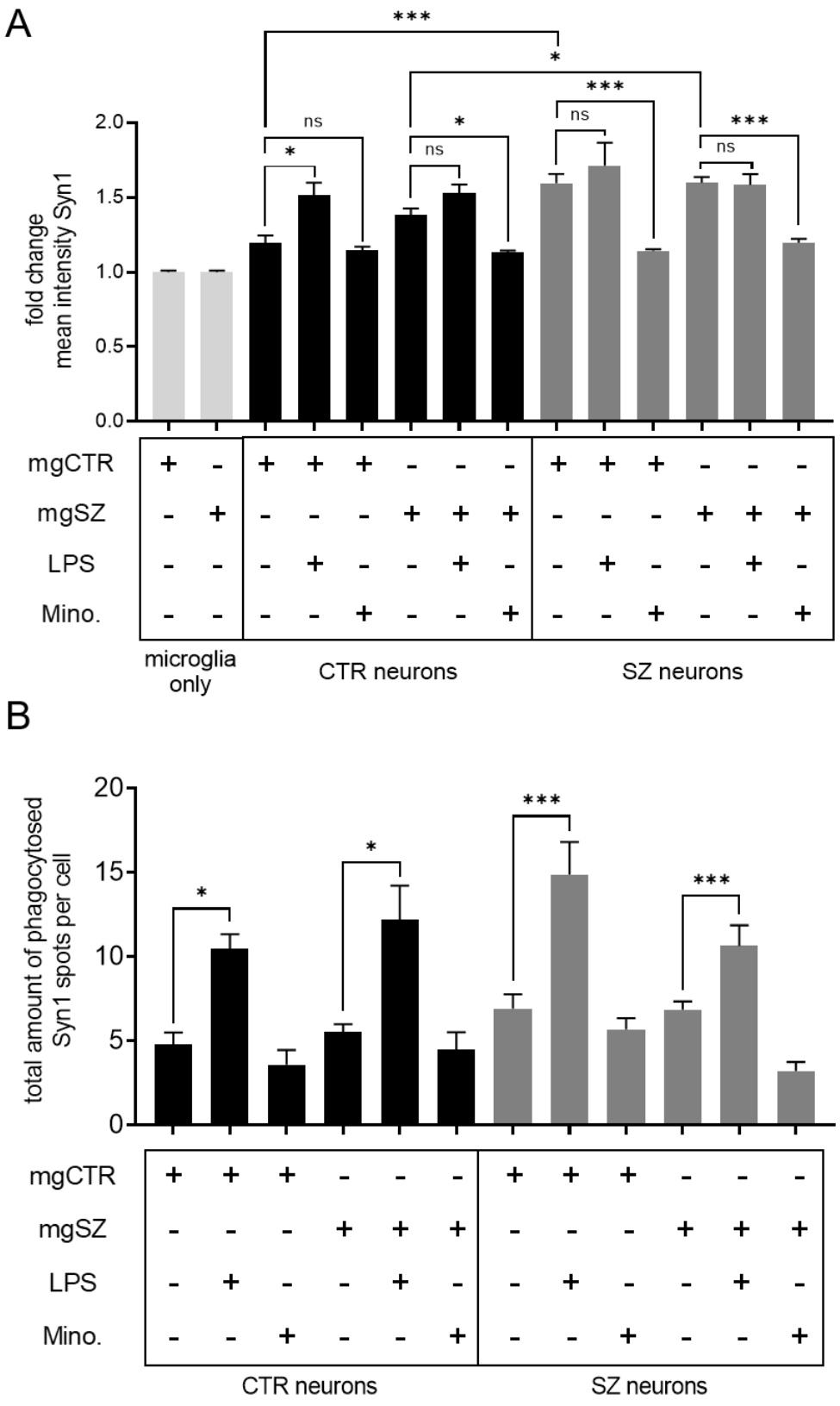

Figure 21. Pro-inflammatory priming increases phagocytosis, while anti-inflammatory inhibits synaptic elimination. (A) Quantification of Syn1 MFI across whole primed microglial cells. MFI is calculated as fold change referring to microglia that were not cultured on neurons. Kruskal-Wallis test with Dunn's post hoc multiple comparisons test, H(12)=116.5, n>35. **(B)** Quantification of the total amount of intracellular, phagocytosed spots within microglia. Kruskal-Wallis Test with Dunn's post hoc multiple comparisons test, H(12)=75.36, n>35, error bars are s.e.m., p<0.05 *, p<0.01 **, p<0.001 ***.

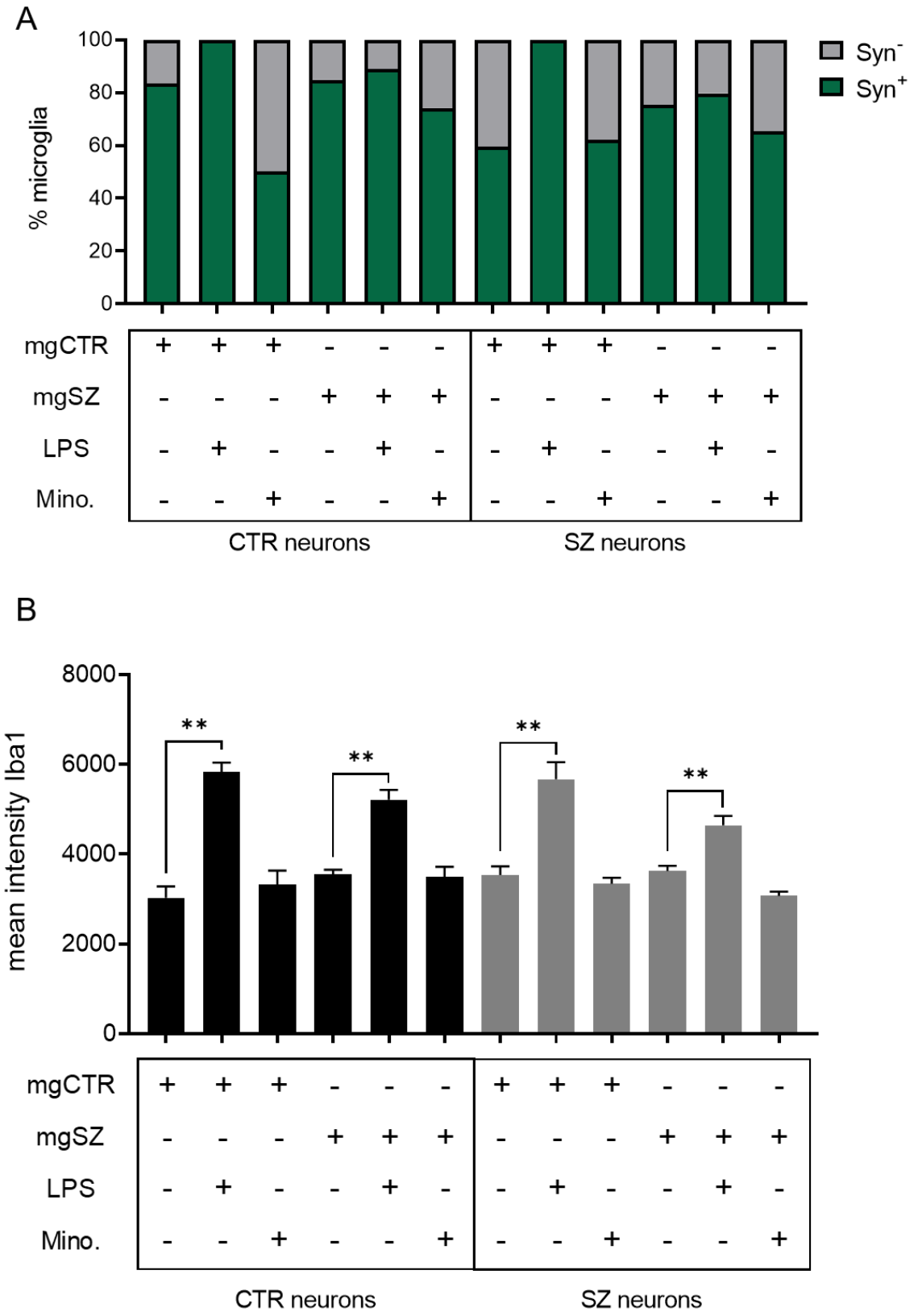

Figure 22. Priming of microglia specifically changes microglial phagocytosis and activation patterns. (A) Primed microglia positive for at least one Syn1 spot were considered as Syn1-positive phagocytosing cells. Determination of percentage of Syn1-positive or negative microglia after co-culture with neurons, n>50. **(B)** Iba1 MFI across whole microglia is increased in primed microglia co-cultured with neurons. Kruskal-Wallis Test with Dunn's post hoc multiple comparisons test, H(11)=93.46, n>50, error bars are s.e.m., p<0.05 *, p<0.01 **, p<0.001 ***.

4. Discussion

Genetic evidence, results of post mortem tissue studies and recently also iPSC-based model systems indicate neurodevelopmental deficits and neuroinflammation as two central implications in the pathology of schizophrenia.

For the first time, iPSC-derived neuronal cultures were able to discriminate pathological phenotypes of schizophrenia and autism spectrum disorder by functional analysis of intracellular calcium signaling. Analysis of developmental pathologies revealed decreased mean neurite lengths and decreased synaptic density in neuronal cultures from patients with schizophrenia compared to healthy controls. Co-culture of neurons and microglia subsequently revealed increased synaptic elimination by SZ-microglia accompanied by increased microglial activation compared to control microglia. Our results suggest that the synaptic loss found in schizophrenia patients relies on the reciprocal interactions between pathological phenotypes of microglia and neurons.

4.1. Functional discrimination of neuronal SZ and ASD disease phenotypes *in vitro*

Studying human neuropsychiatric and neurodevelopmental disorders *in vitro* is limited by the lack of robust and reproducible human test systems. iPSC-based neuronal systems and specific assays may ultimately help to discriminate neurological pathologies from each other and lead to the development of specific patient-derived test systems for drug discovery. Neurodevelopmental disorders, such as schizophrenia (SZ) and autism spectrum disorder (ASD) share several pathological deficits that are characterized by impaired growth and development of the central nervous system. A distinct discrimination of SZ and ASD in patients and patient-derived *in vitro* model systems is however difficult. Transcriptome profiling of SZ and ASD patients is a first attempt to discriminate both disorders based on differentially deregulated genes compared to healthy controls. Functional *in vitro* assays to model early development of impaired synaptic and neuronal connectivity are needed to better dissect both disorders, to find disease-specific biomarkers and to ultimately find treatment opportunities that are optimal for each individual disease.

Neurite outgrowth, length and arborization as well as reduced synaptic structures in form of PSD-95 spots have been reported to be compromised in SZ and ASD-derived neurons [46-48]. However, functional differences between both diseases were not detectable. Neurite outgrowth is a simplified 2D neuronal assay for high throughput compound screening and a valuable parameter to evaluate neuronal development. The assay's short duration of only four days and subsequent fully automated analysis for high content image acquisition make it

feasible for large scale studies to examine promoting or inhibiting effects of drugs and compounds on neuritogenesis, network arborization and activity.

In a first experiment during this study, determination of the mean neurite length (reduced by 14 %) and the percentage of iPSC-derived neurons with outgrown neurites (reduced by roughly 10 %) confirmed previously reported reduced outgrowth in SZ-derived neurons [48], indicating impaired neuritogenesis and neuronal maturation in patients with schizophrenia. However, neurite outgrowth was not a suited parameter to determine the impact of antipsychotic drug treatment on neurite development over 72 hours. Application of routinely used drugs clozapine, haloperidol or olanzapine to treat positive symptoms in SZ-patients had no impact on the mean neurite length in control or SZ-neurons. Additionally, the percentage of SZ-neurons with neurites was not affected by drug treatment compared to DMSO treated control cells. Haloperidol and clozapine treatment induced an increased fold change of neurons forming neurites only in control neurons. By contrast, antipsychotic drug treatment showed no effects on impaired SZ-neurons. Our results suggest that determination of mean neurite lengths is not a suited parameter for drug screening using cells derived from patients with schizophrenia.

Impaired neurite development and network formation is directly linked with reduced neuronal maturation, synaptic connectivity and neuronal activity. Intracellular calcium imaging using calcium sensitive fluorescent dyes is a method for visualization of calcium fluxes within single, spontaneously active neurons. In contrast to previously published results [46], comparative pattern analysis of intracellular calcium levels in the course of this study identified decreased peak frequency with significantly increased peak area and width (FWHM) in SZ-derived neurons compared to control cells [48]. The peak amplitude ($\Delta F/F0$) was unaffected in SZ-derived neurons, whereas ASD-neurons showed a significantly reduced peak amplitude. In contrast to SZ-neurons, peak frequency was unaffected but peak area was slightly increased in ASD-neurons compared to CTR-neurons.

For the first time, intracellular calcium signals could discriminate phenotypes of schizophrenia and autism spectrum disorder *in vitro*. Single cell calcium imaging proved to be a more sensitive parameter than determination of synaptic cluster density or neurite outgrowth analysis to dissect both neuropsychiatric disorders.

Interestingly, comparative RNA sequencing revealed for one clozapine-treated patient (SZ2) a significant upregulation of a set of genes involved in MHC class II processing and presentation. Clozapine treatment of unaffected, healthy control neurons revealed the same upregulation of genes. A direct association of clozapine treatment and MHC class II mRNA deregulation is not known. MHC class II expression in neurons may be a sign of the system’s immaturity, as human fetal neuronal progenitor cells and neural stem cells have been shown to express MHC

class II in contrast to mature neuronal networks, for which MHC class II expression never has been reported [143, 144]. Non-immune association of the MHC class I complex have however been described extensively in the context of schizophrenia involving processes of synaptic plasticity and neuronal maturation [145].

However, aiming to reproduce these findings with our newly, non-invasively reprogrammed iPSC and neurons could not confirm an upregulation of MHC class II in cells derived and differentiated from this one specific patient. Most likely, MHC class II deregulation was an artefact of the invasive reprogramming method used during the first approach of reprogramming, as retroviral integration into the host's chromatin may have affected the chromosomal loci harboring MHC class II associated and deregulated genes by introducing changes in gene expression or somatic mutations [11, 146, 147].

4.2. Reprogramming of patient-derived fibroblasts into iPSC

The urge for a new reprogramming approach arose when iPSCs, previously reprogrammed by retroviral transduction, lost their typical iPSC characteristics. The compact morphology of iPSC growing as dense colonies with clear edges and the ability to form embryoid bodied, necessary for differentiation, were lost and expression of iPSC surface markers such as SSEA-4 and TRA-1-60 declined over time and with increasing passage number. A new, non-integrating reprogramming approach was chosen that excluded the possible induction of *de novo* mutations caused by integrating retroviruses. Fibroblast nucleofection with episomal plasmids encoding the four Yamanaka factors was chosen with the addition of two extra plasmids. EBNA1 expression was added to maximize the entry of all expression plasmids needed for reprogramming into the nucleus and additionally, a dominant-negative variant of p53 was combined to reduce apoptosis after electroporation [12].

First iPSC clones appeared after three weeks in culture and monoclonal colonies could be expanded. All generated iPSC clones showed consistent expression of iPSC markers and were capable to be differentiated into all three germ layers. Chromosomal integrity analysis revealed that even though a non-integrating approach was taken, the procedure of reprogramming induced major genomic aberrations in the majority of generated clones.

Although the differentiation efficiency was increased and iPSC clones could easily be handled and cultivated, the insertion of genomic aberrations during reprogramming and expansion was a limiting factor for iPSC culture. Until today, the molecular mechanisms underlying chromosomal changes during iPSC generation remain unknown. It is generally believed that iPSC cultivation *in vitro* increases the risk of introducing cytogenetic mutations that were not found in parental cells [148-150]. Specific and frequently found point mutations in

reprogrammed iPSC clones were caused by transient cell cycle aberrations during mitosis [151]. Strategies to minimize the insertion of genomic abnormalities are currently developed to reduce the number of clones that need to be excluded due to unwanted genomic mutations. It is hypothesized that increased levels of reactive oxygen species occur during reprogramming that cause DNA double strand breaks posing potential mutation sites [152, 153]. Reduction of reactive species during reprogramming by application of antioxidants may be one approach to reduce insertions, deletions or copy number variations in generated iPS cell line [153, 154].

Several generated clones in this study showed minor chromosomal losses or gains, some revealed even losses of whole chromosomes. Any loss, gain or mosaicism was an exclusion factor. One major drawback was finally the outcome of only one healthy control with genomic integrity. In order to have a proper amount of control donors, two healthy clones were included (CTR3.3 and CTR4.3) that both showed a chromosomal gain within chromosome 11 of roughly 60.000-70.000 base pairs. Both clones showed normal stem cell marker expression and were capable to be differentiated into all germ layers. Additionally, synaptic density and microglia function was unaffected in comparison to the one healthy control clone that revealed chromosomal integrity (CTR1.3). For that reason, both additional control clones were included in the subsequent experiments.

However, for future studies additional healthy control clones without chromosomal aberrations have to be included for a sufficient number of control clones. Especially for isogenic mutation experiments or disease studies with a confirmed strong genetic background like schizophrenia, genomic integrity is an inevitable prerequisite and needs to be controlled on a regular basis to ensure the undifferentiated, naïve state of all included iPSC clones necessary for all subsequent differentiation steps and iPSC-based studies.

4.3. Microglia as pro-inflammatory mediators in the early neurodevelopment of schizophrenia

Microglia are mainly considered as the central players during acute CNS inflammation, but additionally microglia have important functions for proper brain development comprising especially synaptic and neuronal organization and tissue homeostasis [155]. The local CNS microenvironment directly influences microglial activity and varies among brain regions and especially among neurological pathologies. Disease-dependent microglial phenotypes are linked to the progression of individual pathologies and severity of symptoms, as the activation of microglia is tightly regulated by molecules, hormones or neurotransmitters released by surrounding cells [156].

Aberrant microglial activation has been reported for several neurodegenerative disorders, such as Alzheimer's disease [157, 158], Parkinson's disease [159, 160], amyotrophic lateral sclerosis [161] or frontotemporal dementia [162], just as a deregulation of microglia has been confirmed in the course of neurodevelopmental and neuropsychiatric diseases [105, 106, 109]. The central goal of this study was the establishment of microglia-neuron co-cultures to increase our understanding of neuroinflammatory processes mediated by reactive microglia in the pathology of schizophrenia.

4.3.1. New established differentiation protocol yields fully functional microglia expressing unique and specific genes

Differentiation of iPSC into microglia followed a recently published protocol for the generation of monocytes and macrophages with slight modifications for the in this study required microglial maturation [123]. Until today, the number of protocols for the generation of microglia from iPSC rises constantly, all varying in duration, media composition and cytokine or growth factor supplementation [133, 163-168]. The advantages of the applied protocol were the easy handling of cells during differentiation, the very precise addition of specific cytokines needed for myeloid induction and short duration of time until first microglial cells were available for use in experiments. Myeloid progenitor cells were differentiated either towards macrophages by high-dose application of IL-6 and later M-CSF or towards microglia by application of IL-34, TGFβ-1 and GM-CSF for one week before seeding cells to neuronal cultures. Supplementation of IL-34 and TGFβ-1 is required for microglia development and maturation and additionally benefits survival *in vitro* [169, 170]. GM-CSF stimulates proliferation in culture and supports immunological functions [171].

Differentiated microglia were functional as shown by phagocytosis of *Escherichia coli*-derived bacterial particles, an enhanced pro-inflammatory response to LPS treatment and positive immunocytochemical stainings for microglial markers TMEM119 and Iba1.

RNA sequencing proved expression of signature genes that are unique to microglia and are not expressed in other cell types of the CNS or other myeloid cells. iPSC-derived microglia resembled fetal or newborn microglia by expressing genes necessary for synaptic remodeling (*C1qa-c* or *C3*), CNS tissue homeostasis (*CD33*, *Siglecs7/12/14*, *Vsig4*) and immune response associated genes (*Csfr1*, *CD74*, *HLA-DRA*) [110, 130-134].

Transcriptome analysis identified no differences in expression levels between microglia derived from healthy control and patients with schizophrenia. This is on one side due to the fact that only one healthy control clone (CTR1.3) was included in transcriptome analysis, as

the other two clones showed chromosomal aberrations and were only partially and under reserve included in this study. Besides, a similar study based on blood monocyte-derived microglia-like cells reported no altered expression between controls and patients [110] in contrast to post mortem tissues that identified upregulation of immune response and phagocytosis associated genes in schizophrenia brain tissues [172]. Naturally, post mortem tissue or biopsy analysis provide microglia isolated from the complex structures of the aged human brain, while microglia-like cells differentiated *in vitro* over a course of only a few weeks rather resemble human embryonal or newborn microglia. Nevertheless, iPSC-derived microglia expressed specific signature genes proving their functional profile and microglial ontogeny.

Additionally, hierarchical clustering after RNA sequencing gave hints about varying maturation states of differentiated microglia indicating that the differentiation of the included clones was not equally efficient among all analyzed clones. Of note, not every single iPSC-based differentiation yields a pure population of fully active and mature microglia. For further optimization of the differentiation protocol, reproducible checkpoint assays to assess and parallelize microglial differentiation and functionality among clones and replicates are needed before seeding microglia into subsequent co-culture systems. One example could be the enrichment of live $CD34^{+}CD45^{+}$ myeloid progenitor cells at day 9 of the differentiation protocol by fluorescence activated cell sorting (FACS) to exclude cells for which induction of mesodermal differentiation was not achieved. Another feasible checkpoint, would be the enrichment of $CD11b^{+}CD45^{low}CX3CR1^{high}$ microglia to obtain enriched microglia with no other remaining myeloid cells, directly before seeding them into co-culture with neurons [173]. However, live cell sorting tends to compromise cellular integrity and viability and enriched microglia should be given the opportunity to recover for several days before seeding into co-culture with neuronal networks. A direct seeding into cell-culture after live cell sorting could lead to varying numbers of viable microglia in the cell culture afterwards and microglia that become apoptotic due to sorting may impact neuron-microglia co-culture interactions and experiment outcome.

To sum up, the protocol used in this study for differentiation of iPSC into microglia yields functional microglia expressing specific genes involved in brain organization, immune response and tissue homeostasis, and appropriate inflammatory responses to pro-inflammatory stimuli. However, the differentiation protocol requires further optimization regarding purity of microglial populations to increase reproducibility of gained results among all donors and differentiations.

4.3.2. Co-culture model reveals aberrant inflammatory properties of differentiated microglia

Synaptogenesis and synaptic pruning describe two constant processes of synapse formation and elimination throughout the whole human life that are mandatory and necessary for strong brain development and network refinement. Especially during childhood and until late adolescence, weak and redundant synapses are marked with opsonins, so called “Eat-me” signals for microglia to engulf and eliminate tagged synapses. Aberrant synaptic pruning by activated microglia under the influence of the complement system has been reported for human schizophrenia studies [71, 109, 110].

In first experiments during this study, synapsin1 (Syn1) positive presynaptic density was demonstrated to be significantly reduced in all neuronal mono-cultures derived from patients with schizophrenia compared to control cells. These results confirmed previous iPSC-based findings [47, 174] and post mortem brain tissue analysis [42, 43] of reduced synaptic density in schizophrenia patients *in vitro* and *in vivo*.

Addition of iPSC-derived microglia to glutamatergic networks led to further decreased synaptic density and concomitantly, increased microglial phagocytosis and activation, confirming active microglial elimination of synaptic structures. To confirm these results and answer the question if active cell-cell contact is the cause of the decline in synaptic density, neuronal cultures were incubated with conditioned medium derived from previous co-cultures. In contrast to other findings of indirect co-cultures with microglia on inserts and neurons on the well bottom [55], our results suggest that conditioned medium has no effect on synaptic density and that the direct microglia-neuron interaction is responsible for synaptic elimination. In this study, the release of soluble factors, cytokines or hormones by microglia did not induce a decline in synaptic density.

For assessment of active synaptic pruning, different parameters proved that control and patient-derived microglia were capable to phagocytose Syn1 positive presynaptic structures. The increased total amount of Syn1 spots and the significantly enhanced mean fluorescence intensity of Syn1 within Iba1 positive microglia indicate that SZ-neuronal cultures induced increased synaptic pruning in comparison to CTR-neurons with no obvious differences between control and patient-derived microglia. The percentage of actively phagocytosing microglia was however slightly increased by 5 % in SZ-microglia compared to CTR-microglia. This tendency suggests that SZ-microglia more actively engulfed and took up more Syn1 spots (SZ-derived as well as CTR-derived) than CTR-microglia. The phagocytic Syn1 uptake of CTR microglia cultured on CTR neurons was the lowest throughout all experiments. Our initial findings confirm a previous report of increased phagocytosis by SZ-derived microglia-like cells

and an increased uptake of SZ-synaptic structures of neuronal networks [71]. Taken together, these results suggest that both microglial and neuronal factors influence pathological synaptic elimination in patients with schizophrenia. However, which exact biological mechanisms mediate neuron-microglia communication or which specific factors are involved in this imbalanced interplay remains unknown.

To further evaluate phagocytic uptake and degradation of specific Syn1 presynaptic structures, an immunocytochemical co-localization with phagosomal and lysosomal markers, such as Rab7 or LAMP1, could be employed [175-177]. Additionally, live cell imaging of synaptic pruning or the visualization of phagocytosis over time should be considered. Most events of pruning and differential phagocytosis rates likely occurred within the first six hours of co-culture [71, 178, 179], but the co-culture experiments in this study were employed for a total of 72 hours. Most synaptic structures may already have been degraded within the microglial lysosome, making it difficult to detect and measure those early pruning events by immunocytochemistry. Time-dependent analysis of synaptic internalization may reveal more distinct differences in synaptic elimination and activation states between CTR- and SZ-microglia.

In this study, microglia from patients with schizophrenia in mono-cultures without neurons showed an increased activation state by enhanced expression of the activation marker HLA-DR compared to control microglia (Figure 23). However, after co-culture with CTR- or SZ-neurons, the activation state of CTR- and SZ-microglia was not significantly different anymore and upregulated similarly by both CTR- or SZ-neuronal cultures. Interestingly and in addition to our results regarding enhanced synaptic phagocytosis, patient-derived neuronal cultures induced an increased expression of both activation markers HLA-DR and Iba1 in CTR- and SZ-microglia compared to CTR-neurons.For further characterization of differential discrimination of activation states between CTR- and SZ-microglia, another microglial activation biomarker next to HLA-DR should be considered. Pro-inflammatory mechanisms can additionally be evaluated by assessment of biochemical responses to stimuli, e.g. nitric oxide synthases (iNOS) that are activated upon NFκB-mediated inflammatory signaling [180].

Accompanying cytokine secretion, determined by ELISA, resulted in low concentrations of released TNFα into the supernatant. Even though SZ-neurons induced significantly more TNFα secretion of CTR-microglia than CTR-neurons, these findings have to be evaluated with caution. Detection of low abundance cytokines by classical sandwich ELISAs can be challenging, especially when dealing with a low number of cytokine secreting microglia. Employing more sensitive multiplex techniques like the single molecule array (Simoa™, [181]) will improve precision and specificity of results for a panel of pro- and anti-inflammatory cytokines and is especially qualified for detecting low abundant analytes secreted by microglia.

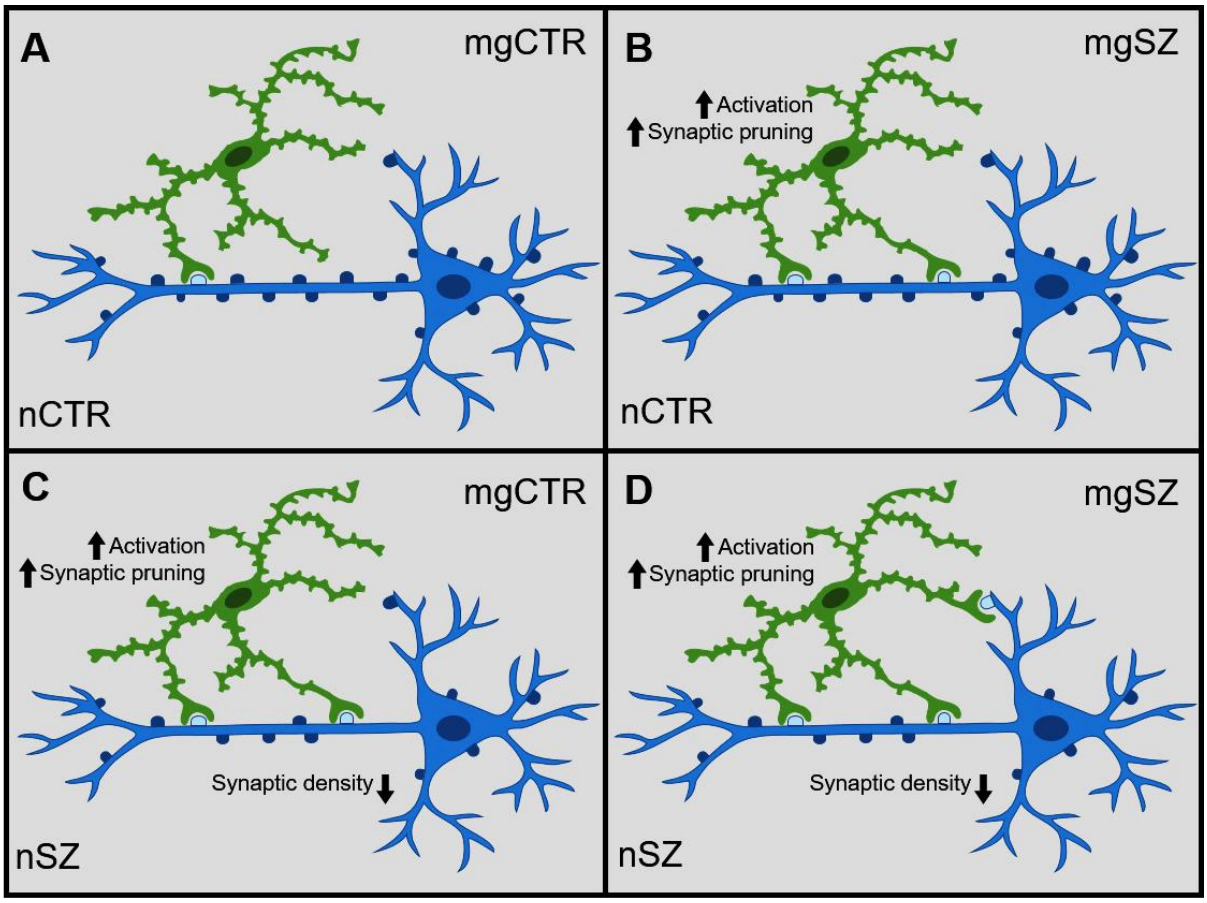

Figure 23. Schematic representation of microglia-neuron interactions in schizophrenia *in vitro* models. (A) In the healthy brain, CTR-microglia (mgCTR) eliminate specific synapses to maintain neuronal circuity and to reduce irrelevant synapses. (B) SZ-microglia (mgSZ) show increased activation and increased synaptic pruning when cultured on CTR-neurons (nCTR) and compared to CTR-microglia. (C) The activation and synaptic elimination capacity of CTR-microglia is increased when cultured on SZ-neurons (nSZ) compared to CTR-neurons. SZ-neurons show *per se* a reduced number of presynaptic structures. (D) The schizophrenia model reveals a maximal activation state and synaptic pruning rate of SZ-microglia cultured on SZ-neurons.

Our results suggest complex interactions and pathological communication between microglia and neurons in the context of schizophrenia. The communication between microglia and neurons is bidirectional and mediated by intrinsic and extrinsic signals. Direct cell-cell contact in combination with the release of soluble factors, extracellular vesicles, fractalkine and purinergic signaling tightly regulate microglial activation states to ensure brain tissue homeostasis [155, 182, 183]. In the healthy brain, surveilling microglia are controlled e.g. by the neuronal release of fractalkine (CX3CL1) that binds to the microglial receptor CX3CR1 to keep microglia in a surveying state [184]. Minor environmental changes or endogenous signals modulating transcription factor expression can trigger communication perturbations between microglia and neurons and cause fatal neurological pathologies of schizophrenia.

In this study, microglia from patients with schizophrenia displayed increased synaptic elimination compared to control microglia. Likewise, the neuronal cultures in our experiments induced activation of microglia and neurons derived from patients with schizophrenia stimulated microglia to eliminate synapses. Usually, damaged, stressed or apoptotic neurons display environmental factors, opsonins, to mark single synapses, dendrites, axons or whole neurons for chemoattraction and degradation by microglia. Classical opsonins are antibodies, proteins of the complement system (C1q or C3b) or bridging proteins (Gas6 or apolipoprotein E) that mediate phagocytosis by strengthening the binding of opsonized neuronal structures and microglial receptors like the complement receptor C3, vitronectin receptor, MER tyrosine kinase receptor (MerTK) or purinergic receptor P2Y6 [185]. The role of the complement system has been described extensively in this context. Mouse models revealed C1q and C3 dependent synapse loss [89] and increased copy numbers of human C4 risk variant were shown to predispose for the development of schizophrenia [71, 109]. Increased C3b deposition by enhanced C4 catalyzation and C3 hydrolysis may contribute to excessive phagocytosis in schizophrenia. Binding of opsonins to microglial receptors induce activation of intracellular NFκB or JAK/STAT signaling pathways with downstream signaling via secondary messengers ERK1/2, AKT or PI3K, ultimately leading to the activation of NFκB transcription factor based expression of inflammatory genes [186, 187].

Pathological association of NFκB and JAK/STAT signaling pathways could be analyzed by adeno-associated viral (AAV) vectors expressing dominant-negative variants of NFκB or its regulatory complex IκB to determine the effects of inhibited pro-inflammatory, NFκB -mediated signaling on subsequent microglial phagocytosis of synaptic structures. Likewise, specific knockdown of associated proteins using siRNAs or treatment with specific NFκB-inhibiting or activating drugs could be employed for a better understanding of the inflammatory mechanisms in microglia in the context of schizophrenia.

In this study, for maximization of NFκB signaling, to enhance microglial activation and thus, increase synaptic elimination, microglia were pre-treated with LPS and minocycline as pro- and anti-inflammatory stimuli, respectively, before seeding them to neuronal cultures. Syn1 spot density was significantly reduced after LPS stimulation, whereas minocycline application could reverse excessive pruning by SZ-microglia significantly when cultured on SZ-neurons (Figure 24).

Addition of minocycline treated microglia to neuronal cultures showed donor-independent lower reduction of Syn1 spots compared to untreated microglia, indicating that minocycline inhibits overreactive, aberrant microglial synaptic elimination. The concentration of 10 µM minocycline for priming was chosen in accordance with previously published results showing a significant anti-inflammatory priming of microglia-like cells but no overstated and fully

inhibition of microglial cellular function [71]. Likewise, minocycline treatment led to reduced levels of phagocytosed Syn1 spots and decreased Syn1 mean fluorescence intensity within Iba1 positive cells compared to untreated microglia. This effect was especially significant for both CTR- and SZ-microglia cultured on SZ-neurons, whereas a culture on CTR-neurons had less distinct effects. Additionally, minocycline pre-treatment decreased the percentage of actively phagocytosing microglia, whereas LPS priming induced significantly increased synapse uptake in all intra- and inter-disease specific combinations with no significant differences between control or patient-derived cells. Likewise, microglial activation assessed by HLA-DR expression levels was significantly increased after LPS. Especially in this case, live cell imaging and time dependent tracking of synaptic elimination can reveal more distinct differences between activity patterns of pro- or anti-inflammatory stimulated CTR- and SZ-microglia.

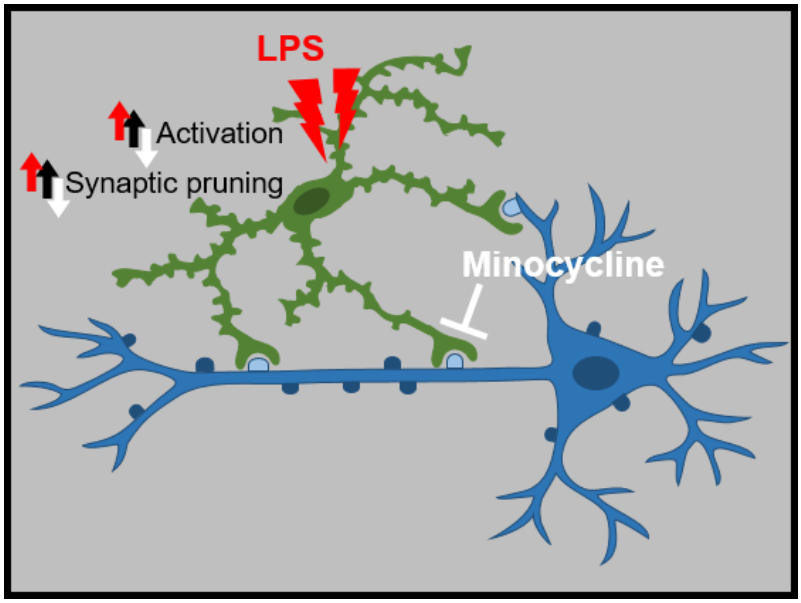

Figure 24. Pro- or anti-inflammatory stimulation directly influences microglial phenotype. LPS stimulation results in increased microglial activation and synaptic elimination, while minocycline treatment can rescue aberrant synaptic pruning and prevent microglial overactivation in schizophrenia disease models.

Recently, RNA sequencing of LPS stimulated microglia-like cells revealed that microglia derived from patients with schizophrenia showed a trend towards a more distinct inflammatory response, but only TNFα expression was significantly increased in SZ-microglia compared to healthy controls [110]. However, one limitation of this study was that cells were cultured as mono-cultures lacking the direct communication with other neuronal or glial cell types that are necessary for proper microglia maturation and functioning *in vitro* [166]. The immaturity of microglial mono-cultures impacts the functional readouts of this system. Nevertheless, upregulation of mRNA levels and peripheral secretion of pro-inflammatory cytokines, such as IL-6 and TNFα have been widely discussed for immune cells derived from patients with schizophrenia [190, 191].

Taken together, our findings underline that SZ-neurons induce a more activated microglial phenotype (CTR-microglia as well as SZ-microglia) compared to CTR-neurons after 72 hours in co-culture. Pro-inflammatory stimulation of microglia amplified this effect, while anti-inflammatory priming using minocycline had beneficial effects and rescued excessive synaptic pruning by SZ-microglia. Our results indicate a pathologically deregulated activity and phagocytosis by microglia, but if a deregulation of phagocytosis arises from pathologically reactive microglia or if phagocytosis signaling per se is defective or if the synaptic tagging mediated by neurons is deregulated, remain open questions.

The exact mechanisms involved in this interplay, the functional aspects of microglial phagocytosis of synapses and the deregulated processes in the course of schizophrenia still remain unclear and need further studies. Live cell imaging of synaptic elimination and single cell RNA sequencing after microglia-neuron co-cultures may detect specific neuronal or microglial characteristics contributing to the pathology of schizophrenia. Additionally, the release of reactive oxygen species by luminescence kits or the classical Griess reagent in combination with more sophisticated analyses like determination of the oxygen consumption rate could be employed to better understand the role of reactive oxygen or nitrogen species in the context of schizophrenia [192-194]. It needs to be considered that such assays are most sensitive at early time points or ideally applied as real time measurements than as endpoint assays after later stages of co-culture.

4.4. Outlook and conclusion

Reciprocal microglia-neuron communication governs homeostasis in the CNS by keeping microglia usually in a surveying, inactive state. In neurological diseases, deregulated communication can lead to a severe activation of microglia and a cascade of inflammatory mechanisms compromising neuronal plasticity. The established microglia-neuron co-culture model based on iPSCs derived from patients with schizophrenia revealed that microglial activity and phagocytosis of synaptic structures in neuronal cultures is increased in schizophrenia. To decipher underlying inflammatory response dynamics in microglia, real time imaging of synaptic elimination and subsequent single cell RNA sequencing could help to identify cell type specifically deregulated genes, associated signaling pathways or cellular mechanisms. The co-culture model offers a novel *in vitro* platform to evaluate the constant interplay of microglia and neurons and to distinguish individual contributions of neuronal networks and microglial inflammatory mechanisms to the pathological phenotype of schizophrenia. For subsequent studies, functional electrophysiological assays, like multi electrode array recordings, patch clamp or calcium imaging, will clarify the influence of microglia on neuronal networks and physiological functionality. Additionally, complex multiplex

cytokine analysis will resolve microglial activation patterns and inflammatory phenotypes. Furthermore, the comparison of inflammatory cytokine release patterns in microglia-neuron co-cultures may be translated and compared to cytokine levels found in the cerebrospinal fluid or peripheral blood of patients diagnosed with schizophrenia. Comparisons of iPSC- and patient-derived results will help to examine the impact and usefulness of iPSC-based co-culture systems to study neuroinflammatory processes. Additionally, mitochondrial deficits have been reported in the progression of schizophrenia [55], thus the release of reactive oxygen species or impairments in mitochondrial functioning should be considered as potentially affected pathologies in patients with schizophrenia.

Neuropsychiatric diseases are disorders with a late onset in patients. Two-dimensional iPSC-derived *in vitro* model systems lack the ability to model aging and to study long term mechanisms occurring during adolescence. Additionally, 2D monolayer models are not able to adequately represent three-dimensional cell-cell contacts and interactions. In 2013, Lancaster et al. developed a protocol for the generation of 3D brain organoids with human brain-like structure [195]. Since then, specific brain regions, such as cortical and subpallial [196] or midbrain region can be differentiated from iPSC and analyzed regarding early neurodevelopmental patterning, cellular migration and cell fate transition [197]. Brain organoids resemble human brains more precisely than cells grown in monolayers and can be cultured for extended longer time periods. Especially for studying activation and phagocytosis pathways in microglia, co-cultures with e.g. cortical brain organoids can reveal long term immunomodulatory mechanisms. Physiological activity of matured neuronal organoids can be analyzed by different electrophysiological assays and is currently especially applied to examine molecular mechanisms of Parkinson’s disease [198]. Disease-specific and patient-derived 3D brain organoids hold great potential for studying neurodegenerative, neuropsychiatric and immunopsychiatric diseases by precisely modeling the human brain in a dish.

5. References

1. Knapp, M., R. Mangalore, and J. Simon, *The global costs of schizophrenia.* Schizophr Bull, 2004. **30**(2): p. 279-93.
2. Saha, S., D. Chant, and J. McGrath, *A systematic review of mortality in schizophrenia: is the differential mortality gap worsening over time?* Arch Gen Psychiatry, 2007. **64**(10): p. 1123-31.
3. Mueser, K.T. and S.R. McGurk, *Schizophrenia.* Lancet, 2004. **363**(9426): p. 2063-72.
4. Patel, K.R., et al., *Schizophrenia: overview and treatment options.* P T, 2014. **39**(9): p. 638-45.
5. Beaulieu, J.M. and R.R. Gainetdinov, *The physiology, signaling, and pharmacology of dopamine receptors.* Pharmacol Rev, 2011. **63**(1): p. 182-217.
6. Tandon, R., et al., *Definition and description of schizophrenia in the DSM-5.* Schizophr Res, 2013. **150**(1): p. 3-10.
7. Millier, A., et al., *Humanistic burden in schizophrenia: a literature review.* J Psychiatr Res, 2014. **54**: p. 85-93.
8. Lewis, D.A. and J.A. Lieberman, *Catching up on schizophrenia: natural history and neurobiology.* Neuron, 2000. **28**(2): p. 325-34.
9. Carbon, M. and C.U. Correll, *Thinking and acting beyond the positive: the role of the cognitive and negative symptoms in schizophrenia.* CNS Spectr, 2014. **19 Suppl 1**: p. 38-52; quiz 35-7, 53.
10. Opoka, S.M. and T.M. Lincoln, *The Effect of Cognitive Behavioral Interventions on Depression and Anxiety Symptoms in Patients with Schizophrenia Spectrum Disorders: A Systematic Review.* Psychiatr Clin North Am, 2017. **40**(4): p. 641-659.
11. Takahashi, K., et al., *Induction of pluripotent stem cells from adult human fibroblasts by defined factors.* Cell, 2007. **131**(5): p. 861-72.
12. Okita, K., et al., *A more efficient method to generate integration-free human iPS cells.* Nat Methods, 2011. **8**(5): p. 409-12.
13. Lichtenstein, P., et al., *Common genetic determinants of schizophrenia and bipolar disorder in Swedish families: a population-based study.* Lancet, 2009. **373**(9659): p. 234-9.
14. Sullivan, P.F., K.S. Kendler, and M.C. Neale, *Schizophrenia as a complex trait: evidence from a meta-analysis of twin studies.* Arch Gen Psychiatry, 2003. **60**(12): p. 1187-92.
15. Brown, A.S. and E.J. Derkits, *Prenatal infection and schizophrenia: a review of epidemiologic and translational studies.* Am J Psychiatry, 2010. **167**(3): p. 261-80.
16. McDonald, C. and K.C. Murphy, *The new genetics of schizophrenia.* Psychiatr Clin North Am, 2003. **26**(1): p. 41-63.
17. Schizophrenia Working Group of the Psychiatric Genomics, C., *Biological insights from 108 schizophrenia-associated genetic loci.* Nature, 2014. **511**(7510): p. 421-7.
18. Pardinas, A.F., et al., *Common schizophrenia alleles are enriched in mutation-intolerant genes and in regions under strong background selection.* Nat Genet, 2018. **50**(3): p. 381-389.
19. Flora, A., et al., *The E-protein Tcf4 interacts with Math1 to regulate differentiation of a specific subset of neuronal progenitors.* Proc Natl Acad Sci U S A, 2007. **104**(39): p. 15382-7.
20. Shi, Y., et al., *Common variants on 8p12 and 1q24.2 confer risk of schizophrenia.* Nat Genet, 2011. **43**(12): p. 1224-7.
21. Wen, Z., et al., *Synaptic dysregulation in a human iPS cell model of mental disorders.* Nature, 2014. **515**(7527): p. 414-8.
22. Millar, J.K., et al., *Disruption of two novel genes by a translocation co-segregating with schizophrenia.* Hum Mol Genet, 2000. **9**(9): p. 1415-23.
23. Ishizuka, K., et al., *A review of Disrupted-In-Schizophrenia-1 (DISC1): neurodevelopment, cognition, and mental conditions.* Biol Psychiatry, 2006. **59**(12): p. 1189-97.

24. Brandon, N.J. and A. Sawa, *Linking neurodevelopmental and synaptic theories of mental illness through DISC1.* Nat Rev Neurosci, 2011. **12**(12): p. 707-22.
25. Devine, M.J., R. Norkett, and J.T. Kittler, *DISC1 is a coordinator of intracellular trafficking to shape neuronal development and connectivity.* J Physiol, 2016. **594**(19): p. 5459-69.
26. Srikanth, P., et al., *Shared effects of DISC1 disruption and elevated WNT signaling in human cerebral organoids.* Transl Psychiatry, 2018. **8**(1): p. 77.
27. Maher, B.J. and J.J. LoTurco, *Disrupted-in-schizophrenia (DISC1) functions presynaptically at glutamatergic synapses.* PLoS One, 2012. **7**(3): p. e34053.
28. Walsh, T., et al., *Rare structural variants disrupt multiple genes in neurodevelopmental pathways in schizophrenia.* Science, 2008. **320**(5875): p. 539-43.
29. Fatemi, S.H. and T.D. Folsom, *The neurodevelopmental hypothesis of schizophrenia, revisited.* Schizophr Bull, 2009. **35**(3): p. 528-48.
30. Knuesel, I., et al., *Maternal immune activation and abnormal brain development across CNS disorders.* Nat Rev Neurol, 2014. **10**(11): p. 643-60.
31. Bergdolt, L. and A. Dunaevsky, *Brain changes in a maternal immune activation model of neurodevelopmental brain disorders.* Prog Neurobiol, 2019. **175**: p. 1-19.
32. Missault, S., et al., *The risk for behavioural deficits is determined by the maternal immune response to prenatal immune challenge in a neurodevelopmental model.* Brain Behav Immun, 2014. **42**: p. 138-46.
33. Scola, G. and A. Duong, *Prenatal maternal immune activation and brain development with relevance to psychiatric disorders.* Neuroscience, 2017. **346**: p. 403-408.
34. Smith, S.E., et al., *Maternal immune activation alters fetal brain development through interleukin-6.* J Neurosci, 2007. **27**(40): p. 10695-702.
35. Hunter, C.A. and S.A. Jones, *IL-6 as a keystone cytokine in health and disease.* Nat Immunol, 2015. **16**(5): p. 448-57.
36. Pepys, M.B. and G.M. Hirschfield, *C-reactive protein: a critical update.* J Clin Invest, 2003. **111**(12): p. 1805-12.
37. Estes, M.L. and A.K. McAllister, *Maternal immune activation: Implications for neuropsychiatric disorders.* Science, 2016. **353**(6301): p. 772-7.
38. Spann, M.N., et al., *Maternal Immune Activation During the Third Trimester Is Associated with Neonatal Functional Connectivity of the Salience Network and Fetal to Toddler Behavior.* J Neurosci, 2018. **38**(11): p. 2877-2886.
39. Brugger, S.P. and O.D. Howes, *Heterogeneity and Homogeneity of Regional Brain Structure in Schizophrenia: A Meta-analysis.* JAMA Psychiatry, 2017. **74**(11): p. 1104-1111.
40. Onwordi, E.C., et al., *Synaptic density marker SV2A is reduced in schizophrenia patients and unaffected by antipsychotics in rats.* Nat Commun, 2020. **11**(1): p. 246.
41. Garey, L.J., et al., *Reduced dendritic spine density on cerebral cortical pyramidal neurons in schizophrenia.* J Neurol Neurosurg Psychiatry, 1998. **65**(4): p. 446-53.
42. Glantz, L.A. and D.A. Lewis, *Decreased dendritic spine density on prefrontal cortical pyramidal neurons in schizophrenia.* Arch Gen Psychiatry, 2000. **57**(1): p. 65-73.
43. Glausier, J.R. and D.A. Lewis, *Dendritic spine pathology in schizophrenia.* Neuroscience, 2013. **251**: p. 90-107.
44. Matosin, N., et al., *Molecular evidence of synaptic pathology in the CA1 region in schizophrenia.* NPJ Schizophr, 2016. **2**: p. 16022.
45. Funk, A.J., et al., *Postsynaptic Density-95 Isoform Abnormalities in Schizophrenia.* Schizophr Bull, 2017. **43**(4): p. 891-899.
46. Brennand, K.J., et al., *Modelling schizophrenia using human induced pluripotent stem cells.* Nature, 2011. **473**(7346): p. 221-5.
47. Robicsek, O., et al., *Abnormal neuronal differentiation and mitochondrial dysfunction in hair follicle-derived induced pluripotent stem cells of schizophrenia patients.* Mol Psychiatry, 2013. **18**(10): p. 1067-76.

48. Grunwald, L.M., et al., *Comparative characterization of human induced pluripotent stem cells (hiPSC) derived from patients with schizophrenia and autism.* Transl Psychiatry, 2019. **9**(1): p. 179.
49. Paulsen Bda, S., et al., *Altered oxygen metabolism associated to neurogenesis of induced pluripotent stem cells derived from a schizophrenic patient.* Cell Transplant, 2012. **21**(7): p. 1547-59.
50. Brennand, K., et al., *Phenotypic differences in hiPSC NPCs derived from patients with schizophrenia.* Mol Psychiatry, 2015. **20**(3): p. 361-8.
51. Ni, P., et al., *iPSC-derived homogeneous populations of developing schizophrenia cortical interneurons have compromised mitochondrial function.* Mol Psychiatry, 2019.
52. Yu, D.X., et al., *Modeling hippocampal neurogenesis using human pluripotent stem cells.* Stem Cell Reports, 2014. **2**(3): p. 295-310.
53. Hook, V., et al., *Human iPSC neurons display activity-dependent neurotransmitter secretion: aberrant catecholamine levels in schizophrenia neurons.* Stem Cell Reports, 2014. **3**(4): p. 531-8.
54. Sarkar, A., et al., *Efficient Generation of CA3 Neurons from Human Pluripotent Stem Cells Enables Modeling of Hippocampal Connectivity In Vitro.* Cell Stem Cell, 2018. **22**(5): p. 684-697 e9.
55. Park, G.H., et al., *Activated microglia cause metabolic disruptions in developmental cortical interneurons that persist in interneurons from individuals with schizophrenia.* Nat Neurosci, 2020. **23**(11): p. 1352-1364.
56. Vermeulen, J., et al., *Antipsychotic medication and long-term mortality risk in patients with schizophrenia; a systematic review and meta-analysis.* Psychol Med, 2017. **47**(13): p. 2217-2228.
57. Miyamoto, S., et al., *Pharmacological treatment of schizophrenia: a critical review of the pharmacology and clinical effects of current and future therapeutic agents.* Mol Psychiatry, 2012. **17**(12): p. 1206-27.
58. Lally, J. and J.H. MacCabe, *Antipsychotic medication in schizophrenia: a review.* Br Med Bull, 2015. **114**(1): p. 169-79.
59. Brenner, H.D., et al., *Defining treatment refractoriness in schizophrenia.* Schizophr Bull, 1990. **16**(4): p. 551-61.
60. Lieberman, J.A., et al., *Effectiveness of antipsychotic drugs in patients with chronic schizophrenia.* N Engl J Med, 2005. **353**(12): p. 1209-23.
61. Remington, G., *Alterations of dopamine and serotonin transmission in schizophrenia.* Prog Brain Res, 2008. **172**: p. 117-40.
62. Aringhieri, S., et al., *Molecular targets of atypical antipsychotics: From mechanism of action to clinical differences.* Pharmacol Ther, 2018. **192**: p. 20-41.
63. Khokhar, J.Y., et al., *Unique Effects of Clozapine: A Pharmacological Perspective.* Adv Pharmacol, 2018. **82**: p. 137-162.
64. Oltra, J.A.E., *Improving Therapeutic Interventions of Schizophrenia with Advances in Stem Cell Technology.* Clin Psychopharmacol Neurosci, 2020. **18**(3): p. 352-361.
65. Wynn, T.A., A. Chawla, and J.W. Pollard, *Macrophage biology in development, homeostasis and disease.* Nature, 2013. **496**(7446): p. 445-55.
66. Shapouri-Moghaddam, A., et al., *Macrophage plasticity, polarization, and function in health and disease.* J Cell Physiol, 2018. **233**(9): p. 6425-6440.
67. Hohlfeld, R., M. Kerschensteiner, and E. Meinl, *Dual role of inflammation in CNS disease.* Neurology, 2007. **68**(22 Suppl 3): p. S58-63; discussion S91-6.
68. Ransohoff, R.M., *How neuroinflammation contributes to neurodegeneration.* Science, 2016. **353**(6301): p. 777-83.
69. Hanson, D.R. and Gottesman, II, *Theories of schizophrenia: a genetic-inflammatory-vascular synthesis.* BMC Med Genet, 2005. **6**: p. 7.
70. Gray, J.A. and B.L. Roth, *The pipeline and future of drug development in schizophrenia.* Mol Psychiatry, 2007. **12**(10): p. 904-22.
71. Sellgren, C.M., et al., *Increased synapse elimination by microglia in schizophrenia patient-derived models of synaptic pruning.* Nat Neurosci, 2019. **22**(3): p. 374-385.

72. Monji, A., T. Kato, and S. Kanba, *Cytokines and schizophrenia: Microglia hypothesis of schizophrenia.* Psychiatry Clin Neurosci, 2009. **63**(3): p. 257-65.
73. Gomez Perdiguero, E., et al., *Tissue-resident macrophages originate from yolk-sac-derived erythro-myeloid progenitors.* Nature, 2015. **518**(7540): p. 547-51.
74. Hashimoto, D., et al., *Tissue-resident macrophages self-maintain locally throughout adult life with minimal contribution from circulating monocytes.* Immunity, 2013. **38**(4): p. 792-804.
75. Bruttger, J., et al., *Genetic Cell Ablation Reveals Clusters of Local Self-Renewing Microglia in the Mammalian Central Nervous System.* Immunity, 2015. **43**(1): p. 92-106.
76. Salter, M.W. and S. Beggs, *Sublime microglia: expanding roles for the guardians of the CNS.* Cell, 2014. **158**(1): p. 15-24.
77. Tay, T.L., et al., *Microglia across the lifespan: from origin to function in brain development, plasticity and cognition.* J Physiol, 2017. **595**(6): p. 1929-1945.
78. Tremblay, M.E., R.L. Lowery, and A.K. Majewska, *Microglial interactions with synapses are modulated by visual experience.* PLoS Biol, 2010. **8**(11): p. e1000527.
79. Schafer, D.P., et al., *Microglia sculpt postnatal neural circuits in an activity and complement-dependent manner.* Neuron, 2012. **74**(4): p. 691-705.
80. Petanjek, Z., et al., *Extraordinary neoteny of synaptic spines in the human prefrontal cortex.* Proc Natl Acad Sci U S A, 2011. **108**(32): p. 13281-6.
81. Salter, M.W. and B. Stevens, *Microglia emerge as central players in brain disease.* Nat Med, 2017. **23**(9): p. 1018-1027.
82. Li, Q. and B.A. Barres, *Microglia and macrophages in brain homeostasis and disease.* Nat Rev Immunol, 2018. **18**(4): p. 225-242.
83. Bachiller, S., et al., *Microglia in Neurological Diseases: A Road Map to Brain-Disease Dependent-Inflammatory Response.* Front Cell Neurosci, 2018. **12**: p. 488.
84. Nimmerjahn, A., F. Kirchhoff, and F. Helmchen, *Resting microglial cells are highly dynamic surveillants of brain parenchyma in vivo.* Science, 2005. **308**(5726): p. 1314-8.
85. Boche, D., V.H. Perry, and J.A. Nicoll, *Review: activation patterns of microglia and their identification in the human brain.* Neuropathol Appl Neurobiol, 2013. **39**(1): p. 3-18.
86. Mills, C.D., et al., *M-1/M-2 macrophages and the Th1/Th2 paradigm.* J Immunol, 2000. **164**(12): p. 6166-73.
87. Martinez, F.O. and S. Gordon, *The M1 and M2 paradigm of macrophage activation: time for reassessment.* F1000Prime Rep, 2014. **6**: p. 13.
88. Murray, P.J., et al., *Macrophage activation and polarization: nomenclature and experimental guidelines.* Immunity, 2014. **41**(1): p. 14-20.
89. Hong, S., et al., *Complement and microglia mediate early synapse loss in Alzheimer mouse models.* Science, 2016. **352**(6286): p. 712-716.
90. Lian, H., et al., *Astrocyte-Microglia Cross Talk through Complement Activation Modulates Amyloid Pathology in Mouse Models of Alzheimer's Disease.* J Neurosci, 2016. **36**(2): p. 577-89.
91. Vom Berg, J., et al., *Inhibition of IL-12/IL-23 signaling reduces Alzheimer's disease-like pathology and cognitive decline.* Nat Med, 2012. **18**(12): p. 1812-9.
92. Bisht, K., K. Sharma, and M.E. Tremblay, *Chronic stress as a risk factor for Alzheimer's disease: Roles of microglia-mediated synaptic remodeling, inflammation, and oxidative stress.* Neurobiol Stress, 2018. **9**: p. 9-21.
93. Morgan, J.T., et al., *Microglial activation and increased microglial density observed in the dorsolateral prefrontal cortex in autism.* Biol Psychiatry, 2010. **68**(4): p. 368-76.
94. Vargas, D.L., et al., *Neuroglial activation and neuroinflammation in the brain of patients with autism.* Ann Neurol, 2005. **57**(1): p. 67-81.
95. Tetreault, N.A., et al., *Microglia in the cerebral cortex in autism.* J Autism Dev Disord, 2012. **42**(12): p. 2569-84.

96. Gupta, S., et al., *Transcriptome analysis reveals dysregulation of innate immune response genes and neuronal activity-dependent genes in autism.* Nat Commun, 2014. **5**: p. 5748.
97. Suzuki, K., et al., *Microglial activation in young adults with autism spectrum disorder.* JAMA Psychiatry, 2013. **70**(1): p. 49-58.
98. Trepanier, M.O., et al., *Postmortem evidence of cerebral inflammation in schizophrenia: a systematic review.* Mol Psychiatry, 2016. **21**(8): p. 1009-26.
99. van Kesteren, C.F., et al., *Immune involvement in the pathogenesis of schizophrenia: a meta-analysis on postmortem brain studies.* Transl Psychiatry, 2017. **7**(3): p. e1075.
100. Bayer, T.A., et al., *Evidence for activation of microglia in patients with psychiatric illnesses.* Neurosci Lett, 1999. **271**(2): p. 126-8.
101. Radewicz, K., et al., *Increase in HLA-DR immunoreactive microglia in frontal and temporal cortex of chronic schizophrenics.* J Neuropathol Exp Neurol, 2000. **59**(2): p. 137-50.
102. Tzioras, M., et al., *Microglial contribution to synaptic uptake in the prefrontal cortex in schizophrenia.* Neuropathol Appl Neurobiol, 2020.
103. Kasai, H., et al., *Structural dynamics of dendritic spines in memory and cognition.* Trends Neurosci, 2010. **33**(3): p. 121-9.
104. Holtmaat, A. and K. Svoboda, *Experience-dependent structural synaptic plasticity in the mammalian brain.* Nat Rev Neurosci, 2009. **10**(9): p. 647-58.
105. Penzes, P., et al., *Dendritic spine pathology in neuropsychiatric disorders.* Nat Neurosci, 2011. **14**(3): p. 285-93.
106. Cannon, T.D., *How Schizophrenia Develops: Cognitive and Brain Mechanisms Underlying Onset of Psychosis.* Trends Cogn Sci, 2015. **19**(12): p. 744-756.
107. Stevens, B., et al., *The classical complement cascade mediates CNS synapse elimination.* Cell, 2007. **131**(6): p. 1164-78.
108. Nesargikar, P.N., B. Spiller, and R. Chavez, *The complement system: history, pathways, cascade and inhibitors.* Eur J Microbiol Immunol (Bp), 2012. **2**(2): p. 103-11.
109. Sekar, A., et al., *Schizophrenia risk from complex variation of complement component 4.* Nature, 2016. **530**(7589): p. 177-83.
110. Ormel, P.R., et al., *A characterization of the molecular phenotype and inflammatory response of schizophrenia patient-derived microglia-like cells.* Brain Behav Immun, 2020. **90**: p. 196-207.
111. Sommer, I.E., et al., *Efficacy of anti-inflammatory agents to improve symptoms in patients with schizophrenia: an update.* Schizophr Bull, 2014. **40**(1): p. 181-91.
112. Kim, H.S. and Y.H. Suh, *Minocycline and neurodegenerative diseases.* Behav Brain Res, 2009. **196**(2): p. 168-79.
113. Chen, X., et al., *Minocycline as adjunct therapy for a male patient with deficit schizophrenia.* Neuropsychiatr Dis Treat, 2018. **14**: p. 2697-2701.
114. Mattei, D., et al., *Maternal immune activation results in complex microglial transcriptome signature in the adult offspring that is reversed by minocycline treatment.* Transl Psychiatry, 2017. **7**(5): p. e1120.
115. Ueno, M., et al., *Layer V cortical neurons require microglial support for survival during postnatal development.* Nat Neurosci, 2013. **16**(5): p. 543-51.
116. Arnoux, I., et al., *Paradoxical effects of minocycline in the developing mouse somatosensory cortex.* Glia, 2014. **62**(3): p. 399-410.
117. Inta, I., et al., *Minocycline exacerbates apoptotic neurodegeneration induced by the NMDA receptor antagonist MK-801 in the early postnatal mouse brain.* Eur Arch Psychiatry Clin Neurosci, 2016. **266**(7): p. 673-7.
118. Shigemoto-Mogami, Y., et al., *Microglia enhance neurogenesis and oligodendrogenesis in the early postnatal subventricular zone.* J Neurosci, 2014. **34**(6): p. 2231-43.
119. Ho, S.M., et al., *Rapid Ngn2-induction of excitatory neurons from hiPSC-derived neural progenitor cells.* Methods, 2016. **101**: p. 113-24.

120. Maherali, N., et al., *A high-efficiency system for the generation and study of human induced pluripotent stem cells.* Cell Stem Cell, 2008. **3**(3): p. 340-5.
121. Zhang, Y., et al., *Rapid single-step induction of functional neurons from human pluripotent stem cells.* Neuron, 2013. **78**(5): p. 785-98.
122. Eminli, S., et al., *Differentiation stage determines potential of hematopoietic cells for reprogramming into induced pluripotent stem cells.* Nat Genet, 2009. **41**(9): p. 968-76.
123. Cao, X., et al., *Differentiation and Functional Comparison of Monocytes and Macrophages from hiPSCs with Peripheral Blood Derivatives.* Stem Cell Reports, 2019. **12**(6): p. 1282-1297.
124. Graham, F.L., et al., *Characteristics of a human cell line transformed by DNA from human adenovirus type 5.* J Gen Virol, 1977. **36**(1): p. 59-74.
125. Nedergaard, M., B. Ransom, and S.A. Goldman, *New roles for astrocytes: redefining the functional architecture of the brain.* Trends Neurosci, 2003. **26**(10): p. 523-30.
126. Allen, N.J. and B.A. Barres, *Neuroscience: Glia - more than just brain glue.* Nature, 2009. **457**(7230): p. 675-7.
127. Schildge, S., et al., *Isolation and culture of mouse cortical astrocytes.* J Vis Exp, 2013(71).
128. Stock, R., et al., *The potential of induced pluripotent stem cells for discriminating neurodevelopmental disorders.* Stem Cells Transl Med, 2020.
129. Stock, R., et al., *Generation and characterization of human induced pluripotent stem cells lines from four patients diagnosed with schizophrenia and one healthy control.* Stem Cell Res, 2020. **48**: p. 101961.
130. Bennett, M.L., et al., *New tools for studying microglia in the mouse and human CNS.* Proc Natl Acad Sci U S A, 2016. **113**(12): p. E1738-46.
131. Gosselin, D., et al., *An environment-dependent transcriptional network specifies human microglia identity.* Science, 2017. **356**(6344).
132. Galatro, T.F., et al., *Transcriptomic analysis of purified human cortical microglia reveals age-associated changes.* Nat Neurosci, 2017. **20**(8): p. 1162-1171.
133. Abud, E.M., et al., *iPSC-Derived Human Microglia-like Cells to Study Neurological Diseases.* Neuron, 2017. **94**(2): p. 278-293 e9.
134. Patir, A., et al., *A core transcriptional signature of human microglia: Derivation and utility in describing region-dependent alterations associated with Alzheimer's disease.* Glia, 2019. **67**(7): p. 1240-1253.
135. Hickman, S.E., et al., *The microglial sensome revealed by direct RNA sequencing.* Nat Neurosci, 2013. **16**(12): p. 1896-905.
136. Butovsky, O., et al., *Identification of a unique TGF-beta-dependent molecular and functional signature in microglia.* Nat Neurosci, 2014. **17**(1): p. 131-43.
137. Chiu, I.M., et al., *A neurodegeneration-specific gene-expression signature of acutely isolated microglia from an amyotrophic lateral sclerosis mouse model.* Cell Rep, 2013. **4**(2): p. 385-401.
138. Linnartz-Gerlach, B., J. Kopatz, and H. Neumann, *Siglec functions of microglia.* Glycobiology, 2014. **24**(9): p. 794-9.
139. Solmi, M., et al., *Systematic review and meta-analysis of the efficacy and safety of minocycline in schizophrenia.* CNS Spectr, 2017. **22**(5): p. 415-426.
140. Lu, Y.C., W.C. Yeh, and P.S. Ohashi, *LPS/TLR4 signal transduction pathway.* Cytokine, 2008. **42**(2): p. 145-151.
141. Oskvig, D.B., et al., *Maternal immune activation by LPS selectively alters specific gene expression profiles of interneuron migration and oxidative stress in the fetus without triggering a fetal immune response.* Brain Behav Immun, 2012. **26**(4): p. 623-34.
142. Stevens, J.R., *Neuropathology of schizophrenia.* Arch Gen Psychiatry, 1982. **39**(10): p. 1131-9.
143. Laguna Goya, R., et al., *Human fetal neural precursor cells can up-regulate MHC class I and class II expression and elicit CD4 and CD8 T cell proliferation.* Neurobiol Dis, 2011. **41**(2): p. 407-14.

144. Vagaska, B., et al., *MHC-class-II are expressed in a subpopulation of human neural stem cells in vitro in an IFNgamma-independent fashion and during development.* Sci Rep, 2016. **6**: p. 24251.
145. McAllister, A.K., *Major histocompatibility complex I in brain development and schizophrenia.* Biol Psychiatry, 2014. **75**(4): p. 262-8.
146. Gore, A., et al., *Somatic coding mutations in human induced pluripotent stem cells.* Nature, 2011. **471**(7336): p. 63-7.
147. Hussein, S.M., et al., *Copy number variation and selection during reprogramming to pluripotency.* Nature, 2011. **471**(7336): p. 58-62.
148. Pasi, C.E., et al., *Genomic instability in induced stem cells.* Cell Death Differ, 2011. **18**(5): p. 745-53.
149. Ronen, D. and N. Benvenisty, *Genomic stability in reprogramming.* Curr Opin Genet Dev, 2012. **22**(5): p. 444-9.
150. Yoshihara, M., Y. Hayashizaki, and Y. Murakawa, *Genomic Instability of iPSCs: Challenges Towards Their Clinical Applications.* Stem Cell Rev Rep, 2017. **13**(1): p. 7-16.
151. Araki, R., et al., *Genetic aberrations in iPSCs are introduced by a transient G1/S cell cycle checkpoint deficiency.* Nat Commun, 2020. **11**(1): p. 197.
152. Kawamura, T., et al., *Linking the p53 tumour suppressor pathway to somatic cell reprogramming.* Nature, 2009. **460**(7259): p. 1140-4.
153. Ji, J., et al., *Antioxidant supplementation reduces genomic aberrations in human induced pluripotent stem cells.* Stem Cell Reports, 2014. **2**(1): p. 44-51.
154. Liang, G. and Y. Zhang, *Genetic and epigenetic variations in iPSCs: potential causes and implications for application.* Cell Stem Cell, 2013. **13**(2): p. 149-59.
155. Paolicelli, R.C., et al., *Synaptic pruning by microglia is necessary for normal brain development.* Science, 2011. **333**(6048): p. 1456-8.
156. Kettenmann, H., et al., *Physiology of microglia.* Physiol Rev, 2011. **91**(2): p. 461-553.
157. Krasemann, S., et al., *The TREM2-APOE Pathway Drives the Transcriptional Phenotype of Dysfunctional Microglia in Neurodegenerative Diseases.* Immunity, 2017. **47**(3): p. 566-581 e9.
158. Venegas, C. and M.T. Heneka, *Danger-associated molecular patterns in Alzheimer's disease.* J Leukoc Biol, 2017. **101**(1): p. 87-98.
159. Perry, V.H., *Innate inflammation in Parkinson's disease.* Cold Spring Harb Perspect Med, 2012. **2**(9): p. a009373.
160. Qian, L., et al., *beta2-adrenergic receptor activation prevents rodent dopaminergic neurotoxicity by inhibiting microglia via a novel signaling pathway.* J Immunol, 2011. **186**(7): p. 4443-54.
161. Cady, J., et al., *TREM2 variant p.R47H as a risk factor for sporadic amyotrophic lateral sclerosis.* JAMA Neurol, 2014. **71**(4): p. 449-53.
162. Guerreiro, R.J., et al., *Using exome sequencing to reveal mutations in TREM2 presenting as a frontotemporal dementia-like syndrome without bone involvement.* JAMA Neurol, 2013. **70**(1): p. 78-84.
163. Pandya, H., et al., *Differentiation of human and murine induced pluripotent stem cells to microglia-like cells.* Nat Neurosci, 2017. **20**(5): p. 753-759.
164. Douvaras, P., et al., *Directed Differentiation of Human Pluripotent Stem Cells to Microglia.* Stem Cell Reports, 2017. **8**(6): p. 1516-1524.
165. van Wilgenburg, B., et al., *Efficient, long term production of monocyte-derived macrophages from human pluripotent stem cells under partly-defined and fully-defined conditions.* PLoS One, 2013. **8**(8): p. e71098.
166. Haenseler, W., et al., *A Highly Efficient Human Pluripotent Stem Cell Microglia Model Displays a Neuronal-Co-culture-Specific Expression Profile and Inflammatory Response.* Stem Cell Reports, 2017. **8**(6): p. 1727-1742.
167. Muffat, J., et al., *Efficient derivation of microglia-like cells from human pluripotent stem cells.* Nat Med, 2016. **22**(11): p. 1358-1367.
168. McQuade, A., et al., *Development and validation of a simplified method to generate human microglia from pluripotent stem cells.* Mol Neurodegener, 2018. **13**(1): p. 67.

169. Greter, M., et al., *Stroma-derived interleukin-34 controls the development and maintenance of langerhans cells and the maintenance of microglia.* Immunity, 2012. **37**(6): p. 1050-1060.
170. Wang, Y. and M. Colonna, *Interkeukin-34, a cytokine crucial for the differentiation and maintenance of tissue resident macrophages and Langerhans cells.* Eur J Immunol, 2014. **44**(6): p. 1575-81.
171. Lee, S.C., et al., *GM-CSF promotes proliferation of human fetal and adult microglia in primary cultures.* Glia, 1994. **12**(4): p. 309-18.
172. Gandal, M.J., et al., *Transcriptome-wide isoform-level dysregulation in ASD, schizophrenia, and bipolar disorder.* Science, 2018. **362**(6420).
173. Kierdorf, K., et al., *Microglia emerge from erythromyeloid precursors via Pu.1- and Irf8-dependent pathways.* Nat Neurosci, 2013. **16**(3): p. 273-80.
174. Brennand, K.J. and F.H. Gage, *Concise review: the promise of human induced pluripotent stem cell-based studies of schizophrenia.* Stem Cells, 2011. **29**(12): p. 1915-22.
175. Harrison, R.E., et al., *Phagosomes fuse with late endosomes and/or lysosomes by extension of membrane protrusions along microtubules: role of Rab7 and RILP.* Mol Cell Biol, 2003. **23**(18): p. 6494-506.
176. Pauwels, A.M., et al., *Patterns, Receptors, and Signals: Regulation of Phagosome Maturation.* Trends Immunol, 2017. **38**(6): p. 407-422.
177. Dayam, R.M. and R.J. Botelho, *Quantitative Immunofluorescence to Study Phagosome Maturation.* Methods Mol Biol, 2017. **1519**: p. 113-123.
178. Hampton, M.B., M.C. Vissers, and C.C. Winterbourn, *A single assay for measuring the rates of phagocytosis and bacterial killing by neutrophils.* J Leukoc Biol, 1994. **55**(2): p. 147-52.
179. Richards, D.M. and R.G. Endres, *The mechanism of phagocytosis: two stages of engulfment.* Biophys J, 2014. **107**(7): p. 1542-53.
180. Green, S.J., et al., *Nitric oxide: cytokine-regulation of nitric oxide in host resistance to intracellular pathogens.* Immunol Lett, 1994. **43**(1-2): p. 87-94.
181. Rissin, D.M., et al., *Polymerase-free measurement of microRNA-122 with single base specificity using single molecule arrays: Detection of drug-induced liver injury.* PLoS One, 2017. **12**(7): p. e0179669.
182. Biber, K., et al., *Neuronal 'On' and 'Off' signals control microglia.* Trends Neurosci, 2007. **30**(11): p. 596-602.
183. Paolicelli, R.C., G. Bergamini, and L. Rajendran, *Cell-to-cell Communication by Extracellular Vesicles: Focus on Microglia.* Neuroscience, 2019. **405**: p. 148-157.
184. Paolicelli, R.C., K. Bisht, and M.E. Tremblay, *Fractalkine regulation of microglial physiology and consequences on the brain and behavior.* Front Cell Neurosci, 2014. **8**: p. 129.
185. Vilalta, A. and G.C. Brown, *Neurophagy, the phagocytosis of live neurons and synapses by glia, contributes to brain development and disease.* FEBS J, 2018. **285**(19): p. 3566-3575.
186. Al-Aoukaty, A., et al., *MIP-3alpha, MIP-3beta and fractalkine induce the locomotion and the mobilization of intracellular calcium, and activate the heterotrimeric G proteins in human natural killer cells.* Immunology, 1998. **95**(4): p. 618-24.
187. Chandrasekar, B., et al., *Fractalkine (CX3CL1) stimulated by nuclear factor kappaB (NF-kappaB)-dependent inflammatory signals induces aortic smooth muscle cell proliferation through an autocrine pathway.* Biochem J, 2003. **373**(Pt 2): p. 547-58.
188. Mackay, C.R., *Chemokines: immunology's high impact factors.* Nat Immunol, 2001. **2**(2): p. 95-101.
189. Mellado, M., et al., *Chemokine receptor homo- or heterodimerization activates distinct signaling pathways.* EMBO J, 2001. **20**(10): p. 2497-507.
190. Upthegrove, R., N. Manzanares-Teson, and N.M. Barnes, *Cytokine function in medication-naive first episode psychosis: a systematic review and meta-analysis.* Schizophr Res, 2014. **155**(1-3): p. 101-8.

191. Hoseth, E.Z., et al., *A Study of TNF Pathway Activation in Schizophrenia and Bipolar Disorder in Plasma and Brain Tissue.* Schizophr Bull, 2017. **43**(4): p. 881-890.
192. Armstrong, J.S. and M. Whiteman, *Measurement of reactive oxygen species in cells and mitochondria.* Methods Cell Biol, 2007. **80**: p. 355-77.
193. Griendling, K.K., et al., *Measurement of Reactive Oxygen Species, Reactive Nitrogen Species, and Redox-Dependent Signaling in the Cardiovascular System: A Scientific Statement From the American Heart Association.* Circ Res, 2016. **119**(5): p. e39-75.
194. Campos, P.B., B.S. Paulsen, and S.K. Rehen, *Accelerating neuronal aging in in vitro model brain disorders: a focus on reactive oxygen species.* Front Aging Neurosci, 2014. **6**: p. 292.
195. Lancaster, M.A., et al., *Cerebral organoids model human brain development and microcephaly.* Nature, 2013. **501**(7467): p. 373-9.
196. Sloan, S.A., et al., *Generation and assembly of human brain region-specific three-dimensional cultures.* Nat Protoc, 2018. **13**(9): p. 2062-2085.
197. Monzel, A.S., et al., *Derivation of Human Midbrain-Specific Organoids from Neuroepithelial Stem Cells.* Stem Cell Reports, 2017. **8**(5): p. 1144-1154.
198. Chlebanowska, P., et al., *Use of 3D Organoids as a Model to Study Idiopathic Form of Parkinson's Disease.* Int J Mol Sci, 2020. **21**(3).
199. Weisman, G.A., et al., *Neuroprotective roles of the P2Y(2) receptor.* Purinergic Signal, 2012. **8**(3): p. 559-78.

6. Supplementary Information

6.1. Analysis of chromosomal integrity, surface marker expression and mycoplasma test of all seven fully validated iPSC clones

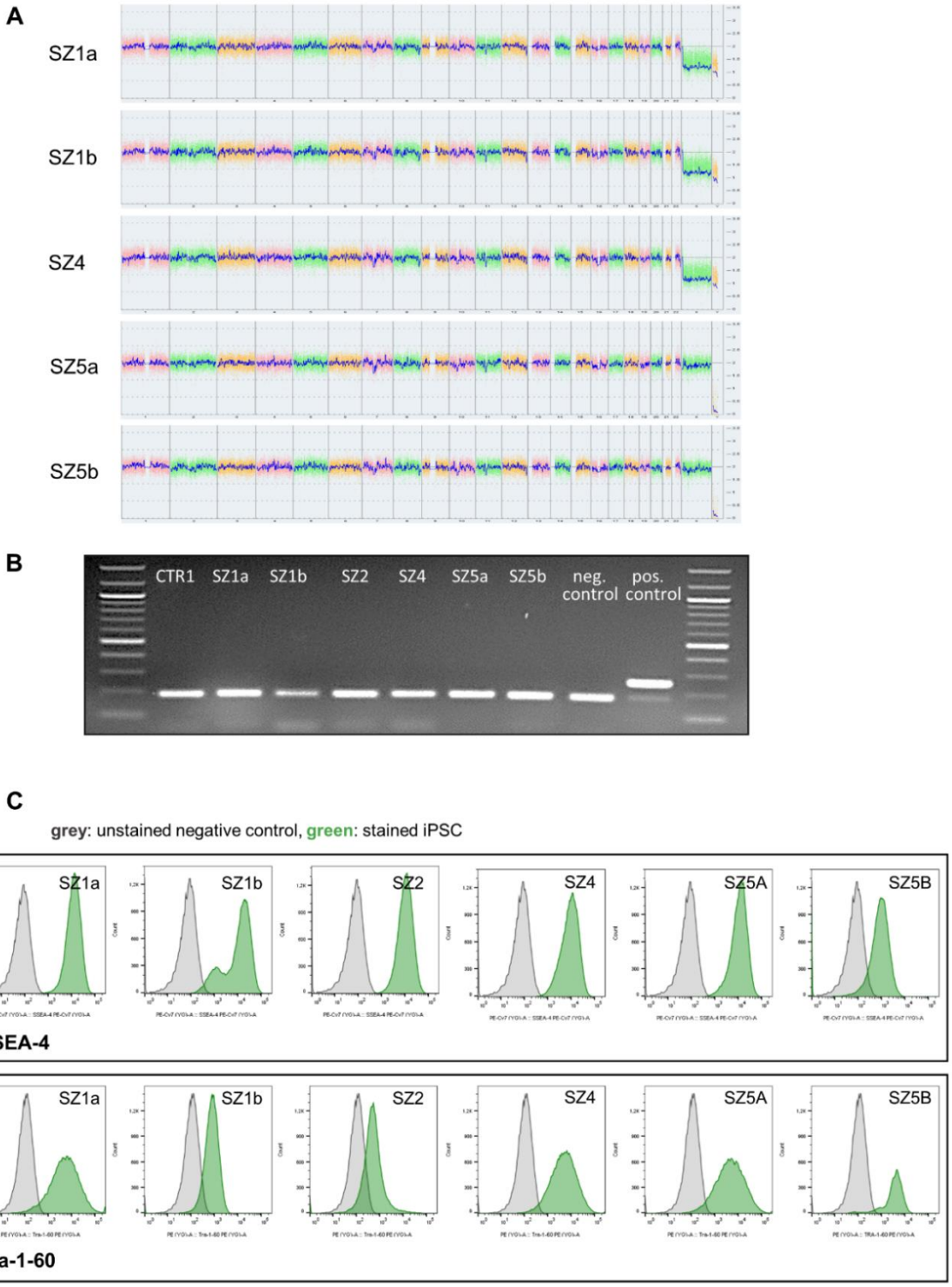

Supplementary Figure 1. Residual characterization of all seven clones regarding (A) their chromosomal integrity, KaryoStat™ analysis performed by Thermo Fisher Scientific, (B) prove of mycoplasma absence and (C) expression of classical iPSC surface markers SSEA-4 and TRA-1-60. Results are published in [129].

6.2. Characterization of control clones CTR3.3 and CTR4.3

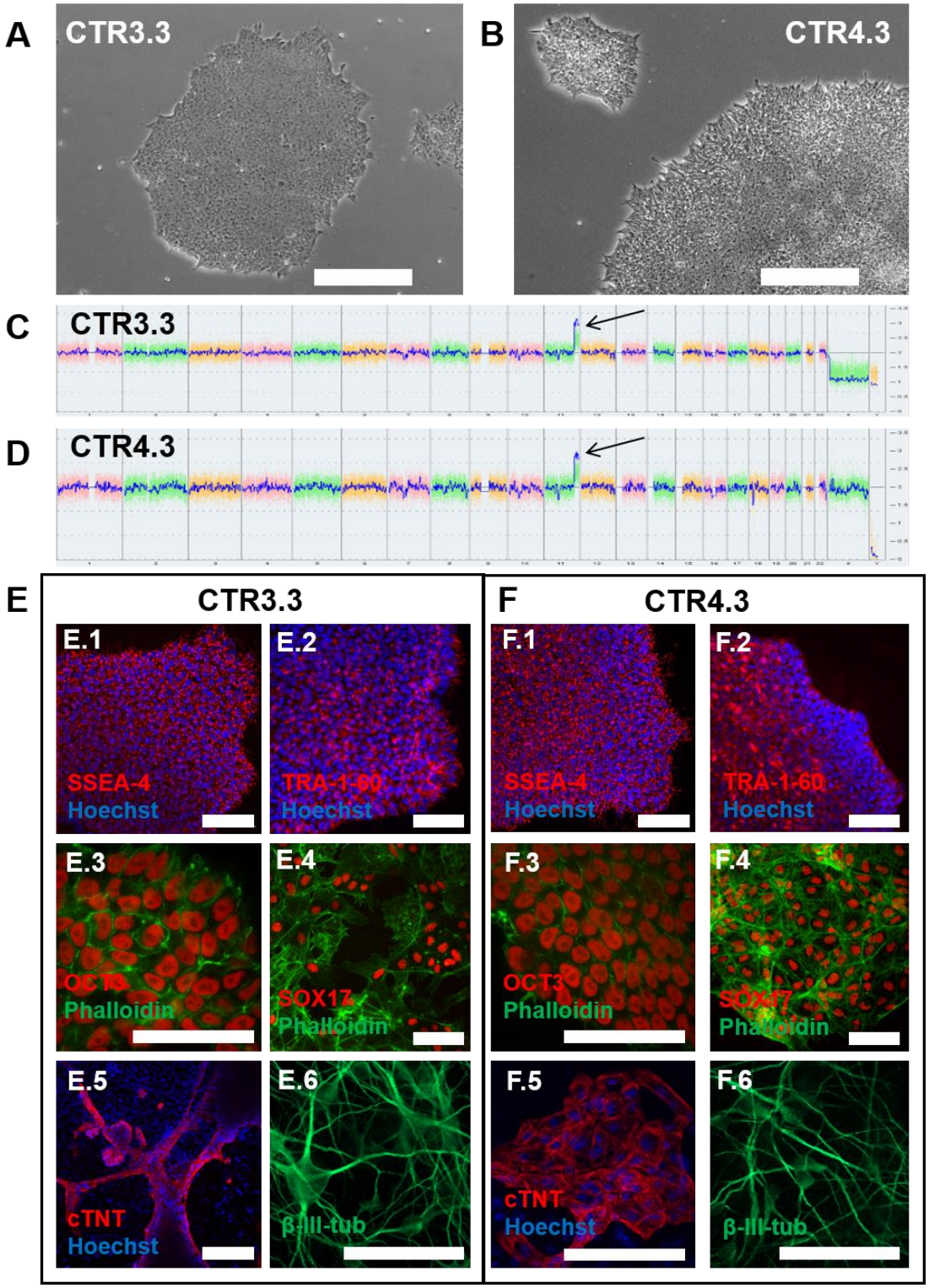

Supplementary Figure 2. Full characterization of additional healthy control clones CTR3.3 and CTR4.3. (A+B) iPSC grew in their classical morphology of tightly packed colonies. (C+D) KaryoStat™ analysis revealed minor genomic aberrations. For both clones, there was a mosaic gain found on chromosome 11 (chromosomal gain for CTR3.3: 69,487 bp; chromosomal gain for CTR4.3: 60,344 bp). (E+F) iPSC clones stably expressed iPSC markers (SSEA-4 (.1), TRA-1-60 (.2) and OCT3 (.3)) and could be differentiated into all three germ layers (positive SOX17 staining (.4) for successful endodermal differentiation, cardiac troponin t (cTNT) staining (.5) for mesodermal differentiation and β-III-tubulin (.6) for ectodermal differentiation).

6.3. Gene expression analysis of differentiated microglia in mono- and co-culture with neurons

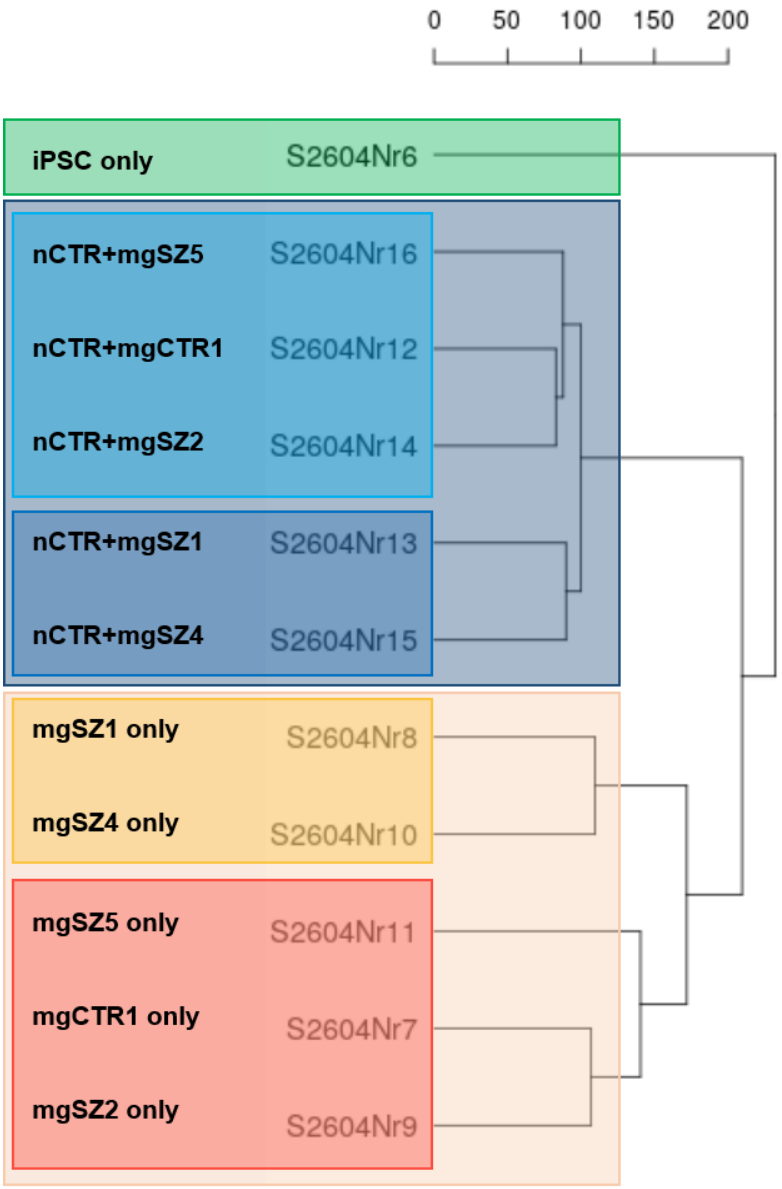

Supplementary Figure 3. Dendrogram depicting the results of an unbiased hierarchical clustering of iPSC-derived microglia in mono- or co-culture with neurons. Undifferentiated iPSC served as negative control for microglial gene expression. Results are based on all genes that achieved at least one read in one sample during RNA sequencing. RNA sequencing was performed by CeGaT GmbH, Tübingen.

Supplementary Table 1. Gene expression profiling of differentiated microglia with raw data as reads per kilo base million. Deregulated genes are compared to undifferentiated iPSC (shown as FPKM+1), log2 fold change (log2FC).

		iPSC only	mgCTR1		mgSZ1		mgSZ2		mgSZ4		mgSZ5	
Gene	**Ref.**	**raw data**	**raw data**	**log2FC to iPSC**	**raw data**	**log2FC to iPSC**	**raw data**	**log2FC to iPSC**	**raw data**	**log2FC to iPSC**	**raw data**	**log2FC to iPSC**
ADORA3	[137]	5,2	4,8	-0,1	366,1	6,1	1,0	-2,4	81,9	4,0	12,0	1,2
APOBEC3C	[132]	906,4	1,9	-8,9	343,8	-1,4	80,9	-3,5	481,1	-0,9	114,3	-3,0
C1QA	[132]	1,0	1,0	0,0	134,6	7,1	1,0	0,0	26,2	4,7	1,0	0,0
C1QB	[132]	1,0	1,0	0,0	455,1	8,8	2,1	1,0	163,7	7,4	6,0	2,6
C1QC	[132]	1,0	1,9	1,0	2333	11,2	1,0	0,0	541,3	9,1	7,0	2,8
C2	[132]	20,3	27,6	0,4	33,1	0,7	7,4	-1,5	21,7	0,1	23,1	0,2
C3	[132]	512,7	20,9	-4,6	1029	1,0	5,3	-6,6	837,1	0,7	68,2	-2,9
C3AR1	[130] [131]	1,0	1,0	0,0	87,4	6,4	1,0	0,0	54,9	5,8	2,0	1,0
C4A	[132]	9,4	16,2	0,8	17,7	0,9	14,8	0,7	9,4	0,0	22,1	1,2
C4B	[132]	10,0	10,5	0,1	6,4	-0,6	7,4	-0,4	10,0	0,0	33,1	1,7
CARD8	[132]	721,6	1126	0,6	1164	0,7	1124	0,6	912,6	0,3	920,4	0,4
CASP8	[130] [131]	180,4	97,8	-0,9	289,5	0,7	109,7	-0,7	304,9	0,8	180,5	0,0
CCL2	[130] [131]	91,3	1,0	-6,5	23,3	-2,0	312,0	1,8	675,3	2,9	4,0	-4,5
CCL3	[137]	1,0	25,7	4,7	100,7	6,7	17,0	4,1	64,8	6,0	2,0	1,0
CCL4	[137]	1,0	1,0	0,0	27,7	4,8	2,1	1,0	22,6	4,5	7,0	2,8
CCR1	[130] [131]	1,0	10,0	3,3	456,0	8,8	4,2	2,1	134,1	7,1	14,0	3,8
CCR5	[130] [131]	1,0	9,0	3,2	59,8	5,9	1,0	0,0	17,2	4,1	11,0	3,5
CCRL2	[137]	1,0	1,9	1,0	18,8	4,2	2,1	1,0	9,1	3,2	5,0	2,3
CD14	[132]	1,6	35,2	4,5	924,3	9,2	18,0	3,5	378,6	7,9	27,1	4,1
CD33	[132]	13,0	3,8	-1,8	90,9	2,8	7,4	-0,8	42,4	1,7	19,0	0,5
CD53	[130] [131]	30,5	1,9	-4,0	226,3	2,9	1,0	-4,9	118,8	2,0	9,0	-1,8
CD58	[132]	91,9	217	1,2	147,0	0,7	313,1	1,8	244,6	1,4	151,4	0,7
CD74	[132]	1183	93,1	-3,7	1615	0,4	55,3	-4,4	1153	0,0	168,4	-2,8
CD84	[130] [131]	1,6	5,7	1,8	370,5	7,9	4,2	1,4	131,4	6,4	8,0	2,3
CIITA	[132]	5,8	6,7	0,2	143,5	4,6	3,1	-0,9	36,1	2,6	18,0	1,6
CLECL1	[132]	1,0	1,0	0,0	8,1	3,0	1,0	0,0	1,0	0,0	8,0	3,0
CMKLR1	[130] [131]	17,9	34,2	0,9	521,9	4,9	59,6	1,7	240,1	3,7	34,1	0,9
CSF1R	[132]	1,6	23,8	3,9	1646	10,0	26,6	4,1	566,5	8,5	53,1	5,1
CSF3R	[130] [131]	1,6	12,4	3,0	439,1	8,1	7,4	2,2	127,8	6,3	20,0	3,6
CTTNBP2	[131]	1668	979	-0,8	3863	1,2	370,6	-2,2	826,3	-1,0	772,0	-1,1
CX3CR1	[132]	1,0	5,7	2,5	23,3	4,5	8,5	3,1	20,8	4,4	13,0	3,7
EGR1	[137]	3734	2776	-0,4	2929	-0,4	3267	-0,2	2106	-0,8	2222	-0,7
F11R	[137]	2901	98,8	-4,9	418,6	-2,8	384,5	-2,9	326,4	-3,2	169,4	-4,1
FOSB	[137]	764,3	1209	0,7	1352	0,8	460,1	-0,7	359,7	-1,1	825,1	0,1
GLDN	[131]	70,8	46,6	-0,6	16,1	-2,1	58,5	-0,3	10,9	-2,7	35,1	-1,0

GNLY	[132]	2,8	10,5	1,9	2,8	0,0	2,1	-0,4	1,0	-1,5	12,0	2,1
GPR34	[135]	1,0	1,0	0,0	101,6	6,7	1,0	0,0	76,5	6,3	1,0	0,0
HEXB	[130]	1327	485	-1,5	1072	-0,3	791,4	-0,7	1164	-0,2	620,6	-1,1
HLA-B	[131]	2613	543	-2,3	1005	-1,4	1356	-0,9	1243	-1,1	2323	-0,2
HLA-DRA	[131]	22,1	6,7	-1,7	140,8	2,7	11,7	-0,9	148	2,7	2,0	-3,5
ICAM1	[132]	542,8	52,3	-3,4	526,3	0,0	126,7	-2,1	439,7	-0,3	99,3	-2,5
IL21R	[137]	19,7	39,9	1,0	21,5	0,1	30,8	0,6	8,2	-1,3	13,0	-0,6
ITGB3	[130] [131]	6,4	8,6	0,4	549,5	6,4	8,5	0,4	359,7	5,8	381,0	5,9
ITGAM	[136]	25,1	17,1	-0,5	376,7	3,9	17,0	-0,6	86,4	1,8	59,2	1,2
KLF4	[12]	141,9	185	0,4	147,0	0,1	141,9	0,0	102,6	-0,5	219,6	0,6
LAG3	[137]	113,6	86,4	-0,4	90,0	-0,3	94,7	-0,3	55,8	-1,0	136,4	0,3
LIN28A	[12]	65349	9671	-2,8	8,1	-13,0	65349	0,0	648,3	-6,7	9079	-2,8
LY96	[130] [131]	1,6	1,9	0,3	11,7	2,9	4,2	1,4	10,0	2,6	7,0	2,1
MERTK	[130]	489,2	223	-1,1	1125	1,2	110,7	-2,1	585,4	0,3	183,5	-1,4
MRC1	[130] [131]	1,0	1,0	0,0	55,3	5,8	9,5	3,3	6,4	2,7	15,0	3,9
MYD88	[132]	418,8	405	0,0	818,4	1,0	402,6	-0,1	847,9	1,0	356,9	-0,2
OLFML2B	[130] [131]	398,3	710	0,8	969,7	1,3	962,9	1,3	1406	1,8	833,2	1,1
P2RY12	[199]	1,0	5,0	2,3	1,0	0,0	2,1	1,0	4,6	2,2	6,0	2,6
P2RY13	[199]	1,0	1,0	0,0	14,4	3,8	1,0	0,0	15,4	3,9	1,0	0,0
P2RY2	[199]	25,1	30,4	0,3	55,3	1,1	73,4	1,5	20,8	-0,3	36,1	0,5
POU5F1	[12]	26275	28847	0,1	4,6	-12,5	26275	0,0	6465	-2,0	18848	-0,5
PROS1	[130]	241,8	748,2	1,6	1391	2,5	795,6	1,7	1119	2,2	662,7	1,5
PTGS1	[137]	135,8	39,0	-1,8	253,9	0,9	15,9	-3,1	98,1	-0,5	24,1	-2,5
ROBO3	[131]	728,8	1785	1,3	341,1	-1,1	1083	0,6	243,7	-1,6	445,1	-0,7
SERPING1	[132]	2349	1926	-0,3	1242	-0,9	2322	0,0	2399	0,0	1445	-0,7
SIGLEC12	[132]	1,0	4,0	2,0	63,3	6,0	1,0	0,0	12,7	3,7	7,0	2,8
SIGLEC14	[132]	1,0	4,0	2,0	42,8	5,4	1,0	0,0	15,4	3,9	3,0	1,6
SIGLEC5	[132]	1,0	1,0	0,0	1,0	0,0	1,0	0,0	2,8	1,5	1,0	0,0
SIGLEC7	[132]	1,0	3,0	1,6	74,9	6,2	5,3	2,4	17,2	4,1	6,0	2,6
SLC17A9	[130] [131]	459,7	44,7	-3,4	371,4	-0,3	45,7	-3,3	246,4	-0,9	220,6	-1,1
SLC2A5	[137]	10,0	4,8	-1,1	32,2	1,7	3,1	-1,7	38,8	2,0	20,0	1,0
SLC37A2	[130] [131]	35,3	15,2	-1,2	455,1	3,7	23,4	-0,6	104,4	1,6	42,1	0,3
SLCO2B1	[130] [131]	1,0	34,0	5,1	1232	10,3	30,8	4,9	347,1	8,4	114,3	6,8
SOX2	[12]	11019	5339	-1,0	82,9	-7,1	11020	0,0	648,3	-4,1	4463	-1,3
SYNDIG1	[131]	241,2	605,8	1,3	160,4	-0,6	382,3	0,7	118,8	-1,0	323,8	0,4
TGFBR1	[130]	3083	3688	0,3	5602	0,9	5444	0,8	10020	1,7	3102	0,0
TMEM106A	[130] [131]	153,3	197,5	0,4	530,8	1,8	195,9	0,4	320,2	1,1	259,7	0,8
TMEM119	[135]	18,5	47,5	1,4	18,5	0,0	85,2	2,2	1042	5,8	65,2	1,8
TREM2	[135]	1,0	1,0	0,0	109,6	6,8	4,2	2,1	39,7	5,3	7,0	2,8
VSIG4	[132]	1,0	6,7	2,7	673,2	9,4	3,1	1,6	137,7	7,1	9,0	3,2

7. Publications

Parts of this thesis are published in:

- Grunwald LM*, **Stock R***, Haag K, Buckenmaier S, Eberle MC, Wildgruber D, Storchak H, Kriebel M, Weißgraeber S, Mathew L, Singh Y, Loos M, Li KW, Kraushaar U, Fallgatter AJ, Volkmer H. Comparative characterization of human induced pluripotent stem cells (hiPSC) derived from patients with schizophrenia and autism. Transl Psychiatry. 2019 Jul 29;9(1):179. doi: 10.1038/s41398-019-0517-3. PMID: 31358727. PMCID: PMC6663940.
- **Stock R**, Vogel S, Mau-Holzmann UA, Kriebel M, Wüst R, Fallgatter AJ, Volkmer H. Generation and characterization of human induced pluripotent stem cells lines from four patients diagnosed with schizophrenia and one healthy control. Stem Cell Res. 2020 Aug 27; 48:101961. doi: 10.1016/j.scr.2020.101961. PMID: 32911325.

Published review articles:

- **Stock R**, Jeckel P, Kraushaar U, Wüst R, Fallgatter A, Volkmer H. The potential of induced pluripotent stem cells for discriminating neurodevelopmental disorders. Stem Cells Transl Med. 2020 Aug 31. doi: 10.1002/sctm.20-0206. PMID: 32864861.
- **Stock R**, Volkmer H. Psychiatrische Erkrankungen mit Stammzelltechnologien verstehen. BIOSpektrum. 2020 Jan. doi: 10.1007/s12268-020-1321-6

*shared first authors